UCLA
UCLA Electronic Theses and Dissertations

Title

Synthetic and Photophysical Investigations of Boron Cluster-Based Luminescent Molecules

Permalink

https://escholarship.org/uc/item/83k4x2sz

Author

Anderson, Kierstyn

Publication Date

2022

Peer reviewed|Thesis/dissertation

UNIVERSITY OF CALIFORNIA

Los Angeles

Synthetic and Photophysical Investigations of Boron Cluster-Based Luminescent Molecules

A dissertation submitted in partial satisfaction of the

requirements for the degree Doctor of Philosophy

in Chemistry

by

Kierstyn Phyllis Anderson

2022

ABSTRACT OF THE DISSERTATION

Synthetic and Photophysical Investigations of Boron Cluster-Based Luminescent Molecules

by

Kierstyn Phyllis Anderson

Doctor of Philosophy in Chemistry

University of California, Los Angeles, 2022

Professor Alexander Michael Spokoyny, Chair

Luminescent boron cluster-based compounds have gained recent attention for their potential use in optoelectronic applications due to their three-dimensional aromaticity, synthetic tunability, and stability profiles. Functionalization of individual boron cage vertices provides a route toward precise structural modification that ultimately affects the photoluminescent and photophysical properties of the overall molecule. For many boron clusters, however, synthetic modification methods are limited, and the structure-function relationships of luminescence are not well understood. In this dissertation, the syntheses and characterization of new luminescent polyhedral borane cluster compounds are described. Chapter 1 focuses on the development of an S_NAr method for C-carborane ($C_2B_{10}H_{12}$) functionalization capable of procuring new molecular architectures containing (hetero)aryl groups. We envision that these carborane-based compounds could serve as

sterically bulky, rigid ligands in organometallic complexes, which could lend the molecule properties such as high energy emission and high quantum yield. The remaining chapters focus on the synthetic and photoluminescent investigations of the only inherently fluorescent boron hydride cluster known to date, *anti*-$B_{18}H_{22}$. Despite its unique luminescence, only a handful of reports on the synthetic reactivity of *anti*-$B_{18}H_{22}$ exist, and little is understood about how structural changes affect its innate fluorescence. Therefore, in Chapters 2-4, *anti*-$B_{18}H_{22}$ is derivatized through halogenation with iodine, bromine and chlorine, and the photoluminescence and stability properties of the resulting analogues are benchmarked. Finally, Chapter 5 describes both palladium-catalyzed cross-coupling and metal-free nucleophilic substitution reactions on 7-I-$B_{18}H_{21}$, which result in boron-iodine bond substitution to forge B-N, B-O, and B-S connectivities with the boron cluster cage. Overall, this work advances the fundamental synthetic knowledge of the fluorescent *anti*-$B_{18}H_{22}$ cluster and provides a foundation for the generation of new luminescent boron-cluster-based molecules.

The dissertation of Kierstyn Phyllis Anderson is approved.

Neil Kamal Garg

Justin Ryan Caram

Paula Loredana Diaconescu

Alexander Michael Spokoyny, Committee Chair

University of California, Los Angeles

2022

Dedication Page

This work is dedicated to my loving and ever supportive family, who have never stopped cheering me on and challenging me. I could not ask for a more supportive partner, Jeff, who has been by my side through the tears (of joy and frustration), failures, and successes of my research. Thank you for providing the much needed mental, emotional, and financial support over these past several years, and thank you for feigning interest while I explain complex chemistry concepts to you.

I owe much of my early success to my phenomenal mentors Dr. Kent Kirlikovali and Dr. Jon Axtell, who provided immense guidance through the first two turbulent years of graduate school. They set a high bar for what a graduate student and postdoc should be, and I hope that what I've accomplished over the past five years lives up to their legacies. Thank you to my wonderful coworkers who made the slow days go by faster and the difficult days pass easier. An enormous thanks to Dr. Peter Djurovich, who taught me almost all that I know about luminescent molecules and took a genuine interest in my research.

Finally, I would like to thank Alex, who let me explore the chemistry I found most interesting and supported me every step of the way. My only regret is that I did not take your advice ("A day in the library saves a month in the lab!") seriously enough until my 4th year. Thank you for providing a research environment that provided a challenging, rewarding, and fascinating graduate school experience. It is invaluable to me.

Table of Contents

List of Figures

Acknowledgements

A. M. S. PI and edited the manuscript

Chapter 3 is a version of K. P. Anderson, A. S. Hua, J. B. Plumley, A. D. Ready, A. L. Rheingold, T. L. Peng, P. I. Djurovich, C. Kerestes, N. A. Snyder, A. Andrews, J. R. Caram and A. M. Spokoyny. Benchmarking the dynamic luminescent properties and UV stability of $B_{18}H_{22}$-based materials. *Dalton Trans.* **2022**, Advance Article. DOI: 10.1039/D2DT01225A.

K. P. A. designed and performed experiments and wrote the manuscript.

A. S. H. and J. R. C. designed and assisted in UV imaging experiments.

J. B. P., T. L. P., C. K., N. A. S. and A. A. designed and conducted light soaking studies.

A. D. R. performed ICP experiments.

A. L. R. performed crystallography experiments.

P. I. D. assisted with luminescence measurements and data interpretation.

A. M. S. PI and edited the manuscript

Chapter 4 is a version of K. P. Anderson, A. L. Rheingold, P. I. Djurovich, O. Soman and A. M. Spokoyny. Synthesis and luminescence of monohalogenated $B_{18}H_{22}$ clusters. *Submitted*.

K. P. A. designed and performed experiments and wrote the manuscript.

A. L. R. performed crystallography experiments.

P. I. D. assisted with luminescence measurements and data interpretation.

O. S. performed experiments.

A. M. S. PI and edited the manuscript

Chapter 5 is a version of K. P. Anderson, P. I. Djurovich, V. P. Rubio, A. Liang, and A. M. Spokoyny. Metal-Catalyzed and Metal-Free Nucleophilic Substitution of 7-I-$B_{18}H_{21}$. *Submitted.*

K. P. A. designed and performed experiments and wrote the manuscript.

P. I. D. assisted with luminescence measurements and data interpretation.

V. P. R. and A.L. assisted with experiments.

A. M. S. PI and edited the manuscript.

Biographical Sketch

Kierstyn Anderson earned a BS in Chemistry at Northeastern University, where she studied fuel cell membranes under Prof. Eugene Smotkin. She also conducted research on drug development for neurodegenerative diseases and microneedle vaccine patches. As a graduate student in Prof. Alexander Spokoyny's research group, her primary research interests involve investigating the structure-function relationships of luminescent boron cluster molecules, specifically *anti*-$B_{18}H_{22}$.

Awards and Honors

M. Frederick Hawthorne Inorganic Chemistry Dissertation Award, 2022 | Air Force Research Laboratory (AFRL) Space Scholar, 2021 and 2022 | Jim and Barbara Tsay Excellence in Second Year Research and Academics, 2020 | National Science Foundation Graduate Research Fellowship (NSF GRF), 2019 | Outstanding Undergraduate Research Award, 2017 | Provost Undergraduate Research and Creative Endeavors Award, 2015

Peer-Reviewed Publications (ψ indicates co-first authorship)

1. **<u>Anderson, K.P.</u>,*** Djurovich, P.I., Rubio, V. P., Liang, A. and Spokoyny, A.M. Metal Catalyzed and Metal-Free Nucleophilic Substitution of $7\text{-}I\text{-}B_{18}H_{21}$. *Submitted.*

2. **<u>Anderson, K.P.</u>,*** Rheingold, A.L., Djurovich, P.I., Soman, O. and Spokoyny, A.M. Synthesis and luminescence of monohalogenated $B_{18}H_{22}$ clusters. *Submitted.*

3. Mills, H.A., Jones, C.G., **<u>Anderson, K.P.,</u>** Ready, A.D., Djurovich, P.I., Khan, S.I., Hohman, N., Nelson, H.M., and Spokoyny, A.M.* Sterically Invariant Carborane-Based Ligands for the Morphological and Electronic Control of Metal-Organic Chalcogenolate Assemblies. *Accepted.*

4. Ready, A.R., Becwar, S.M., Jung, D., Schueller, E., **Anderson, K.P.,** Kubena, R., Seshadri, R. Chmelka, B.F., and Spokoyny, A.M* Advance Article. DOI: 10.1039/D2DT01292H.

5. **Anderson, K.P.,** Hua, A., Plumley, J., Ready, A., Rheingold, A.L., Peng, T.L., Djurovich, P.I., Caram, J.R., and Spokoyny, A.M.* Advance Article. DOI: 10.1039/D2DT01225A.

6. **Anderson, K.P.,** Waddington, M. A., Balaich, G. J., Stauber, J. M., Caram, J. R.,* Djurovich, P. I., and Spokoyny, A.M.* *Dalton Trans.* **2020**, 49, 16245-16251.

7. **Anderson, K.P.,**$^{\psi}$ Mills, H.A.,$^{\psi}$ Mao, C., Kirlikovali, K.O., Axtell, J.C., Rheingold, A.L., and Spokoyny, A.M.* *Tetrahedron*. **2018**, 75, 187- 191.

8. Kirlikovali, K.O., Axtell, J.C., **Anderson, K.,** Djurovich, P.I., Rheingold, A.L., and Spokoyny, A.M.* *Organometallics*. **2018,** 37, 3122-3131.

9. Choi, S., Calder, A.N., Miller, E.H., **Anderson, K.P.,** Fiejtek, D.K., Rietz, A., Li, H., Cherry, J.J., Quist, K.M., Xing, X., Glickman, M.A., Cuny, G.D., Lorson, C.L., Androphy, E.A., and Hodgetts, K.J.* *Bioorganic & Medicinal Chemistry Letters.* **2017,** 27, 5144-5148.

10. **Anderson, K.,** Kingston, E., Romeo, J., Doan, J., Loupe, N., Dimakis, N., and Smotkin, E.S.* *Polymer*. **2016,** 93, 65-71.

11. Doan, J., Navarro, N.E., Kumari, D., **Anderson, K.,** Kingston, E., Johnson, C., Vong, A., Dimakis, N., and Smotkin, E.S.* *Polymer.* **2015,** 73, 34-41.

12. Doan, J., Kingston, E., Kendrick, I., **Anderson, K.,** Dimakis, N., Knauth, P., Di Vona, M.L., and Smotkin, E.S.* *Polymer*. **2014,** 55, 4671-676.

Introduction

Boron-containing compounds offer a variety of advantageous properties that are distinctly different from the typical carbon-based molecules investigated in organic chemistry. Boron has historically found use in glass, ceramics, insecticides, and detergents, but only in the past 15-30 years has it been applied for broader purposes ranging from organic light emitting diode (OLED) displays to cancer therapeutics. The emergence of research on boron-containing compounds over the past half century can be traced back to boron's unique electron-deficient bonding motif discovered by Lipscomb,[1] which affords molecular architectures not typically found in carbon compounds. Specifically, the ability for boron to form multicenter bonds results in large, three-dimensional delocalized cluster compounds that display aromaticity similar to that of benzene. Pioneered by Hawthorne[2] in the 1950's, the field of boron cluster molecules has now found a prominent place in chemistry research. One of these areas, and the focus of this work, involves the generation and modulation of boron cluster-based luminescent compounds that are useful for a variety of optoelectronic applications such as OLEDs, solar cells, and sensors. The implementation of boron clusters in these areas can provides advantages over the carbon-based molecules currently employed, such as improved thermal and photostability and improved luminescence efficiency.

My work primarily focuses on understanding a particularly unique boron cluster molecule, *anti*-$B_{18}H_{22}$, which is a rare example of a boron hydride possessing innate fluorescence. Despite this, very few studies investigating the synthetic and photoluminescent properties of this molecule exist. My goals focus first on the generation of B_{18}-based analogues that could permit access to more complex and interesting luminescent molecular structures. Synthetic alteration of $B_{18}H_{22}$ *via* appending functional groups on the boron vertices of the cage alters the luminescent properties of the overall molecule, potentially generating derivatives with a variety of emission wavelengths.

Thus, the second goal of this work centers on the investigation and characterization of the photoluminescent properties of *anti*-$B_{18}H_{22}$ derivatives. Through these efforts we can gain insight into the structure-function relationships relevant to the design of $B_{18}H_{22}$ chromophores and further the field luminescent boron cluster chemistry.

Bonding in boron

Like any element, the origins of boron's unique properties are reflected by its position on the periodic table. Residing in the 13th group and 2nd period, boron is the leftward neighbor of carbon, and hence possesses one less valence electron to give a total of three. As one can surmise based on their proximity in the periodic table, carbon and boron share several similar chemical properties. However, the comparatively electropositive nature of boron originating from its single p-orbital electron renders it unable to form stable electron octets in the same manner as carbon. Consequently, boron exists in a 3+ oxidation state and prefers to form just three covalent bonds, resulting in stable compounds such as boric acid, or $B(OH)_3$. This bonding motif also has implications for boron-boron bonds; while carbon easily forms classical single, double, or triple carbon-carbon bonds, there is insufficient orbital overlap for these to form between boron atoms. Instead, boron-boron bonds generally exist as a non-classical, three-center, two-electron system in which two electrons are delocalized over three atoms.[1] For example, ethane (C_2H_6) is comprised of a carbon-carbon single bond, with each carbon possessing three singly bonded hydrogens to form a complete octet in which all 14 valence electrons are involved in bonding (Figure I.1, top). The boron analogue B_2H_6, however, does not exhibit the same bonding motif due to the presence of only 12 available valence electrons. Instead of being bound by a single bond, the boron atoms are held together by two bridging hydrogens. These bridging hydrogens share two electrons across three atoms, giving a boron-hydrogen-boron bond that satisfies the need for a stable octet (Figure

2
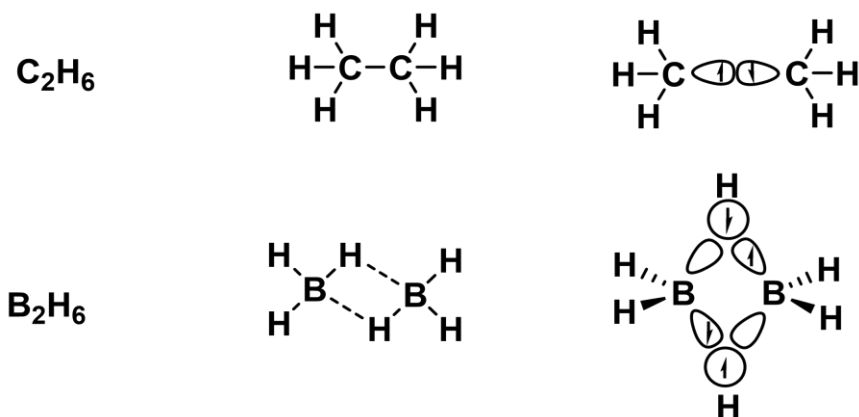
Figure I.1. Top) Classical bonding in C_2H_6. Bottom) Non-classical bonding in B_2H_6, showing the three-center two-electron bonding characteristic of boron compounds.

I.1, bottom).[3] This delocalized manner of bonding is what permits the formation of stable polyhedral boron hydride clusters such as carboranes ($C_2B_{10}H_{12}$), dodecaborate clusters ($B_{12}H_{12}^{2-}$), and decaborane ($B_{10}H_{14}$), among several others. Like carbon-based compounds. these three-dimensional boron cluster molecules can undergo synthetic modification to afford a broad scope of versatile molecular architectures.

Photoluminescence

Luminescence is a process in which electrons within molecules become energetically excited and subsequently release this excess energy in the form of light. Electrons are organized into orbitals with increasing energies, and only those in the highest energy orbitals are able to participate in light-activated processes. These outermost electrons, residing in the Highest Occupied Molecular Orbital (HOMO), will be most susceptible to energetic excitation through light absorption. Molecules exist at the lowest point in their potential energy surfaces (ground state), with each successive orbital up to and including the HOMO being filled with paired electrons. This ground state is termed the electronic singlet ground state (S_0), where the singlet term arises from the spin multiplicity of the system. Spin multiplicity is calculated from the equation *M = 2S + 1*, where S

3
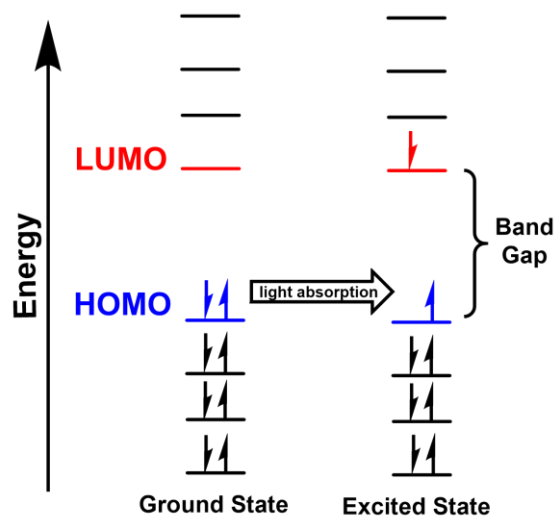
Figure I.2. Schematic representation of HOMO and LUMO in the singlet ground state and, after light absorption, the singlet excited state.

is the total spin of the system. The spin of a single electron is assigned a value of ½, and if all electrons are paired with opposite spins, the total spin S is zero ($+½ + -½ = 0$). Therefore, the spin multiplicity M in this scenario is 1.

Absorption and non-radiative decay

If excited by light (absorption), a single electron in the HOMO can be excited into the next unoccupied orbital of higher energy, termed the Lowest Unoccupied Molecular Orbital (LUMO), provided the energy of absorbed light is sufficient to cross the band gap (difference in energy between the HOMO and LUMO, Figure I.2). The excited electron will maintain its spin orientation and therefore singlet character is preserved; however, because this electron resides in a higher energy orbital (*i.e.* the molecule is not at the lowest possible energy) the molecule is deemed to be in a singlet excited state (Figure I.2 and I.3). Within each electronic state (*e.g.*, S_1, S_2, depicted as bold lines in Figure I.3) there are a variety of vibronic energy states that can couple with the electronic state (Figure I.3, non-bold lines). Therefore, upon excitation of the electron there is a spread of electronic and vibrational states that it can access.[4] There are both radiative (transitions

associated with light) and non-radiative (transitions not associated with light) pathways through which the excess energy can dissipate. In the Jablonski diagram in Figure I.3, the former are depicted as straight arrows while the latter are denoted as curvy arrows. The first type of transition, vibrational relaxation (VR), is likely to take place immediately after absorption. This non-radiative process involves kinetic energy loss through either intermolecular or intramolecular means, resulting in the electron transitioning between vibrational energy levels within an electronic excited state. Similarly, the electron can undergo internal conversion (IC) to transition between electronic excited states (*e.g.*, S_2 to S_1, Figure I.3), which is also a non-radiative process that occurs due to the coupling between vibrational levels and electronic states. Both vibrational relaxation and internal conversion are exceedingly fast ($\sim 10^{-14}$ to 10^{-11} seconds),[4] and therefore occur
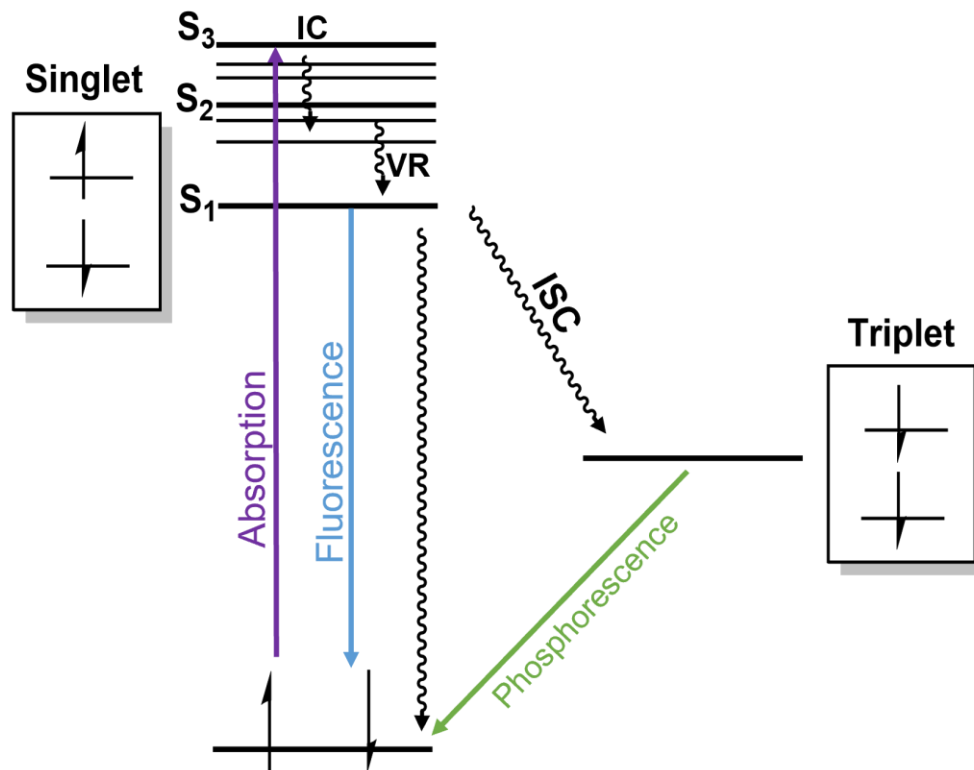
Figure I.3. Jablonski diagram showing possible radiative (straight arrows) and non-radiative (curved arrows) processes. Absorption (purple) occurs from the singlet ground state, which Internal Conversion (IC, black arrow) and Vibrational Relaxation (VR, black arrow) can occur. Subsequent radiative decay (fluorescence, blue) or non-radiative Intersystem Crossing (ISC, black arrow) can occur from S_1. ISC leads to the formation of a triplet state, from which non-radiative or radiative decay (phosphorescence, green) can take place.

5

immediately after absorption. The majority of molecules do not display luminescence due to either the inability to promote an electron (large band gap), or due to the several favorable non-radiative decay pathways, such as energy loss through molecular collisions or through electron transfer between molecules.

Fluorescence

Once an excited electron has decayed to the lowest energy of its electronic excited state, likely the first excited singlet state (S_1), it can decay non-radiatively back to the singlet ground state without the emission of light. Alternatively, relaxation can occur radiatively to result in fluorescence. In comparison to non-radiative decay, fluorescence is exceptionally slow (~10^{-9} to 10^{-11} sec),[4] and therefore is less likely to occur. For this reason, emission originating from the higher excited states is generally not feasible, and thus fluorescence will only be able to compete with vibrational relaxation processes from the first singlet excited state. The energy, or wavelength, of the emitted light from fluorescence will always be lower than that of the absorption process due to the fact that energy loss through non-radiative processes (vibrational relaxation and internal conversion) will take place prior to fluorescence (Figure I.3).

Intersystem Crossing and Phosphorescence

The mechanisms of light absorption and electron decay discussed so far have focused on processes within the same spin multiplicity. However, transitions between spin multiplicities are possible through a process called Intersystem Crossing (ISC, Figure I.3). This is a forbidden process, which means that it should not be possible according to electronic selection rules. However, if we take into consideration the fact that electronic states can couple to vibrational levels, the transition becomes weakly allowed. Because this is a disfavored process, a specific set of conditions must

be met for it to be feasible for an excited molecule. Namely, the vibrational levels of the two electronic excited states involved in the transition must overlap, and the degree of overlap will dictate the feasibility of ISC. In most cases, this is achieved through the presence of heavy atoms such as halogens or metals, which lend the molecular Spin-Orbit Coupling (SOC) that increases the likelihood of ISC.[5] This is because the presence of heavy atoms will enhance vibronic coupling (coupling between vibrational and electronic states). When ISC occurs, the electron will undergo a spin flip, resulting in a total spin S of 1 ($S = \frac{1}{2} + \frac{1}{2}$) and therefore a multiplicity M of 3, which is aptly termed a triplet state. From the excited triplet state (T_1) the electron can undergo non-radiative decay, as discussed earlier, or radiative decay. Radiative decay from the excited triplet state is called phosphorescence and involves another change in multiplicity back to the singlet ground state (Figure I.3). This is also a forbidden process and is extraordinarily slow ($\sim 10^{-4}$ to 10^{-1} seconds).[4] As a result, phosphorescence occurs over a much longer timescale compared to fluorescence, and the long-lived nature (lifetime, τ) of this process is usually the distinguishing feature between the two types of emission.[4] The efficiency of fluorescence and phosphorescence is measured through quantum yield (Φ), which is a term that represents the number of photons that are emitted by the molecule divided by the number of photons absorbed by the molecule. Therefore, a quantum yield of 1 means that all of the photons that are absorbed by the molecule are also re-emitted in a fluorescent or phosphorescent process; a quantum yield of 0.5 means that only 50% of the absorbed photons are re-emitted, and so on. Given the numerous opportunities for an electron to decay without emitting light, one can appreciate how difficult it is to achieve luminescence in general, let alone quantum yields nearing unity. It is this complex landscape that must be considered throughout the design, synthesis, and characterization of luminescent molecules, rendering it a particularly challenging- yet fascinating- field of research.

Boron cluster-based luminescent compounds

Carboranes as ligands in organometallic compounds

Luminescent boron cluster materials have recently gained attention due to their unique properties that can provide advantages over typical carbon moieties. For example, square planar platinum-based organometallic compounds bearing chelating biaryl ligands have shown promise as OLED materials, however their use is limited in part due to their propensity toward aggregation.[6] The intermolecular platinum-platinum metal interactions that arise cause diminished quantum yields and red-shifted emission. To address this, a biscarborane ligand was incorporated into the molecular structure;[7] the icosahedral polyhedral carborane cluster possesses benzene-like aromaticity and significant three-dimensional steric bulk. The former permits broad-scope functionalization of the boron vertices, essentially rendering it a three-dimensional analogue of benzene. Therefore, the corresponding square planar platinum complex with a C,C-bound biscarborane ligand can be easily procured. The bulky nature of the boron cluster proved sufficient in preventing the unwanted metal center interactions and thus luminescence quenching. Another advantage to incorporating boron clusters in luminescent compounds is their highly tunable nature; this was shown through the synthesis and characterization of the platinum complex bearing a B,C-bound biscarborane ligand, which exhibited distinctly different emission properties from its C,C-bound congener.[8] Despite the advantages offered by carborane-based ligands, these molecules were found to undergo significant distortion in the excited state. We hypothesized that this could be mitigated through the development of a more rigid, tetradentate carborane-containing ligand. It is the development of such ligands that initiated work on the S_NAr method described in Chapter 1.

Chemistry and luminescence of anti-B$_{18}$H$_{22}$

With the aforementioned descriptions of boron cluster bonding and luminescence, one can begin to appreciate the exceptional case of *anti*-B$_{18}$H$_{22}$ as the only inherently luminescent boron-hydride known to date. Hawthorne and Pitochelli initially synthesized this molecule and noted its blue fluorescence in 1962,[9] however its exact bonding motif was not established until 1963 by Simpson and Lipscomb.[10] The cluster can be procured in a multi-step synthesis from sodium borohydride (NaBH$_4$) to yield decaborane (B$_{10}$H$_{14}$), which undergoes thiolation to yield the disubstituted diethyl sulfide cluster [(C$_2$H$_5$)$_2$S]$_2$B$_{10}$H$_{12}$. Deboronation of this cluster occurs at one of the substituted boron vertices when the compound is heated in methanol, giving (C$_2$H$_5$)$_2$SB$_9$H$_{13}$. Deprotonation *via* reaction with tetramethylammonium hydroxide in ethanol produces B$_9$H$_{12}^-$, which oxidatively combines to form *anti*-B$_{18}$H$_{22}$ (Figure I.4).[11]

Naturally, the origins of the anomalous luminescence in *anti*-B$_{18}$H$_{22}$ warrants investigation, particularly because the other known B$_{18}$H$_{22}$ isomer, *syn*-B$_{18}$H$_{22}$, is completely non-emissive. The only difference between these two isomers is the way in which the two cluster halves are fused together, with the *syn* isomer possessing C$_2$ symmetry and the *anti* isomer C$_i$, or inversion, symmetry (Figure I.5). This seemingly slight difference results in changes in the potential energy surfaces of each molecule.[12] In the case of *anti*-B$_{18}$H$_{22}$, absorption of light leads to excitation of an electron, followed by immediate non-radiative decay to the lowest point of the potential energy surface of the S$_1$ excited state. This results in the electron coming to "rest" in an energy well
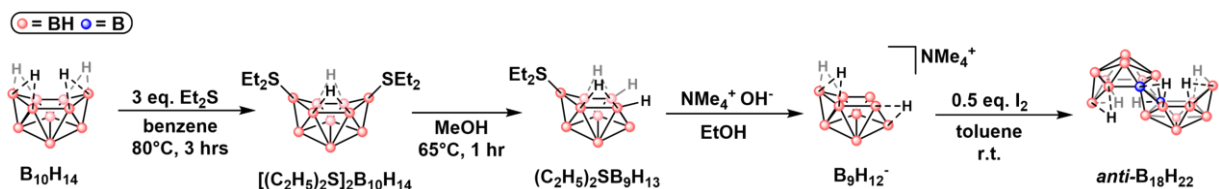
Figure I.4. Synthetic scheme for *anti*-B$_{18}$H$_{22}$, beginning from decaborane(14).

9

approximately 0.5 eV deep, which provides enough time for radiative decay to occur and thus gives fluorescence with exceptional efficiency ($\Phi = 0.97$).[12,13] For *syn*-$B_{18}H_{22}$, absorption and non-radiative decay occur in a similar manner, however the energy well in the S_1 state is shallow (~0.04 eV) and renders non-radiative decay more favorable than fluorescence. Consequently, the molecule will return to the ground state, S_0, by losing energy through molecular vibrations, specifically between boron vertices 5 and 7 (Figure I.5, red line).[12] From these observations, the rarity of luminescence in boranes is better contextualized, as the fluorescence observed in *anti*-$B_{18}H_{22}$ is a circumstance of precise molecular geometry that is not easily achieved in other polyhedral borane clusters.

Studies on the properties of *anti*-$B_{18}H_{22}$ indicate that it could offer advantages over luminescent materials typically used in optoelectronic applications, including carbon-based dyes and non-molecular compounds. For example, a laser-induced fluorescence study demonstrated that *anti*-
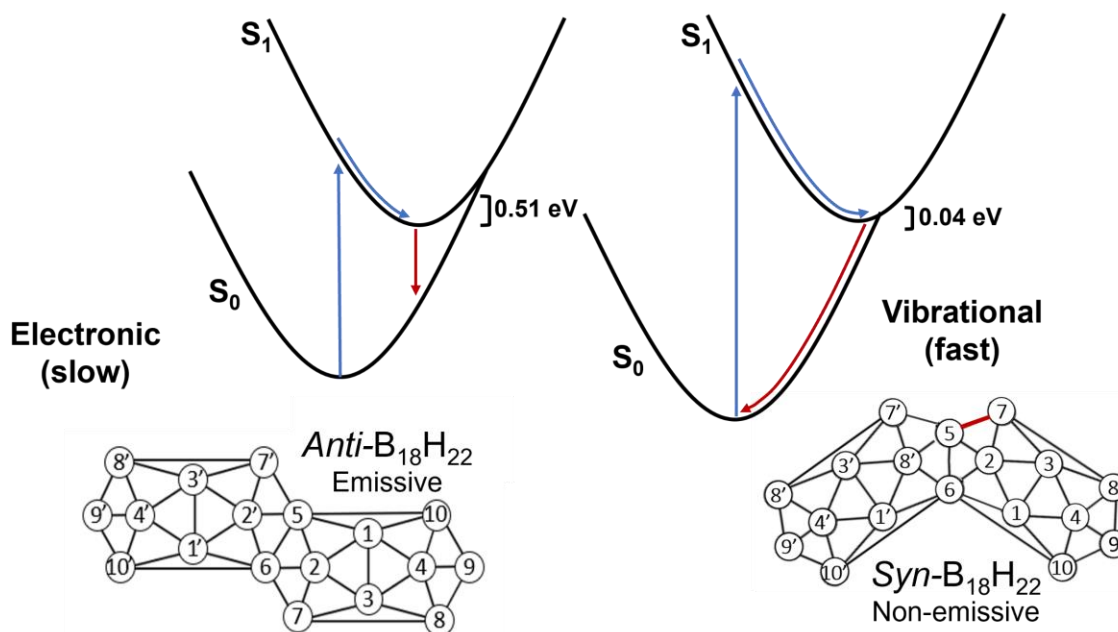
Figure I.5. Comparison of the two isomers of $B_{18}H_{22}$, showing how the slight differences in geometry result in changes of the potential energy surfaces of the molecules. The differences in potential energy surfaces result in fluorescence in *anti*-$B_{18}H_{22}$ and the absence of luminescence in *syn*-$B_{18}H_{22}$.

10

$B_{18}H_{22}$ possesses remarkable photostability, exceeding that of both coumarin dyes and CdSeS/ZnS quantum dots.[13] Because it can be synthetically altered through basic organic chemistry reactions, *anti*-$B_{18}H_{22}$ luminescence can be easily altered in a manner similar to emissive carbon-based molecules.[14] It is also highly processable, meaning that *anti*-$B_{18}H_{22}$ can be dissolved in a variety of organic solvents or cast into films, marking a distinct advantage over non-molecular chromophores.[15] Still, our knowledge of this unique borane remains nascent; only a handful of synthetic procedures describing how to append groups to the 18-vertex boron cage have been reported. Consequently, methods for achieving vertex-selective functionalization and new types of connectivities (*e.g.*, B-O, B-Br bonds) remain unknown. Furthermore, guiding principles on how these structural alterations affect the absorption, nature of emission (fluorescence vs. phosphorescence), emission wavelength, quantum yield, and lifetime are severely lacking. Should *anti*-$B_{18}H_{22}$ gain prominence as a potentially useful material, this knowledge will be essential for the design and preparation of chromophores with specific photoluminescent and photostability properties. Therefore, a significant portion of the work described within this dissertation provides a foundation for the synthetic chemistry of *anti*-$B_{18}H_{22}$ and the resulting properties of its analogues.

References

1. Eberhardt, W.H.; Crawford, B.; Lipscomb, W.N. *J. Chem. Phys.* **1954**, *22*, 989.

2. Tolman, W.B.; Evans, W.; Spokoyny, A.M. *Inorg. Chem.* **2021**, *60*, 12621-12624.

3. Lipscomb, W.N. *Boron Hydrides.* Courier Corporation, 2013.

4. (a) Turro, N.J.; Ramamurthy, V.; Scaiano, J.C. *Modern Molecular Photochemistry of Organic Molecules*. University Science Books, 2010. (b) Jaffé, H.H. and Miller, A.L. *J. Chem. Educ.* **1966**, *9*, 469.

5. Lower, S. K. and El-Sayed, M.A. *Chem. Rev.* **1966**, *66*, 199-241.

6. (a) P.-T. Chou, P.-T. and Chi, Y. *Chem.–Eur. J.*, **2007**, *13*, 380-395. (b) Chi, Y. and Chou, P.-T. *Chem. Soc. Rev.*, **2010**, *39*, 638-655. (c) Brooks, J.; Babayan, Y.; Lamansky, S.; Djurovich, P.I.; Tsyba, I.; Bau, R.; Thompson, M.E. *Inorg. Chem.*, **2002**, *41*, 3055-3066. (d) Hudson, Z.M.; Sun, C.; Helander, M.G.; Amarne, H. Lu, Z.-H., Wang, S. *Adv. Funct. Mater.*, **2010**, *20*, 3426-3439.

7. Kirlikovali, K.O.; Axtell, J.C.; Gonzalez, A.; Phung, A.C.; Khan, S.I.; Spokoyny, A.M. *Chem. Sci,* **2016**, *7*, 5132-5138.

8. Kirlikovali, K.O.; Axtell, J.C.; Anderson, K..; Djurovich, P.I.; Rheingold, A.L.; Spokoyny, A.M. *Organometallics,* **2018**, *37*, 3122-3131.

9. Pitochelli, A.R. and Hawthorne, M.F. *J. Am. Chem. Soc.*, **1962**, *84*, 3218.

10. Simpson, P.G. and Lipscomb, W.N. *J. Chem. Phys.* **1963**, *39*, 26-34.

11. (a) Graybill, B.M.; Ruff, J.K.; Hawthorne, M.F. *J. Am. Chem. Soc.*, **1961**, *83*, 2669-2670. (b) Li, Y. and Sneddon, L.G. *Inorg. Chem.* **2006**, *45*, 470-471.

12. Londesborough, M.G.S.; Hnyk, D.; Bould, J,; Serrano-Andrés, L.; Sauri, V.; Oliva, J.M.; Kubát, P.; Polívka T.; Lang, K. *Inorg. Chem.*, **2012**, *51*, 1471-1479.

13. Cerdán, L.; Braborec, J.; Garcia-Moreno, I.; Costela, A.; Londesborough, M.G.S. *Nature Commun.* **2015**, *6*, 5958.

14. (a) Londesborough, M. G. S.; Dolanský, J.; Bould, J.; Braborec, J.; Kirakci, K.; Lang, K.; Císařová, I.; Kubát, P.; Roca-Sanjuán, D.; Francés-Monerris, A.; Slušná, L.; Noskovičová, E.; Lorenc, D. *Inorg. Chem.* **2019**, *58*, 10248-10259. (b) Londesborough, M. G. S.; Dolanský, J.; Jelínek, T.; Kennedy, J.D.; Císařová, I.; Kennedy, R.D.; Roca-Sanjuán, D.; Francés-Monerris, A.; Lang. K.; Clegg, W. *Dalton Trans.* **2018**, *47*, 1709-1725. (c) Saurí, V.; Oliva, J.M.;0 Hnyk, D.; Bould, J.; Braborec, J.; Merchán, M.; Kubát, P.; Císařová, I.; Lang, K.; Londesborough, M.G.S. *Inorg. Chem.* **2013**, *52*, 9266-9274.

15. Hamilton, E. J. M.; Kultyshev, R.G.; Du, B.; Meyers, E.A.; Liu, S.; Hadad, C.M.; Shore, S.G. *Eur. J. Chem.*, **2006**, *12*, 2571.

Chapter 1 – Improved synthesis of icosahedral carboranes containing exopolyhedral C-C bonds

1.1 Abstract

Carboranes are boron-rich molecular clusters possessing electronic characteristics that allow for orthogonal approaches to vertex-selective modifications. We report improved functionalization methods utilizing orthogonal chemistry to achieve efficient substitution at electron-poor C-vertices of carborane. This transition metal-free approach to the substitution of carborane with (hetero)aryl substrates has been developed under nucleophilic aromatic substitution (S_NAr) conditions. The selective substitution of carboranes afforded by this reaction holds potential for the rational synthesis of heterofunctionalized boron clusters with substituents on both boron and carbon-based vertices.

1.2 Introduction

Since the discovery of neutral carboranes ($C_2B_{10}H_{12}$) more than 50 years ago, these icosahedral clusters have emerged as diverse building blocks for a variety of applications, including organic light emitting diodes,[1] biomedicine,[2] batteries,[3] catalysis[4], self-assembled materials[5] and medicinal drug design.[6] These compounds, which exist as three constitutional isomers (*ortho, meta,* and *para*) depending on relative positions of the two C-H vertices on the cage, feature several unique properties, such as three dimensional aromaticity, a large HOMO-LUMO gap, tunable dipole

moments as a function of cluster symmetry, and thermal stability.[7] The diversity of carborane applications, however, requires synthetic methods that can provide access to vertex-selective modification. Under basic conditions the acidic protons bound to the carbon vertices can undergo facile deprotonation and subsequent selective functionalization with electrophiles.[8] Nevertheless, current synthetic methods are still limited in their ability to achieve efficient substitution of carboranes. For example, current C-vertex substitution methods can install (hetero)aryl groups but often require the use of transition metal reagents (Figure 1.1).[8a-c] To improve on these procedures, we report a transition metal-free C-vertex substitution of (hetero)aryl substrates. Importantly, this can be performed on existing B-functionalized carboranes, producing a convenient and straightforward strategy to form B- and C-substituted clusters.

1.3 C-Vertex Substitution

C-vertex substitution methods are perceived as more straightforward than the B-vertex
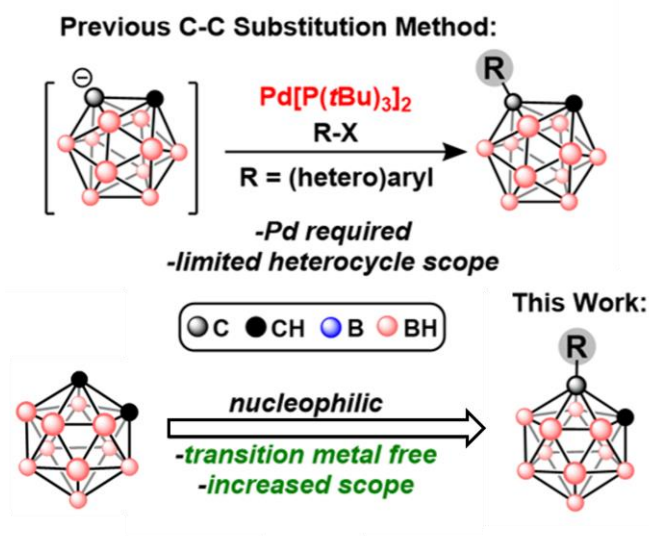
Figure 1.1: Previous substitution method for C-(hetero)arylation and this work.

functionalization: due to the acidic nature of the C–H bond, C-vertices can be deprotonated and
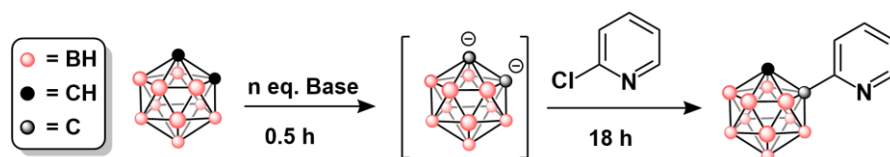
treated with electrophiles or used as nucleophiles.[8] While the metalation of carboranes and subsequent reactivity towards alkyl halides has produced a library of C-alkyl carboranes,[7] C-vertex (hetero)arylation has been achieved through less straightforward procedures, such as metal-catalyzed cross-coupling that requires either stoichiometric or catalytic amounts of transition-metal reagents.[8] For example, Cu-mediated coupling with (hetero)aryl iodides or bromides can yield C-pyridyl- and C-aryl-carboranes, but requires 25-90 h reaction times and can tolerate only a select group of functionalized (hetero)aryl substrates.[8b] More recent methods, such as Ni- and Pd-catalyzed cross coupling, demonstrate improved functional group tolerance for C-arylation, but are limited to attaching chloro- and methyl-pyridine.[8a,c] Transition metal-free C-substitution methods have been investigated, but require the reaction between a C-monosubstituted *ortho*-carborane (oCB) and a fluoroarene possessing a strong electron withdrawing group.[11] This selectively produces 1,2-diaryl-*ortho*-carboranes, but this methodology was not applied to heterocyclic substrates. Overall, procedures for C-(hetero)arylation are currently limited by their use of transition metal reagents and small substrate scopes. Previous reports have demonstrated the possibility of C-vertex substitution under S_NAr conditions,[1a,9,10] prompting us to expand the number and type of substrates that can be appended to carborane using this approach.

For the initial optimization studies we tested 2-chloropyridine, estimating that it would be less reactive than fluoroheterocycles and more reactive than fluoroarenes. Typically, C–H deprotonation and successive metalation of carborane have been achieved with *n*BuLi in either diethyl ether or THF.[7] Nevertheless, we found that *n*BuLi was unable to facilitate the heteroarylation of carborane to 1-(2-pyridyl)-*ortho*-carborane (2A) under these conditions (Table 1.1, Entry 1). We previously observed that KHMDS deprotonates 1,1'-bis-(*ortho*-carborane),[11] indicating that it could potentially be applicable to our system. While 2 and 1 equivalents of

5

KHMDS yielded sub-quantitative conversions (Entries 2 and 3, respectively), 3 equivalents of this base led to 99% conversion of oCB to product (Entry 4). Testing the effect of the disilazide counterion on the reaction, we observed 45% and 90% conversion with LiHMDS and NaHMDS, respectively (Entries 5 and 6), suggesting the cation significantly influences the reaction progression. High conversion efficiency with KHMDS led us to continue its use throughout the optimization studies. Next, we examined the effect of other ethereal solvents on the reaction progress. With conversions ranging from 86%-98% (Entries 7-9), we selected THF as our primary solvent.

Under the optimized conditions, 2A (Figure 1.2A) can be isolated in 61% yield after purification *via* silica gel column chromatography. This method tolerates bipyridine-based electrophiles, producing compounds 2B and 2C in 43% and 73% isolated yields, respectively. These bipyridine-based compounds would be difficult to synthesize using metal-catalyzed cross-coupling methods. The ability to generate 2C suggests that multiple C–C bond forming processes can be achieved at the electrophile under these conditions. Testing this method with (hetero)aryl fluorides resulted in

Entry #	Base	Base eq.	Solvent	% Conv.
1	^{n}BuLi	2	THF	0
2	KHMDS	2	THF	92
3	KHMDS	1	THF	80
4	KHMDS	3	THF	99
5	LiHMDS	3	THF	45
6	NaHMDS	3	THF	90
7	KHMDS	3	MTBE[a]	86
8	KHMDS	3	Ether [b]	90
9	KHMDS	3	DME [c]	98

Table 1.1: Optimization table of S_NAr reaction between 2-chloropyridine and *ortho*-carborane. % Conv. indicates the % of 1-(2-pyridine)-oCB present in the crude reaction mixture as determined by GC-MS. a Methyl-tert-butyl ether [b]Diethyl ether [c]1,2-Dimetheoxyethane

the desired product formation under the optimized conditions (Figure 1.2, 2D-I see SI for experimental details). The lower room temperature reactivity of substrates originating from products 2D and 2E was circumvented by heating the reaction mixture to 80°C. This initially afforded 2E in 27% yield, and analysis of the ^{11}B NMR data suggested the presence of deboronated products, which is consistent with previous reports of deboronation of oCB in the presence
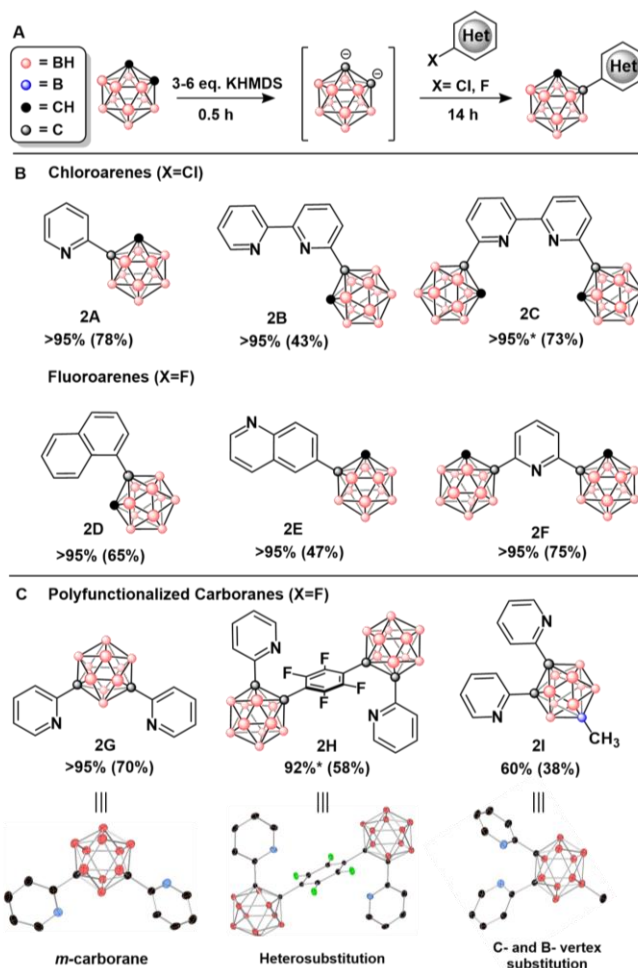
Figure 1.2: A) C-functionalization reaction scheme B) Products with GC-MS conversions and isolated yields in parentheses. C) Polyfunctionalized carboranes with associated single crystal X-ray structures obtained by extrapolating the general method in A. (*) indicates that conversion was determined through ^{1}H NMR instead of GC-MS. See Table S4 in SI for exact reaction conditions. [a]See SI for corresponding single crystal X-ray structures.

7

fluoride.[12] To sequester fluoride ions and potentially prevent cage degradation, we used one equivalent of isopropoxytrimethylsilane under otherwise identical conditions, which increased the isolated yield of 2E to 44%. Similar observations were made with the 2,6-difluoropyridine substrate, but the yield remained nearly identical even with the addition of the fluoride scavenger. However, upon changing the solvent from THF to diethyl ether, the isolated yield for 2F increased to 75%. We attribute this observation to the likely lower solubility of the KF byproduct in diethyl ether, thereby decreasing its reactivity towards deboronation. The present S_NAr method also proceeds with *meta*-carborane under similar conditions, as exemplified by the formation of 2G (Figure 1.2C). We also assessed the viability of conducting sequential C-vertex heterosubstitutions. Deprotonation of 2A and subsequent treatment with perfluorobenzene selectively produced the para-substituted product 2H in 29% isolated yield. Upon further optimization, we found that excess perfluorobenzene resulted in higher conversion to desired product. The best results were achieved with DME and 2 equivalents of KHMDS, resulting in 74% isolated product yield. Similar carborane-substituted phenylene molecules have been investigated for their luminescent properties, but are typically synthesized *via* cross coupling procedures that require multiple reagents such as CuI and $Pd(PPh_3)_2Cl_2$.[13] Overall, we demonstrate that S_NAr methodology can be applied to both chloro- and fluoro(hetero)aryl substrates, however, in the latter case a competing reactivity of the fluoride byproduct needs to be mitigated by the judicious use of the additional reagents and solvents.

Lastly, the described method for forming C–C bonds in carboranes prompted us to explore whether this can be used on B-functionalized carboranes. Treatment of 9-methyl-carborane with excess 2-fluoropyridine produced product 2I, demonstrating that both B- and C- vertex functionalization methods can be used in a sequential manner. This compound was isolated in 38% yield. Single

crystals of 2I were grown with hexanes and analyzed using X-ray crystallography, ultimately confirming its structural assignment (Figure 1.2C).

1.4 Conclusion

We have developed an improved C-vertex functionalization method that can effectively afford previously inaccessible carborane derivatives. Specifically, we have expanded the scope of C-vertex substitution while circumventing the requirement for transition metal-catalyzed cross-coupling. By utilizing the nucleophilic nature of the C-metalated carboranes, mild conditions can be used to achieve substitutions of heterocycles on carboranes. This represents a robust addition of transformations now available to the practitioners in boron cluster chemistry.

1.5 References

1. (a) Axtell, J. C.; Kirlikovali, K. O.; Djurovich, P. I.; Jung, D.; Nguyen, V. T.; Munekiyo, B.; Royappa, A. T.; Rheingold, A. L.; Spokoyny, A. M. *J. Am. Chem. Soc.* **2016,** *138* (48), 15758; (b) Prokhorov, A. M.; Hofbeck, T.; Czerwieniec, R.; Suleymanova, A. F.; Kozhevnikov, D. N.; Yersin, H. *J. Am. Chem. Soc.* **2014,** *136* (27), 9637.

2. (a) Paxton, R. J.; Beatty, B. G.; Hawthorne, M. F.; Varadarajan, A.; Williams, L. E.; Curtis, F. L.; Knobler, C. B.; Beatty, J. D.; Shively, J. E. *Pro. Natl. Acad. Sci.* **1991,** *88* (8), 3387; (b) Hawthorne, M. F.; Maderna, A. *Chem. Rev.* **1999,** *99* (12), 3421; (c) Neirynck, P.; Schimer, J.; Jonkheijm, P.; Milroy, L. G.; Cigler, P.; Brunsveld, L. *J. Mater. Chem. B* **2015,** *3* (4), 539.

3. McArthur, S. G.; Geng, L.; Guo, J.; Lavallo, V. *Inorg. Chem. Front.* **2015,** *2* (12), 1101.

4. Selg, C.; Neumann, W.; Lönnecke, P.; Hey-Hawkins, E.; Zeitler, K. *Chem. Eur. J.* **2017,** *23* (13), 7932.

5. (a) Farha, O. K.; Spokoyny, A. M.; Mulfort, K. L.; Hawthorne, M. F.; Mirkin, C. A.; Hupp, J. T. *J. Am. Chem. Soc.* **2007,** *129* (42), 12680; (b) Serino, A. C.; Anderson, M. E.; Saleh, L. M. A.; Dziedzic, R. M.; Mills, H.; Heindreich, L. K.; Spokoyny, A. M.; Weiss, P. S. *ACS Appl. Mater. Interfaces* **2017**, 9, 40, 34592; (c) Kim, J.; Rim, Y. S.; Liu, Y.; Serino, A. C.; Thomas, J. C.; Chen, H.; Yang, Y.; Weiss, P. S. *Nano Lett.* **2014**, *14* (5), 2946; (d) Spokoyny, A.M.; Farha, O.K.; Mulfort, K.L.; Hupp, J.T.; Mirkin, C.A. *Inorg. Chim. Acta.* **2010**, *364* (1), 266.

6. (a) Issa, F.; Kassiou, M.; Rendina, L. M. *Chem. Rev.* **2011,** *111* (9), 5701; (b) Leśnikowski, Z.J. *J. Med. Chem.* **2016**, *59* (17), 7738; (c) Adamska, A.; Rumijowska,-Galewicz, A.; Ruszczynska, A.; Studzińska, M.; Jablońska, A.; Paradowska, E.; Bulska, E.; Munier-Lehman, H.; Dziadek, J.; Leśnikowski, Z.J.; Olejniczak, A.B. *Eur. J. Med. Chem.* **2016**, *121* (4), 71.

7. R. N. Grimes, Carboranes, 3rd edn, Elsevier, Oxford, 2016.

8. For a general overview of C-vertex substitution: (a) Lu, J.-Y.; Wan, H.; Zhang, J.; Wang, Z.; Li, Y.; Du, Y.; Li, C.; Liu, Z.-T.; Liu, Z.-W.; Lu, J. *Chem. Eur. J.* **2016,** *22* (49), 17542; (b) Coult, R.; Fox, M. A.; Gill, W. R.; Herbertson, P. L.; MacBride, J. A. H.; Wade, K. *J. Organomet. Chem.* **1993**, *462* (1), 19; (c) Tang, C.; Xie, Z. *Angew. Chem. Int. Ed.* **2015**, *54* (26), 7662; (d) Chan, A.L.; Estrada, J.; Kefalidis, C.E.; Lavallo, V. *Organometallics* **2016**, *35* (19), 3257; (e) Cabrera-González, J.; Viñas, C.; Haukka, M.; Bhattacharyya, S.; Gierschner, J.; Núñez, R. *Chem. Eur. J.* **2016**, *22* (38), 13588; (f) Powley, S.L.; Schaefer, L.; Man, W.Y.; Ellis, D.; Rosair, G.M.; Welch, A.J. *Dalton Trans.* **2016**, *45*, 3635.

9. Ohta, K.; Goto, T.; Endo, Y. *Tetrahedron Lett.* **2005**, *46* (3), 483.

10. (a) Henly, T.J.; Knobler, C.B.; Hawthorne, M.F. *Organometallics* **1992**, *11*, 2313; (b) Islam, M.J.; Smith, M.D.; Peryshkov, D.V. *J. Organomet. Chem.* **2018,** *867*, 208.

11. Kirlikovali, K. O.; Axtell, J. C.; Anderson, K.; Djurovich, P. I.; Rheingold, A. L.; Spokoyny, A. M. *Organometallics* **2018**, *37* (18), 3122.

12. (a) Getman, T.D. *Inorg. Chem.* **1998**, 37, 3422-3423; (b) Fox, M.A.; MacBride, J.A.H.; Wade, K. *Polyhedron* **1996**, *16* (14), 2499; (c) Yoo, J.; Hwang, J.-W.; Do, Y. *Inorg. Chem.* 2001, *40* (3), 568.

13. Bae, H. J.; Kim, H.; Lee, K. M.; Kim, T.; Lee, Y. S.; Do, Y.; Lee, M. H. *Dalton Trans.* **2014**, *43* (13), 4978.

Chapter 2 – A molecular boron cluster-based chromophore with dual emission

This chapter is a version of K. P. Anderson, M. A. Waddington, G. J. Balaich, J. M. Stauber, N. A. Bernier, J. R. Caram, P. I. Djurovich and A. M. Spokoyny. A molecular boron cluster-based chromophore with dual emission. *Dalton Trans.* **2020**, *49*, 16245-16251. Supplementary information can be found free of charge at DOI: 10.1039/d0dt00826e

2.1 Abstract

Bromination of the luminescent borane, *anti*-$B_{18}H_{22}$, via electrophilic substitution using $AlCl_3$ and Br_2, yields the monosubstituted derivative 4-Br-*anti*-$B_{18}H_{21}$ as an air-stable crystalline solid. In contrast to the unsubstituted parent compound, 4-Br-*anti*-$B_{18}H_{21}$ possesses dual emission upon excitation with UV light and exhibits fluorescence at 410 nm and phosphorescence at 503 nm, with $\Phi_{total} = 0.07$ in oxygen-free cyclohexane. Increased oxygen content in cyclohexane solution quenches the phosphorescence signal. The fluorescent signal intensity remains unaffected by oxygen, suggesting that this molecule could be used as a ratiometric oxygen probe.

2.2 Introduction

Boron-containing luminescent molecules have been widely known and researched over decades for a variety of applications, including intracellular imaging,[1] sensors,[2] organic light emitting diodes[3] photovoltaics,[4] and lasers.[5] While the properties of molecules such as triarylboranes and borate-based dyes have received considerable attention, research into luminescent boron-rich hydride-based materials remains an underexplored field in which *closo*-dicarbadodecaboranes, also known as carboranes, have remained a central focus. This research has successfully developed emissive materials that incorporate carboranyl groups as components in metal complexes or luminescent polymers and oligomers.[3c, 6] However, due to the large band gap of carboranes (~8

eV), substitution onto the icosahedral cage is usually required for the molecule to participate in visible light transitions.[7] Consequently, a significant amount of work has focused on carborane functionalization methods.[8] In fact, only one known polyhedral borane to date, *anti*-$B_{18}H_{22}$, possesses inherent luminescence. This unique cluster best resembles two *nido*-$B_{10}H_{14}$ molecules fused at two vertices, forming an 18-vertex borane (Figure 2.1). Of the two known isomers of $B_{18}H_{22}$, *anti*-$B_{18}H_{22}$ and *syn*-$B_{18}H_{22}$, only the former is luminescent, featuring intense blue fluorescence at 407 nm when irradiated at 340 nm with a high quantum yield ($\Phi_{fluor} = 0.97$).[9] Despite its discovery in 1962,[10] detailed analyses of luminescence from *anti*-$B_{18}H_{22}$ have only recently been described,[9,11] which found that both the HOMO and LUMO are distributed evenly across the boron cage. The absorbed energy in the S_1 state is redistributed throughout the σ bonding framework resulting in a prolonged S_1 lifetime and, consequently, fluorescence.[9,11] Since then, however, only a handful of synthetic derivatives of *anti*-$B_{18}H_{22}$ have been reported (Figure 2.1),[12] and a comprehensive synthetic foundation for this fascinating boron cluster system has yet to be established. From the existing reports it is clear that functionalization of the cluster dramatically alters its emissive properties.[10] For example, thiolation of the cluster gives 4,4'-$(HS)_2$-*anti*-$B_{18}H_{20}$,
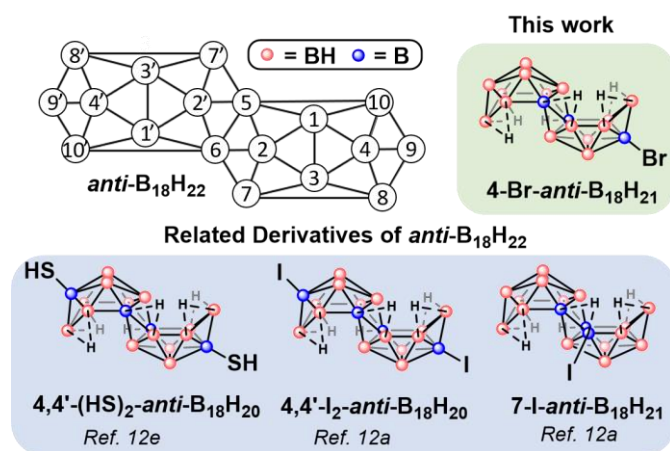
Figure 2.1: Top) Two-dimensional projection of *anti*-$B_{18}H_{22}$ and the brominated derivative discussed in this work. Bottom) Representations of select previously reported derivatives of *anti*-$B_{18}H_{22}$.

which displays red-shifted luminescence with fluorescent emission at 536 nm and phosphorescent emission at 597 nm.[12e] Reaction with pyridine yields a rearranged boron cage derivative, $B_{18}H_{20}(NC_5H_5)_2$, that exhibits thermochromic luminescence ranging from 585 nm (8 K) to 620 nm (300 K), which is caused by the constraint of the pyridine substituents at lower temperatures.[13] Most recently, the iodination of this cluster was reported, which described the green phosphorescence of both 7-I-*anti*-$B_{18}H_{21}$ and 4,4'-I_2-*anti*-$B_{18}H_{20}$ at 525 nm and 545 nm, respectively.[12a] Still, the relationship between $B_{18}H_{22}$ cluster structure and resulting photophysical properties has yet to be elucidated. It is therefore of great interest to explore functionalization methods and investigate the effect that such changes have on the photoluminescence profile. Following the first account of halogenated *anti*-$B_{18}H_{22}$, we were interested in how other halogens affect the luminescent properties of this cluster. Herein we report a synthesis for the first brominated derivative of *anti*-$B_{18}H_{22}$, 4-Br-*anti*-$B_{18}H_{21}$, and its unique photophysical characteristics distinctively different from the other halogenated analogues.

2.3 Results and Discussion

Synthesis and Structural Characterization of 4-Br-*anti*-$B_{18}H_{21}$

Following conventional electrophilic bromination protocols used previously with other polyhedral boron clusters,[14] we treated *anti*-$B_{18}H_{22}$ with Br_2 (1 equiv) and $AlCl_3$ (15 mol%) in dichloromethane under an N_2 atmosphere at room temperature. Formation of the monobrominated cluster was observed after several hours, as suggested by an *in situ* mass spectrometry assay of the reaction mixture, although a significant amount of unreacted *anti*-$B_{18}H_{22}$ was still present after 18 hours. Increasing the amount of $AlCl_3$ (20 mol%) resulted in higher conversion to $B_{18}H_{21}Br$ with concomitant formation of the dihalogenated species, $B_{18}H_{20}Br_2$. Attempts to separate these two products were successful, but resulted in poor recovered yield of $B_{18}H_{21}Br$. Consequently, the

procedure was further modified to improve the conversion to $B_{18}H_{21}Br$, which required fewer than 1 equiv of Br_2. These optimized conditions (15 mol% $AlCl_3$ and 0.70 equiv Br_2 in DCM) afforded a reaction mixture containing $B_{18}H_{22}$, $B_{18}H_{20}Br_2$, and $B_{18}H_{21}Br$ as major products as judged by *in situ* mass spectrometry analysis. Subsequently, $B_{18}H_{21}Br$ was purified from the crude mixture obtained from this reaction via high performance liquid chromatography (HPLC) using methanol/water mixture as an eluent on C-18 modified silica stationary phase,[15] giving a 22% yield. While the isolated material appeared pure by ^{11}B NMR spectroscopy, an impurity comprising ca. 5% of the bulk material was indicated by LC-MS analysis. Consequently, further purification via HPLC was required to obtain >99% pure $B_{18}H_{21}Br$ as determined by LC-MS (see Figure S6, Table S1). The yield after the second purification was 8%. This product is stable when stored as a solid at 5°C.

Single crystal X-ray diffraction analysis was used to determine the structure of 4-Br-*anti*-$B_{18}H_{21}$. Single, X-ray quality colorless crystals of 4-Br-*anti*-$B_{18}H_{21}$ were grown by dissolution of the >95% pure compound in benzene followed by storage of the resulting solution at 5 °C (see SI). The resulting crystal structure indicated the possibility of co-crystallized impurities, $B_{18}H_{20}Br_2$ and
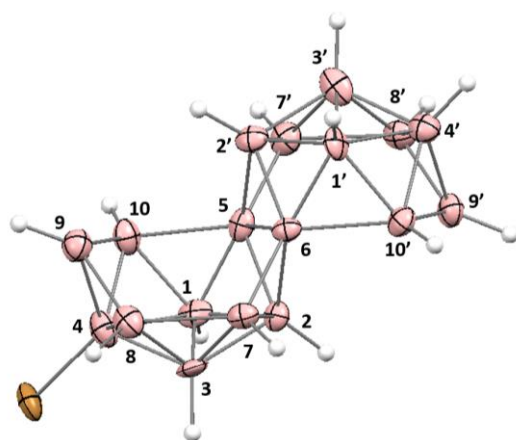
Figure 2.2: Single crystal X-ray structure of 4-Br-*anti*-$B_{18}H_{21}$•($2C_6H_6$) with labeled boron vertices. For clarity, the bridging hydrides, benzene solvent molecules are not shown. Displacement ellipsoids are drawn at a 50% probability level.

15

$B_{18}H_{21}Cl$. The solid-state structure of 4-Br-*anti*-$B_{18}H_{21}$ (Figure 2.2) indicates that the boron atom connectivity in the cluster remains the same compared to the parent molecule, and that the bromine atom is located on the 4 position of the octadecaborane cage. Prior analyses of *anti*-$B_{18}H_{22}$[12a, 16] revealed that the 4 and 4' boron vertices are the most electron rich and therefore the most likely to undergo electrophilic substitution. Indeed, the doubly iodinated cluster, synthesized with I_2 and $AlCl_3$, is substituted at the 4 and 4' boron vertices.[12a] Therefore, electrophilic substitution of bromide at these locations is expected under the given experimental conditions. Even so, it is worthy to note that bromide substitution on vertices other than 4 and 4' was not indicated by other analytical methods including ^{11}B NMR spectroscopy. The selectivity of electrophilic substitution may consequently be a helpful synthetic tool in the exploration of *anti*-$B_{18}H_{22}$ chemistry.

Photophysical Properties

The absorption spectra of 4-Br-*anti*-$B_{18}H_{21}$ and *anti*-$B_{18}H_{22}$ are shown in Figure 2.3. Both compounds display transitions in the ultraviolet (UV) region with only minor changes in energy found for the lowest absorption bands in 4-Br-*anti*-$B_{18}H_{21}Br$ (λ_{max} = 300 nm and 343 nm) compared to *anti*-$B_{18}H_{22}$, (λ_{max} = 283 nm and 332 nm). However, the molar absorptivity of 4-Br-*anti*-$B_{18}H_{21}$ (ε_{342} = 1900 $M^{-1}cm^{-1}$) is significantly lower than that of *anti*-$B_{18}H_{22}$ (ε_{332} = 6800 $M^{-1}cm^{-1}$).

Upon exposure to UV light, 4-Br-*anti*-$B_{18}H_{21}$ exhibits luminescence that is blue-green in a mixture of isomeric hexanes solution at room temperature and green when the solution is cooled to 77 K. Likewise, this green luminescence is present in the solid state (Figure 2.3, inset). Since *anti*-$B_{18}H_{22}$ is brightly fluorescent, we hypothesized that the bromide functionalized cluster would display some phosphorescent character due to the heavy atom effect.[17] The attached bromine would presumably enhance spin-orbit coupling (SOC) and improve spin-forbidden intersystem crossing

(ISC) between singlet and triplet states that are close in energy. This permits the population of triplet states that may undergo radiative decay to produce phosphorescence. Intersystem crossing as it relates to SOC and the singlet-triplet energy gap is described by the equation

$$k_{ISC} \sim \frac{|\langle \Psi_{S1} | \mathcal{H}_{SO} | \Psi_{T1} \rangle|^2}{(\Delta E_{S1-T1})^2}$$

where $|\langle \Psi_{S1} | \mathcal{H}_{SO} | \Psi_{T1} \rangle|$ represents spin-orbit coupling and ΔE_{S1-T1} is the difference between the energies of the S_1 and T_1 states. Consequently, a smaller energy difference between the singlet and triplet states results in a large SOC value and more efficient intersystem crossing. To probe the possibility of phosphorescence, photophysical data of 4-Br-*anti*-$B_{18}H_{21}$ were first obtained under ambient conditions in cyclohexane. While the absorption spectra of *anti*-$B_{18}H_{22}$ and *anti*-$B_{18}H_{21}Br$ displayed in Figure 2.3 reveal slight differences in their λ_{max} values, the emission spectra exhibit
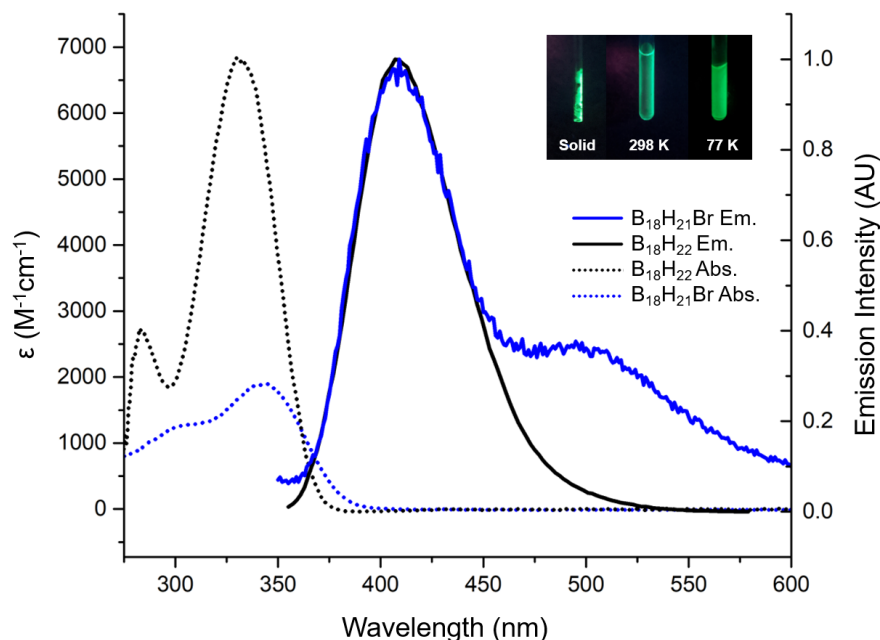
Figure 2.3: Absorption (dotted) and emission (solid) spectra of 4-Br-*anti*-$B_{18}H_{21}$ (blue) and *anti*-$B_{18}H_{22}$ (black). The wavelengths of excitation are 350 nm and 340 nm, respectively. All measurements were conducted in cyclohexane solution. Inset: Luminescence of 4-Br-*anti*-$B_{18}H_{21}$ in the solid state at 298 K and in hexanes at 298 K and 77 K.

17

more pronounced differences, with the brominated cluster displaying a shoulder at 503 nm. The variability in emission color, illustrated in Figure 2.3, prompted us to conduct more photoluminescence studies under various conditions. We suspected that the 503 nm shoulder observed could be phosphorescent in nature, but because room temperature phosphorescence is often difficult to observe the emission data were gathered at 77K. Under these conditions, bimolecular and diffusional quenching processes are minimized and molecular motions are restricted due to the molecule existing within a solid glass matrix.[18] With these pathways diminished, any occurring phosphorescence is likely to be detected. Indeed, at 77K the 503 nm peak is intense, nearly obscuring the 410 nm signal (Figure 2.4). To investigate the possibility of oxygen-quenched phosphorescence, the photophysical data in degassed (O_2-free) cyclohexane were gathered at 298 K. The emission spectrum shows the 410 nm peak and a considerably more
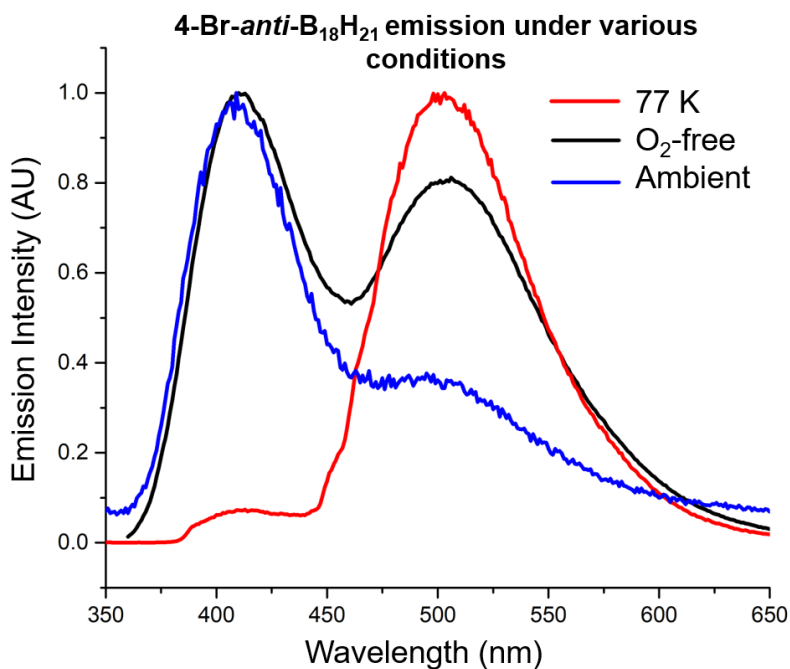
Figure 2.4: Emission spectra of 4-Br-*anti*-$B_{18}H_{21}$ in cyclohexane at 298 K under ambient conditions (blue), at 298 K in O_2-free cyclohexane (black), and at 77 K in methylcyclohexane (red). The wavelengths of excitation are 330 nm, 350 nm, and 340 nm, respectively.

18

intense 503 nm signal (Figure 2.4), indicating that oxygen is at least partially responsible for the low peak intensity initially observed.

The quantum yield (Φ) data, summarized in Table 2.1, also supports this hypothesis. Both cyclohexane solutions and PMMA films of 4-Br-*anti*-$B_{18}H_{21}$ possess smaller quantum yields when exposed to oxygen. The quantum yield of 4-Br-*anti*-$B_{18}H_{21}$ in cyclohexane under ambient conditions is 0.05, which increases to 0.07 when the measurement is conducted in oxygen-free solution. These low values are surprising considering that both iodinated clusters possess QY values no less than 0.41 in oxygen-free solution.[12a] The contribution to QY from fluorescence and phosphorescence (Φ_{fluor} and Φ_{phos}) was also determined (see Figures S9 and S10). Under ambient conditions in cyclohexane, both $\Phi_{fluor-amb}$ and $\Phi_{phos-amb}$ are 0.025, while in oxygen-free solution $\Phi_{fluor} = 0.024$ and $\Phi_{phos} = 0.046$. Because the fluorescence quantum yield remains the same within error for both conditions, the decrease in quantum yield from 0.07 to 0.05 is most likely due to oxygen-quenched phosphorescence. The quantum yield of a 4-Br-*anti*-$B_{18}H_{21}$ PMMA film was also assessed, increasing from <0.01 to 0.08 when under N_2, which is similar with the low values of the solid-state iodinated clusters (0.06 for 7-I-*anti*-$B_{18}H_{21}$ and 0.11 for 4,4'-I_2-*anti*-$B_{18}H_{20}$).[12a]

4-Br-*anti*-$B_{18}H_{21}$Br	emission λ_{max}	$\Phi_{ambient}$	$\Phi_{O2-free}$	τ (ns)	k_r 10^6 (s^{-1})	k_{nr} 10^6 (s^{-1})
Cyclohexane O_2-free[a]	503		0.07[a]	11600[e]	0.0040[h]	0.082[h]
	410	-	0.024/0.046[d]	10.3[fe]	2.3[i]	95[i]
Cyclohexane[b]	410	0.05[b]	-	10.6[f]	2.3[g]	92[g]
		0.025/0.025[d]				
Methylcyclohexane[c]	503			552000[e]	-	-
	407	-	-	9.8[f]	-	-

Table 2.1: Summary of photophysical properties of 4-Br-*anti*-$B_{18}H_{21}$. [a]Collected at 298 K under N_2 atmosphere. [b]Collected at 298 K under ambient conditions. [c]Collected at 77 K. [d]Quantum efficiency of fluorescence (φ_{fluor})/Quantum efficiency of phosphorescence (φ_{phos}), calculated by multiplying peak percent by the quantum yield of the cyclohexane solution under ambient or O_2-free conditions (Figures S9 and S10). [e]Obtained by exciting at 372 nm and observing at 525 nm. [f]Obtained by exciting at 331 nm and observing at 410 nm. Error in the excited state lifetime measurement is ±14% and ±10%, respectively. [g,h,i]Calculated according to the equations $k_r = \varphi/\tau$ and $k_{nr} = (1 - \varphi)/\tau$, where k_r is the radiative rate constant, k_{nr} is the nonradiative rate constant, φ is the quantum efficiency under ambient conditions ($\varphi_{ambient}$),[g] of φ_{phos} under N_2,[h] or φ_{fluor} under N_2,[i] and τ is the excited state lifetime.

Because diffusion of oxygen at room temperature in PMMA is significantly slower than in cyclohexane, the system was allowed to equilibrate under the flow of O_2 for over 30 minutes (see Figure S8).[19] Finally, the fluorescent and phosphorescent nature of these peaks were further explored through lifetime (τ) decay experiments. For a cyclohexane solution of 4-Br-*anti*-$B_{18}H_{21}$, the 410 nm peak lifetime is 10.6 ns under ambient conditions (Table 2.1, Figure S11), compared to that of the parent borane (11.2 ns).[9] This value remains consistent under oxygen-free atmosphere ($\tau = 10.3$ ns) and decreases slightly at 77 K ($\tau = 9.8$ ns). The lifetime decay data was also gathered for the 503 nm peak, revealing a lifetime of 11.6 µs in oxygen-free cyclohexane at 298 K. At 77 K, the lifetime is extended dramatically ($\tau = 552$ µs) (Table 2.1, Figure S11), which further supports the photoluminescence data in Figure 3.4. The photoluminescence, quantum yield, and lifetime data for 4-Br-*anti*-$B_{18}H_{21}$ under the conditions studied are summarized in Table 2.1. This data can be further contextualized through a comparison to the other reported monohalogenated derivative, 7-I-*anti*-$B_{18}H_{21}$.[12a] The iodinated cluster contains only a single emission peak that is attributed to phosphorescence, which is probably due to the increased singlet and triplet state overlap that results from the heavy iodine atom.[12a, 20] The monobrominated cluster displays attenuated ISC in comparison, achieving a balance between singlet and triplet states that permits dual fluorescent/phosphorescent emission.

The simultaneous fluorescence and oxygen-sensitive phosphorescence demonstrated by 4-Br-*anti*-$B_{18}H_{21}$ is a property not commonly observed by small molecule metal-free emitters.[20] Although dual emission was reported for thiolated *anti*-$B_{18}H_{22}$, the two luminescence bands in this molecule overlap significantly, obscuring small changes in the oxygen-sensitive phosphorescence signal.[10e] In contrast, the energy difference between the two emission events for 4-Br-*anti*-$B_{18}H_{21}$ is large enough that the fluctuating intensity of the phosphorescence peak is easily observed. These

combined characteristics make the 4-Br-*anti*-B$_{18}$H$_{21}$ chromophore potentially useful for oxygen sensing. Emissive oxygen sensors have been intensely studied due to their wide applicability in biological imaging.[21] Although oxygen can be detected and measured based on a single emission signal, a ratiometric probe based on dual-emissivity is more reliable due to the presence of a reference signal. Many dual-emitting sensors are nanoparticle or heavy-metal based, or require the combination of two different luminophores (one fluorescent, the other phosphorescent).[20] This is due to the difficulty involved in rationally designing a single dual-emitting small molecule with the appropriate balance of populated singlet and triplet states that would give rise to dual emission. This phenomenon is especially difficult to achieve with entirely organic systems, and most dual-emissive organic small molecules are based on polycyclic aromatic molecules such as pyrene[22] or naphthalene.[23] However, each of these methods are accompanied by a host of disadvantages, such as unequal stability between mixed dyes, weak phosphorescence, photobleaching, and bio-incompatibility. The ideal ratiometric oxygen probe exhibits intense oxygen-sensitive phosphorescence, long lifetime, resistance to photobleaching, and stability.[20] To assess the applicability of 4-Br-*anti*-B$_{18}$H$_{21}$ as a small molecule oxygen sensor, preliminary sensing studies were conducted. Mixtures of nitrogen and oxygen gas containing varying amounts of oxygen were bubbled through a cyclohexane solution of 4-Br-*anti*-B$_{18}$H$_{21}$ before measurements were conducted (see Table S4). As shown in Figure 2.5, phosphorescence decreases significantly with increasing oxygen content while the fluorescence peak maintains its intensity. This system functions as a ratiometric probe through comparison of the reference signal (the oxygen-insensitive fluorescence peak) to the intensity of the oxygen-quenchable phosphorescence peak. The intermolecular, collisional quenching process by oxygen follows Stern-Volmer kinetics (see inset of Figure 2.5). Using a previously reported value for the solubility of oxygen in cyclohexane[24] and the Stern-

Emission under varying oxygen concentrations
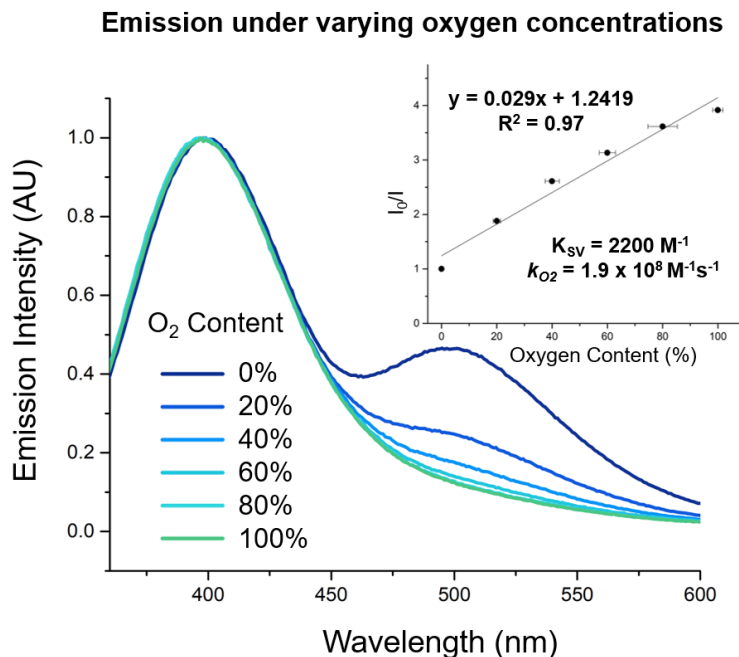
Figure 2.5: Emission spectra of 4-Br-*anti*-$B_{18}H_{21}$ in cyclohexane degassed with N_2 and O_2 gas mixtures containing varying amounts of oxygen. The wavelength of excitation was 320 nm. Inset) Stern-Volmer plot of phosphorescence quenching of the 503 nm peak. The quenching constant K_{SV} and bimolecular rate constant of T_1 state quenching k_q were calculated using 0.00116 mole fraction atm^{-1} as the solubility of O_2 in cyclohexane[24] and the Stern-Volmer equation: $I^0/I = 1+K_{SV}[O_2]$, $K_{SV} = k_{O2}\tau_0$.

Volmer relationship, the Stern-Volmer quenching constant was calculated, $K_{SV} = 2200$ M^{-1} along with the bimolecular rate quenching constant, $k_{O2} = 1.9$ x 10^8 M^{-1}s^{-1}. The latter value can be directly compared to the quenching rate of 7-I-*anti*-$B_{18}H_{21}$ (4.1 x 10^7 M^{-1}s^{-1}) and 4,4'-I_2-*anti*-$B_{18}H_{20}$ (6.8 x 10^7 M^{-1}s^{-1}).[12a] It is evident that oxygen quenching occurs an order of magnitude faster in the brominated borane than its iodinated counterparts. Finally, the electrochemical properties of both *anti*-$B_{18}H_{22}$ and 4-Br-*anti*-$B_{18}H_{21}$ were assessed through cyclic voltammetry (see Figure S12). Both compounds exhibit an irreversible reduction, with a potential that shifts cathodically from -1.36 V (*anti*-$B_{18}H_{22}$) to -1.18 V (4-Br-*anti*-$B_{18}H_{21}$) vs the ferrocene couple at 0 V Fc$^+$/Fc.

DFT Analysis of Photophysical Data

As a supplement to experimental data, computational calculations were conducted using TD-DFT on ADF software. A DFT hybrid PBE0 functional and DZP basis set was used with scalar relativistic effects considered. Optimized geometry coordinates and frequency calculations can be found in Tables S6-9. First, the absorption spectrum was calculated based on the optimized singlet ground state geometry, S_0. As shown in Figure 2.6, three vertical absorption (λ_{VA}) events with oscillator strengths > 0.02 occur between 290-350 nm, the approximate range in which the molecule was excited in the photoluminescence experiments. While these transitions originate from the HOMO (-8.31 eV), HOMO-1 (-8.42 eV), or HOMO-2 (-9.18 eV), they are all singlet-singlet processes that excite into the LUMO (-4.09 eV). Importantly, there are two calculated bands at 347 nm and 357 nm that correspond to the broad experimental band at 343 nm. The relatively small oscillator strengths for these transitions (~3-4 times smaller than those of *anti*-$B_{18}H_{22}$, Table S5), are in accordance with the absorption spectrum and ε values in Figure 2.3. The emission spectrum, based on the optimized geometry of the S_1 state, was calculated, resulting in a vertical emission wavelength (λ_{VE}) at 374 nm, which best corresponds to the experimental λ_{max} at 410 nm. In order to determine the origin of phosphorescence, the T_1 optimized geometry was calculated.

	State Transition	Composition	λ_{VA} or λ_{VE} (nm)	f
Excitation	$S_0 \rightarrow S_1$	HOMO → LUMO	357	0.0443
		HOMO-1 → LUMO	347	0.0336
		HOMO-2 → LUMO	288	0.0909
Emission	$S_0 \rightarrow S_1$	HOMO → LUMO	374	-
	$S_0 \rightarrow T_1$	HOMO → LUMO	487	-
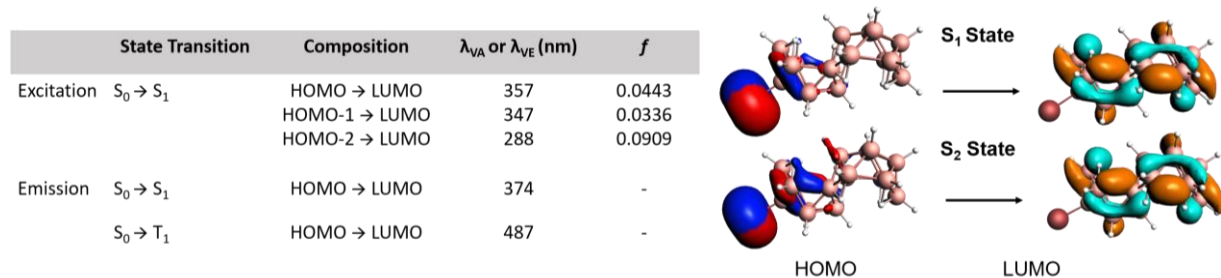
Figure 2.6: Left) Summary of relevant calculated absorption and emission spectra (Hybrid PBE0 DZP) for 4-Br-*anti*-$B_{18}H_{21}$, where λ_{VA} is the calculated vertical absorption wavelength, λ_{VE} is the calculated vertical emission wavelength, f is the oscillator strength, and λ_{max} is the corresponding experimental wavelength. Excitation calculations were based on the S_0 optimized geometry and emission calculations were based on the S_1, S_2 or T_1 optimized geometries. Right) Natural Transition Orbitals (NTOs) for the electronic transitions of the S_1 and S_2 states. The remaining relevant NTOs are shown in Figure S14.

The energy difference between the S_1 and T_1 states is 0.22 eV, a relatively small gap in which intersystem crossing would be possible. Therefore, phosphorescence will most likely occur from the T_1 state. The emission spectrum based on the optimized geometry of the T_1 state was calculated, giving $\lambda_{VE} = 487$ nm, which matches well with the experimental band maximum $\lambda_{max} = 503$ nm. The natural transition orbitals (NTOs) for the S_1, and S_2 states are shown in Figure 2.6, whereas the NTO for the T_1 state, which is similar to the S_1 state, is included in Figure S14. The NTOs show that the HOMO for S_1 and S_2 states have predominantly bromine p-orbital (n_{Br}) character. Furthermore, the bromine p-orbital in the S_2 state is orthogonal to the S_1 state, which will consequently favor SOC and therefore ISC. This feature is consistent with the fast ISC process observed in the experimental lifetime decay experiments. All of these excited states have a common LUMO, which is distributed exclusively on the boron cluster. Therefore, while fluorescence from the parent borane can be characterized as a $^1(\sigma \rightarrow \sigma^*)$ transition involving B-B and B-H bonds (Figure S13), emission from 4-Br-*anti*-$B_{18}H_{21}$ can be assigned to $^1(n_{Br} \rightarrow \sigma^*)$ and $^3(n_{Br} \rightarrow \sigma^*)$ charge transfer transitions, which

2.4 Conclusion

This work presents the synthesis and photophysical characterization of the dually emissive *anti*-$B_{18}H_{21}Br$ molecule, which was prepared from *anti*-$B_{18}H_{22}$ through electrophilic substitution with $AlCl_3$ and Br_2. This molecule is a rare example of a boron-based dual emitting chromophore. Its simultaneous fluorescence and phosphorescence originate from a delicate balance of S_1 and T_1 state population afforded by the bromo substituent. While the phosphorescence is quenched by oxygen, the fluorescence signal maintains its intensity, suggesting that this molecule could be useful as a ratiometric oxygen probe. The synthesis of 4-Br-*anti*-$B_{18}H_{21}$ offers a contribution to the synthetic toolbox for *anti*-$B_{18}H_{22}$, while also elucidating the relationship between cluster

structure and photophysical properties. More broadly, this work presents further advances in the burgeoning field of boron-containing luminescent and photoactive materials.[25]

2.5 References

1. (a) T. Kowada, H. Maeda, K. Kikuchi, *Chem. Soc. Rev.*, 2015, **44** (14), 4953. (b) A. Sutter, M. Elhabiri, G. Ulrich, *Chem. Eur. J.* 2018, **24**, 11119.

2. (a) K. Rurack, M. Kollmannsberger, J. Daub, *Angew.*, 2001, **40** (2), 385; (b) S. Yamaguchi, S. Akiyama, K. Tamao, *J. Am. Chem. Soc.*, 2001, **123** (46), 11372. (c) S. K. Mellerup, S. Wang, *Chem. Soc. Rev.* 2019, **48**, 3537.

3. Recent select examples (see references within): (a) K. S. Mellerup and S. Wang, Trends in Chem. 2019, **1** (1), 77. (b) J. Lei, S. Griesbeck, T. B. Marder, *Chem. Sci.* 2017, **8**, 846. (c) K. O. Kirlikovali, J. C. Axtell, A. Gonzalez, A. C. Phung, S. I. Khan, A. M. Spokoyny, *Chem. Sci.*, 2016, **7** (8), 5132.

4. (a) S. Yruegas, J. J. Martinez, C. D. Martin, *Chem. Comm.*, 2018, **54** (50), 6808; (b) T. C. Li, F. Fabregat-Santiago, O. K. Farha, A. M. Spokoyny, S. R. Raga, J. Bisquert, C. A. Mirkin, T. J. Marks, J. T. Hupp, *J. Phys. Chem. C* 2011, **115** (22), 11257.

5. R. T. Kuznetsova, Y. V. Aksenova, E. N. Tel'minov, L. G. Samsonova, G. V. Maier, T. N. Kopylova, S. L. Yutanova, E. V. Antina, M. B. Berezin, G. B. Guseva, *Opt. Spectrosc.*, 2012, **112** (5), 746.

6. (a) B. P. Dash, R. Satapathy, E. R. Gaillard, J. A. Maguire, N. S. Hosmane, *J. Am. Chem. Soc.*, 2010, **132** (18), 6578. (b) S. Mukherjee, P. Thilagar, *Chem. Comm.*, 2016, **52** (6), 1070; (c) K. Kokado, Y. Tokoro, Y. Chujo, *Macromolecules*, 2009, **42** (8), 2925.

7. R. N. Grimes, *Carboranes, 3rd ed.* Academic Press: 2016.

8. Representative examples (see references within): (a) R. Núñez, M. Tarrés, A. Ferrer-Ugalde, F. F. de Biani, F. Teixidor, *Chem. Rev.*, 2016, **116** (23), 14307; (b) Y. Quan, Z. Xie, *Chem. Soc. Rev.*, 2019, **48** (13), 3660; (c) S. P. Fisher, A. W. Tomich, S. O. Lovera, J. F. Kleinsasser, J. Guo, M. J. Asay, H. M. Nelson, V. Lavallo, *Chem. Rev.,* 2019, **119** (14), 8262.

9. M. G. S. Londesborough, D. Hnyk, J. Bould, L. Serrano-Andrés, V. Sauri, J. M. Oliva, P. Kubát, T. Polívka, K. Lang, *Inorg. Chem.*, 2012, **51** (3), 1471.

10. A. R. Pitochelli, M. F. Hawthorne, *J. Am. Chem. Soc.*, 1962, **84** (16), 3218.

11. L. Cerdán, J. Braborec, I. Garcia-Moreno, A. Costela, M. G. S. Londesborough, *Nat. Commun.*, 2015, **6**, 5958.

12 (a) M. G. S. Londesborough, J. Dolanský, J. Bould, J. Braborec, K. Kirakci, K. Lang, I. Císařová, P. Kubát, D. Roca-Sanjuán, A. Francés-Monerris, L. Slušná, E. Noskovičová, D. Lorenc, *Inorg. Chem.*, 2019, **58** (15), 10248; (b) M. G. S. Londesborough, J. Dolanský, T. Jelínek, J. D. Kennedy, I. Císařová, R. D. Kennedy, D. Roca-Sanjuán, A. Francés-Monerris, K. Lang, W. Clegg, *Dalton Trans.,* 2018, **47** (5), 1709; (c) M. G. S. Londesborough, R. Macías, J. D. Kennedy, W. Clegg, J. Bould, *Inorg. Chem.*, 2019, **58** (19), 13258; (d) R. L. Sneath, L. J. Todd, *Inorg. Chem.*, 1973, 12 (1), 44; (e) V. Saurí, J. M. Oliva, D. Hnyk, J. Bould, J. Braborec, M. Merchán, P. Kubát, I. Císařová, K. Lang, M. G. S. Londesborough, *Inorg. Chem.*, 2013, **52** (16), 9266.

13. M. G. S. Londesborough, J. Dolanský, L. Cerdán, K. Lang, T. Jelínek, J. M. Oliva, D. Hnyk, D. Roca-Sanjuán, A. Francés-Monerris, J. Martinčík, M. Nikl, J. D. Kennedy, *Adv. Opt. Mater.*, 2017, **5** (6), 1600694.

14. R. M. Dziedzic, L. M. Saleh, J. C. Axtell, J. L. Martin, S. L. Stevens, A. T. Royappa, A. L. Rheingold, A. M. Spokoyny, *J. Am. Chem. Soc.*, 2016, **138** (29), 9081.

15. L. C. Sander, S. A. Wise, S. A., *Anal. Chem.* 1984, **56** (3), 504.

16. P. G. Simpson, W. N. Lipscomb, *J. Chem. Phys.*, 1963, **39** (1), 26.

17. K. N. Solov'ev, E. A. Borisevich, *Physics-Uspekhi* 2005, **48** (3), 231.

18. N. J. Turro, V. Ramamurthy, J. C. Scaiano, *Principles of molecular photochemistry : an Introduction*. University Science Books: 2009.

19. (a) I. M. Krieger, G. W. Mulholland, C. S. Dickey, *J. Phys. Chem.*, 1967, **71** (4), 1123; (b) E. I. Hormats, F. C. Unterleitner, *J. Phys. Chem.*, 1965, **69** (11), 3677; (c) H. Y. Kaptan, *J. Appl. Polym. Sci.*, 1999, **71** (7), 1203.

20. Y. Feng, J. Cheng, L. Zhou, X. Zhou, H. Xiang, *Analyst*, 2012, **137** (21), 4885.

21. Y. Zhao, L. Liu, T. Luo, L. Hong, X. Peng, R. H. Austin, J. Qu, *Sensor. Actuat. B- Chem.*, 2018, **269**, 88.

22. B. J. Basu, A. Thirumurugan, A. R. Dinesh, C. Anandan, K. S. Rajam, *Sensor. Actuat. B- Chem.*, 2005, **104** (1), 15.

23. E. D. Lee, T. C. Werner, W. R. Seitz, *Anal. Chem.*, 1987, **59** (2), 279.

24. J. D. Wild, T. Sridhar, O. E. Potter, *Chem. Eng. J.,* 1978, **15** (3), 209.

25. Key representative examples (see references within): (a) X. Li, Y. Shi, N. Wang, T. Peng, S. Wang, *Chem. Eur. J.,* 2019, **25**, 5757; (b) L. Dong, F. Saraci, K. Yuan, X. Wang, S. Wang, *Org. Biomol. Chem.,* 2019, **21** (26), 6470; (c) M. Ito, E. Ito, M. Hirai, S. Yamaguchi, *J. Org. Chem.*, 2018, **83** (15), 8449; (d) C. D. Entwistle, T. B. Marder, *Chem. Mater.*, 2004, **16** (23), 4574; (e) X. Jia, J. Nitsch, L. Ji, Z. Wu, A. Friedrich, F. Kerner, M. Moos, C. Lambert, T. B. Marder, *Chem.*

Eur. J., 2019, **25** (46), 10845; (f) M. Vanga, R. A. Lalancette, F. Jäkle, *Chem. Eur. J.*, 2019, **25** (43), 10133; (g) K. Liu, R. A. Lalancette, F. Jäkle, *J. Am. Chem. Soc.*, 2019, **141** (18), 7453; (h) M. Gorbe, A. M. Castro, F. Sancenón, R. Martínez-Máñez, R. Ballesteros-Cillero, L. E. Ochando, K. Chulvi, R. Gotor, S. Gil, *Dyes Pigm.,* 2019, **160**, 198; (i) C. Ray, C. Schad, E. Avellanal-Zaballa, F. Moreno, J. Bañuelos, B. L. Maroto, S. de la Moya, *Proceedings*, 2019, **41** (1), 54; (j) Z. Domíngez, V. F. Paid, D. Collado, P. Vázquez-Domínguez, F. A. Albendín, A. Pérez-Inestrosa, A. Ros, U. Pischel, *J. Org. Chem.*, 2019, **84** (21), 13384. (k) J. S. Ishibashi, C. Darrigan, A. Chrostowska, B. Li, S.-Y. Liu, *Dalton Trans.*, 2019, **48** (8), 2807. (l) D. Jung, L. M. A. Saleh, Z. J. Berkson, M. F. El-Kady, J. Y. Hwang, N. Mohamed, A. I. Wixtrom, E. Titarenko, Y. Shao, K. Mccarthy, J. Guo, I. B. Martini, S. Kraemer, E. C. Wegener, P. Saint-Cricq, B. Ruehle, R. R. Langeslay, M. Delferro, J. L. Brosmer, C. H. Hendon, M. Gallagher-Jones, J. Rodriguez, K. W. Chapman, J. T. Miller, X. Duan, R. B. Kaner, J. I. Zink, B. F. Chmelka, A. M. Spokoyny, *Nature Mater.* 2018, **17**, 341. (m) J. C. Axtell, M. S. Messina, J.-Y. Liu, D. Galaktionova, J. Schwan, T. M. Porter, M. D. Savage, A. I. Wixtrom, A. L. Rheingold, C. P. Kubiak, J. R. Winkler, H. B. Gray, P. Kral, A. N. Alexandrova, A. M. Spokoyny, *Inorg. Chem.* 2019, **58** (16), 10516, (n) H. L. van de Wouw, R. S. Klausen, *J. Org. Chem.* 2019, **84** (3), 1117.

Chapter 3 – Benchmarking the dynamic luminescent properties and UV stability of $B_{18}H_{22}$-based materials

This chapter is a version of K. P. Anderson, A. S. Hua, J. B. Plumley, A. D. Ready, A. L. Rheingold, T. L. Peng, P. I. Djurovich, C. Kerestes, N. A. Snyder, A. Andrews, J. R. Caram and A. M. Spokoyny. Benchmarking the dynamic luminescent properties and UV stability of $B_{18}H_{22}$-based materials. *Dalton Trans.* **2022**, Advance Article. DOI: 10.1039/D2DT01225A.

3.1 Abstract

The dynamic photoluminescent properties, and potential quenching mechanisms, of *anti*-$B_{18}H_{22}$, 4,4'-Br_2-anti-$B_{18}H_{20}$, and 4,4'-I_2-anti-$B_{18}H_{20}$ are investigated in solution and polymer films. UV stability studies of the neat powders show no decomposition occurring after intense 7 day light soaking. In contrast, clusters incorporated into polymer films are found to degrade into smaller borane fragments under the same irradiation conditions. To highlight the utility of these compounds, we leverage their favorable optical properties in a prototype UV imaging setup.

3.2 Introduction

Boron-containing luminescent molecules have gained attention for their application in areas such as OLEDs, (bio)sensing, and imaging.[1] These compounds normally consist of a boron atom nested in an aromatic organic framework, which interacts with the vacant p orbital of boron to produce charge transfer processes responsible for luminescence. Despite the abundance of hybrid (boron and carbon containing) luminescent molecules, only one boron hydride framework, *anti*-$B_{18}H_{22}$, exhibits fluorescence without the aid of any carbon-based functional groups. This 18-vertex borane has bright blue emission and a quantum yield nearing unity ($\phi = 0.97$).[2] Since its discovery by Pitochelli and Hawthorne in 1962,[3] multiple follow-up investigations showed how

30

functionalization of the boron vertices can have dramatic effects on its emission, quantum yield and stability.[4] With a limited number of synthetic derivatives reported to date, further work into defining the luminescent properties of B_{18}-based compounds *via* molecular design is needed. The recent research on *anti*-$B_{18}H_{22}$, led by Londesborough *et al.*, has so far focused on its application in lasers and OLEDs;[5] however, the lack of knowledge on its dynamic luminescent properties and UV stability- especially in polymer films- has so far thwarted such efforts.

This work considers the luminescence and UV stability of *anti*-$B_{18}H_{22}$-based molecules, with a focus on how and why these properties are subject to change in solution, neat powders, and polymer films. Specifically, we investigate *anti*-$B_{18}H_{22}$ (**1**) and two of its halogenated derivatives, 4,4'-Br_2-*anti*-$B_{18}H_{20}$ (**2**) and 4,4'-I_2-*anti*-$B_{18}H_{20}$ (**3**) (Figure 3.1). The parent borane **1** was selected to establish a baseline for these studies, while the halogenated clusters have luminescent properties
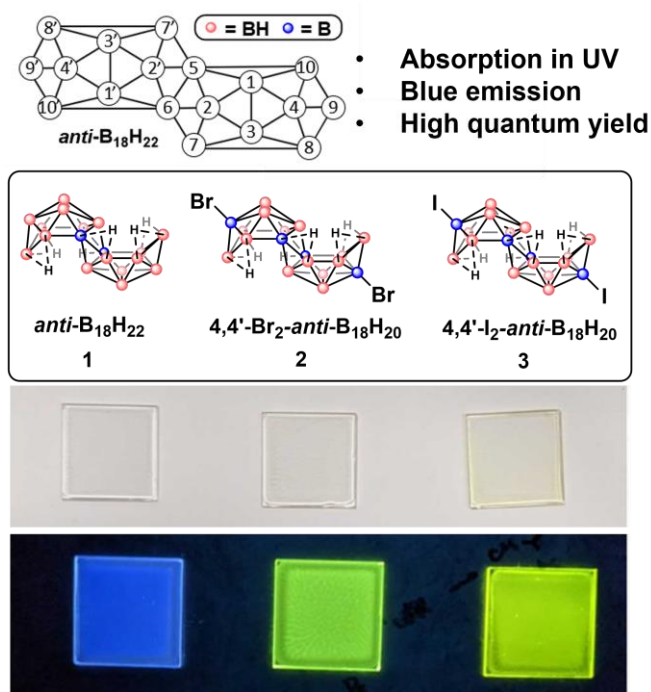
Figure 3.1: Structures of the three luminescent compounds explored in this study (top) in polystyrene-toluene films under normal lighting (middle) and UV light (bottom).

31

favourable to optoelectronic application, such as absorption in the UV region, large Stokes' shifts, and high quantum yields.[4a] In this work, we show that the UV stability of **1**-**3** dramatically depends on the host matrix. Furthermore, we observe unique cage deconstruction chemistry that results in a loss of luminescence. Guided by this new knowledge, we were able to develop a proof-of-concept prototype UV-imaging setup using **1**-**3**. Importantly, this research identifies several interesting areas of *anti*-$B_{18}H_{22}$ chemistry that should be further addressed to achieve meaningful application of these clusters in optical devices.

3.3 Results and Discussion

Incorporation of emitters into polymer films

Halogenated compounds 2 and 3 were selected for these studies due to their straightforward syntheses and large Stokes shifts that minimize reabsorption loss. While compound 3 has already been reported,[4a] its brominated counterpart, 4,4'-Br_2-*anti*-$B_{18}H_{20}$, is synthesized here for the first time. Substitution occurs via electrophilic halogenation by reacting ***anti*-$B_{18}H_{22}$** with $AlCl_3$ and Br_2 over 1 hour (see SI, Figures S1-S5). All three compounds are stable when stored under ambient conditions. With 1-3 in hand, we sought suitable formulations for their incorporation into polymer films. Ideal films are uniform and should preserve the molecular photoluminescence and stability of the parent compound. However, embedding small molecules into polymer films can dramatically affect their properties. This, coupled with the poor solubility of inorganic emitters in organic solvents,**[6]** make developing and optimizing luminescent films extremely challenging. Previous studies demonstrated the ability to incorporate *anti*-$B_{18}H_{22}$ into polystyrene,[5] but only partial characterization of these films was conducted, and no other polymer matrices were explored. In this study, we investigate if and how the properties of **1**-**3** change when incorporated into four widely available and inexpensive polymers: poly(methyl methacrylate) (PMMA),

poly(lauryl methacrylate) (PLMA), ethyl vinyl acetate copolymer (EVA), and polystyrene (PS). PMMA films loaded with 2 wt% **1**, **2**, and **3** were stable, but were also bright yellow in colour with significantly diminished luminescence when observed under a UV lamp (Figure S6). Both the PLMA and EVA films were colourless, but the emissive species degraded in the PLMA films after just 3 days and the EVA films were non-uniform and brittle. Only polystyrene yielded uniform, mostly colourless films that are stable under ambient conditions (Figure 3.1), making it the most suitable polymer matrix for the proceeding experiments.

Photoluminescent Characterization

Because molecular luminescence often changes when incorporated into films, photophysical characterization was conducted on cyclohexane solutions of **1-3** to establish baseline properties of each species. While the parent borane and its brominated analogue maintain absorption strictly within the UV region, 4,4'-I$_2$-*anti*-B$_{18}$H$_{20}$ tails slightly into the visible spectrum (Figure 3.2, left). Out of the three, **1** absorbs light most strongly (ε = 6800 M^{-1}cm^{-1}),[4b] followed by **3** (ε = 4900 M^{-1}cm^{-1}) and **2** (ε = 2200 M^{-1}cm^{-1}). Emission spectra, also gathered in cyclohexane solution, show peak maxima at 408, 525, and 526 nm for **1**, **2**, and **3**, respectively. The significant red-shifts in the emission spectra of **2** and **3** compared to the parent borane are due to the presence of the heavy halogen atoms, which lend spin-orbit coupling to the molecule. Previous reports have already noted that **1** exhibits fluorescence[2] and that the addition of heavy iodine atoms produces phosphorescence in **3**.[4a] Likewise, substitution with bromine results in phosphorescence, which occurs through a ^{3}(n$_{Br}$ → σ*) charge transfer transition (Figure S43). Phosphorescence can be confirmed by the long 7 μs lifetime of **2**, which increases to 43 μs when nitrogen is bubbled through
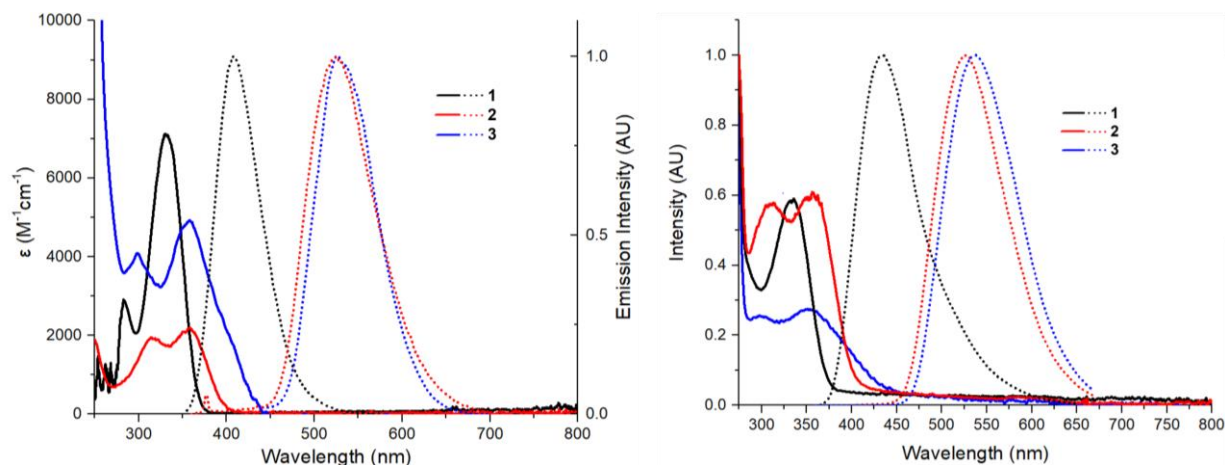
Figure 3.2: Absorption and emission spectra of **1**-**3** in cyclohexane solution (left) and as 2 wt% polystyrene films (right), where the solid lines are absorption and the dotted lines are emission. λ_{exc} = 340 nm.

the solution (Figure S7). The quantum yields (ϕ) of the phosphorescent compounds improve under oxygen-free conditions, from ϕ = 0.08 to ϕ = 0.55 in **2** and from ϕ = 0.41 to ϕ = 0.71 in **3** (Table 3.1). We also note that **1**-**3** were stable in these solutions for at least several weeks, with no degradation observed.

Polystyrene films of these clusters, **PS-1**, **PS-2** and **PS-3**, were subjected to similar characterization, summarized in Table 3.1, Figures S8-S9, and Table S2. The optical properties of the films exhibit low reflectance and high transmittance (~90% at 500-2500 nm) with optical densities less than 1 for all three compounds (Figure S10). The absorption spectra remained largely unchanged from that of the cyclohexane solutions, while the emission peak maxima, particularly for **PS-1** and **PS-3**, exhibited noticeable bathochromic shifts of 25 nm and 10 nm, respectively (Figure 3.2, right). These shifts have been observed previously and are found to increase or decrease with higher and lower emitter loading, respectively; these changes could be caused by cluster-cluster or cluster-polymer interactions.[5b,7] The quantum yields also changed considerably from solution to films, with ϕ = 0.28 for **PS-1**, which is in stark contrast to the 0.97 value observed

	Anti-$B_{18}H_{22}$ (1)	4,4'-Br_2-anti-$B_{18}H_{20}$ (2)	4,4'-I_2-anti-$B_{18}H_{20}$ (3)
$\lambda_{em\ cyclohexane}$ (nm)	408	525	526
$\lambda_{em\ film}$ (nm)	434	526	538
$\phi_{cyclohexane}$	0.97*	0.55[a]	0.71[a]*
ϕ_{film}	0.28	0.41	0.44
	0.30[b]	0.74[b]	0.46[b]
τ_{film} (µs)	0.0022[c,d]	58[c]	3.8[c]
k_r (µs^{-1})	86[d]	0.013	0.12
k_{nr} (µs^{-1})	370[d]	0.0045	0.14

Table 3.1: Emission (λ_{em}), quantum yield (ϕ), lifetime (τ) and radiative ($k_r = \phi_{film}{}^b/ \tau_{film}$) and non-radiative ($k_{nr} = (1- \phi_{film}{}^b)/ \tau_{film}$) decay rates for downshifting molecules. [a]In oxygen-free cyclohexane, [b]Under nitrogen atmosphere, [c]Under vacuum. [d]Data from PS films prepared with dichloromethane, see SI. Excitation wavelength (λ_{exc}) = 340 nm for emission and quantum yield, λ_{exc} = 331 nm for **1** and 405 nm for **2** and **3**. *From refs 2 and 4a.

in cyclohexane solution.[2] Likewise, **3** exhibits a decrease from ϕ = 0.71 in solution[4a] to ϕ = 0.46 in film. Interestingly, only **PS-2** demonstrated improved quantum yield, increasing from φ = 0.41 to φ = 0.74 under nitrogen and exceeding the φ = 0.55 observed in oxygen-free cyclohexane. Diminished fluorescence of **1** in PS films was noted previously[5b] which the authors attributed to the high proton affinity (PA) of polystyrene that causes unfavourable interaction with the borane. They also reported that the quantum yield of PS films is negatively affected if they were cast with high PA solvents. Based on these findings, we prepared another batch of polystyrene films using dichloromethane which, in contrast to the previous report, exhibited slightly lower quantum yields than those cast with toluene (Table S2). Additionally, films cast with THF changed from yellow to opaque white upon drying, suggesting that the effects of the casting solvent are not well maintained in the dried films.

To gain more specific insight into the conditions that quench luminescence, absorption and fluorescence spectra were gathered from solutions of **1-3** in cyclohexane, 1,2,-difluorobenzene, benzene, toluene, THF, acetone, and methanol (Figure S11-S13). The absorption maxima in each remain largely unchanged except for THF, acetone, and methanol, which show significantly (~60

nm) red-shifted peaks. Interestingly, 1,2-difluorobenzene also shifts the absorption of **2**. These changes are characteristic of a ground-state complex between the solvent and cluster forms that prevents luminescence.[8] To further investigate potential ground-state interactions between the borane and solvent molecules, **1-3** were analysed by ^{11}B and ^{1}H{^{11}B} NMR in deuterated THF, acetone, and methanol (Figures S14-23) and compared to their NMR spectra in deuterated chloroform solution. The effects of solvent on the ^{11}B NMR ranged from slight broadening of the boron resonances to wide, poorly defined peaks. For example, while the ^{11}B NMR spectrum of **1** in THF exhibits sharp boron resonances, the analogous spectrum in methanol is significantly broadened (Figures S14 and S16). These changes were often accompanied by increased number of resonances indicating decreased symmetry of the cluster. In several cases, sharp singlets indicative of tetracoordinate boron environments were observed (Figures S16-17, S22). Furthermore, broadening of the proton peaks in ^{1}H{^{11}B} NMR spectra points to the likelihood of exchange between solvent molecules and borane species. Interestingly, several proton resonances were completely absent in some methanol solution ^{1}H{^{11}B} NMR spectra, which is likely due to deuterium exchange between the cluster and solvent (Figure S16, S22). These data, in addition to the red-shifted absorption spectra (see above), strongly support the existence of ground-state complexes that prevent luminescence in coordinating solvents.

The minimal changes in the absorption spectra of compounds **1-3** in polystyrene and toluene suggest that the diminished quantum yield in these cases is due to a dynamic, excited-state process. Therefore, we conducted lifetime measurements in cyclohexane, 1,2-difluorobenzene, benzene, and toluene to investigate the variations in excited state dynamics in these solvents (Figure S24). The lifetime of **1** is longest in cyclohexane (10.4 ns) followed by 1,2-difluorobenzene (8.9 ns), toluene (4.8 ns), and benzene (3.3 ns). These successively shorter lifetimes, assuming

monoexponential decay kinetics, signify stronger quenching caused by solvent. Interestingly, the decay kinetics of **1** in toluene are not monoexponential but are indicative of exciplex formation in the excited state.[8b] Propensity for toluene to strongly interact with **1** correlates to the severely diminished quantum yield observed in **PS-1**. In contrast to **1**, compound **2** exhibited the least amount of quenching from toluene, followed by benzene and 1,2-difluorobenzene (1,2-difluorobenzene also appears to form a ground-state complex with **2**). Notably, **3** only displays strong luminescence in cyclohexane and therefore the lifetime measurements in other solvents were not attempted.

These quenching mechanisms also manifest in polymer films: the less fluorescent yellow PMMA films likely indicate an interaction with the cluster that bears resemblance to that of the THF, methanol, and acetone solutions (Figure S6), while quenching by polystyrene could occur through excited state processes. **PS-2** and **PS-3** are less affected by the polymer matrix than **PS-1**, potentially because of the steric bulk of the substituents that mitigate cluster-polystyrene interactions, particularly in the solid state. At the same time, the progressively increasing polarizability from **1** to **3** could also render the halogenated molecules more susceptible to cluster-solvent interactions that diminish luminescence; it is therefore possible that **2** strikes a balance between these two quenching pathways that ultimately results in its superior quantum yield in polystyrene films. Still, while the exact quenching mechanisms cannot be definitively discerned from these studies, it is evident that quantum yield is dependent on the polymer host matrix, and it is essential that practitioners in future studies assess the intricate relationship between luminescence quenching by solvents and polymers.

Photostability of powders and polymer films

Data gathered for this report shows that polymers can greatly affect both the luminescence and stability of these boron clusters. We had previously identified two polymers, PMMA and PS, in which the clusters were stable under ambient conditions. However, we sought to gauge the extent of this stability under more relevant circumstances (i.e., light exposure). The photostability of **1** in polystyrene films has been previously investigated, with evidence of degradation observed after 30 minutes of light exposure, evidenced by diminished emission intensity.[5b] However, the degradation products of **1** are unknown and the photostability of **2** and **3** remain completely unexplored. Therefore, we conducted a more extensive study to assess the photostability of **1**-**3** as neat powders. To assess the degradation products of doped films, two different polymer hosts containing **1**-**3** were included in the study. Polystyrene and PMMA films as well as powders of **1**-**3** were subjected to intense UV irradiation over 7 days. All films except **PMMA-1** exhibited decreased luminescence after light exposure. Each irradiated film was analysed by NMR spectroscopy and ESI-MS to identify the boron species present. Based on the NMR spectroscopy data, **PMMA-1** remained intact, while **PMMA-2** and **PMMA-3** showed little to no cluster present (Figure S25). Mass spectra for all three PMMA films dissolved in methanol show their respective boron cluster masses, indicating that at least some intact cluster remained (Figures S26-28). There was, however, no detectable intact cluster for **PS-1**, **PS-2**, and **PS-3** by NMR spectroscopy (Figure S29). The mass spectra showed no **1** or **2** present in the PS films, and only a small amount of **3** (Figures S30-32). We found the absence of detectable boron in these samples surprising; even if degradation had occurred, we would expect to see corresponding signals in the ^{11}B NMR spectra. To see if the boron content in the films was consistent before and after irradiation, Inductively Coupled Plasma – Optical Emission Spectrometry (ICP-OES) studies were conducted. Because

the PMMA films were initially spin coated and the recovery of the PS films resulted in some lost fragments, we anticipated that the measured boron content would be slightly inaccurate or lower than the control samples. Nevertheless, the ICP results align well with the NMR and MS observations and show significantly less boron than expected (Tables S3-S4). In all films, the detected boron content was under 50% of the expected amount. In accordance with the MS and NMR spectroscopy data, the parent borane **1** performed best in the PMMA film, with 47% of the expected boron content present. The detected boron in the remaining PS and PMMA films was very low, apart from **PS-3** which had 32% remaining. Interestingly, a mass corresponding to $B_{10}H_{14}$ is present in the **PS-1** mass spectrum (Figure S33), suggesting that degradation could proceed through the deconstruction of the cluster cage into its synthetic precursor, decaborane.[10] To further probe this observation, irradiation of polystyrene films was conducted in sealed quartz tubes under ambient atmosphere. After irradiation, the contents of the quartz tubes were dissolved in deuterated chloroform for NMR analysis (Figure S34). The $^{11}B\{^{1}H\}$ NMR for **PS-1** contains several peaks that do not correspond to **1** but rather decaborane (Figure S35). At least another set of boron hydride peaks is clearly visible in the NMR spectrum which we were unable to definitively assign. There was no detectable boron by NMR spectroscopy for **PS-2** and **PS-3**. The mass spectra showed some intact cluster in **PS-1**, but most masses appeared to be degradation products, with one corresponding to decaborane ($B_{10}H_{14}$) (Figure S36). Interestingly, the MS of **PS-2** and **PS-3** did not contain the mass of $B_{10}H_{14}$, but rather its halogenated counterparts $B_{10}H_{13}Br$ and $B_{10}H_{13}I$, respectively (Figures S37-38). This suggests that degradation does not take place through cleavage of the boron-halogen bond, but through deconstruction of the B_{18}-based framework to form $B_{10}H_{14}$ (Figure 3.3). The relatively high vapor pressure of decaborane (0.2
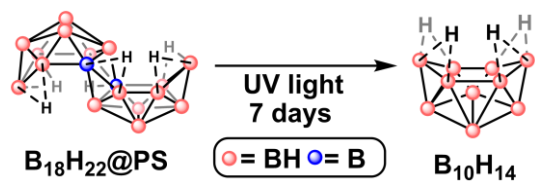
Figure 3.3: Schematic of the deconstruction of **1** into its synthetic precursor, decaborane, after irradiation.

mmHg)[11] explains its absence from the initial non-sealed samples, as it could easily escape the film after forming. Masses corresponding to other clusters, namely $B_{11}H_{14}^-$ and $B_{12}H_{16}O$, were also observed in the **PS-1** mass spectrum along with the corresponding halogenated masses for $B_{11}H_{13}X^-$, $B_{11}H_{13}XO^-$ and $B_{12}H_{15}XO$ in **PS-2** and **PS-3**. This suggests that cluster deconstruction proceeds through similar mechanisms for all three compounds tested. Despite the degradation observed in the films, the powder samples of compounds **1**, **2** and **3** were stable after the week-long irradiation (Figures S39-42). Evidence of intact **2** and **3** as well as $B_{18}H_{19}Br_3$ and $B_{18}H_{19}I_3$ by MS indicates that B-X bonds are less susceptible, but not inert, to photodegradation. Overall, these studies suggest that photostability of B_{18}-based compounds needs to be considered as a function of the host material.

UV-Visible imaging

Current UV-imaging technology is limited by its inability to simultaneously observe UV and visible light, mainly due to the opaque phosphors used.[12] With the appropriate setup,[13] our transparent, UV-absorbing films would permit the simultaneous visualization of UV and visible light. As a proof-of-concept to demonstrate the utility of compounds **1**-**3**, a prototype imaging setup was constructed using a 340 nm LED (Figure 3.4A). To ensure the purity of the LED, a 340 nm bandpass filter and focusing lens was placed in front of the light. A UV absorbing molecule,
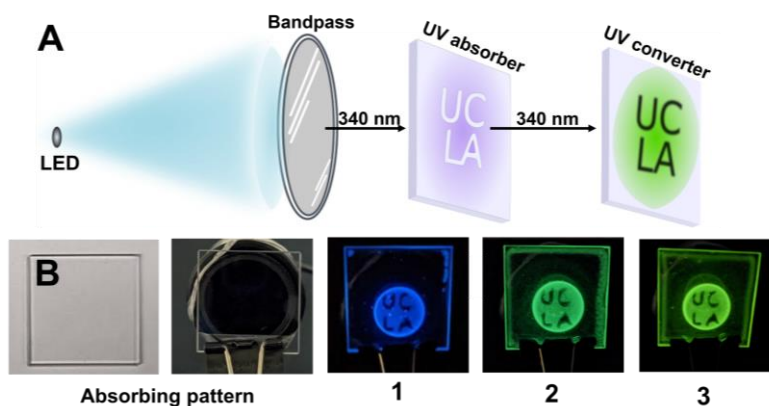
Figure 3.4: A) Schematic of UV-imaging setup, viewed from the side B) Polystyrene films, from left to right: absorber film under ambient light, 340 nm light, the absorber film paired with emissive films **1**, **2**, and **3** under 340 nm illumination.

benzophenone, was dissolved in a solution of toluene and polystyrene and cast in a pattern ("UCLA") on a quartz substrate. The pattern is completely transparent and colourless, and it is not visible when placed in front of the bandpass filter in the presence of 340 nm light (Figure 3.4B, left). However, when polystyrene films of **1-3** are placed in front of the UV-absorbing pattern, the 340 nm light that is not absorbed by the benzophenone pattern is transmitted through the quartz and converted to a wavelength visible to the human eye or camera. Consequently, the UV absorber becomes visible (Figure 3.4B, right). One could further envision the incorporation of these emissive films onto the surface of camera lenses for the detection of UV radiation or UV absorbing objects, especially if better polymer formulations can be identified.

3.4 Conclusion

While *anti*-$B_{18}H_{22}$ and its derivatives remain a promising material for luminescence applications, the development of a suitable polymer formulation that yields transparent films, retains high quantum yield, and is stable to UV radiation is a major bottleneck for their broader applications. This work provides a foundation for future studies by benchmarking dynamic photoluminescence

and UV stability/degradation of B_{18}-based compounds as solids and in polymer films. We established that polymer matrices are intricately tied to luminescence and UV stability of the corresponding polymer films containing emissive boron clusters. The stability profile for these compounds under the same UV irradiation can be extreme, ranging from no noticeable degradation to nearly complete cage deconstruction. This study further serves as a broader reminder to practitioners in the field to carefully consider specific conditions and environmental factors when evaluating photostability of luminescent materials.

3.5 References

1. Recent representative examples: (a) Z. Huang, S. Wang, R. D. Dewhurst, N. V. Ignat'ev, M. Finze, H. Braunschweig, *Angew. Chem., Int. Ed.,* 2020, **59**, 8800-8816. (b) S. M. Berger and T. B. Marder, *Mater. Horiz.*, 2022, **9**, 112-120. (c) X. Su, T. A. Bartholome, J. R. Tidwell, A. Pujol, S. Yruegas, J. J. Martinez and C. D. Martin, *Chem. Rev*., 2021, **121**, 4147-4192. (d) A. John, M. Bolte, H.-W. Lerner, G. Meng, S. Wang, T. Peng and M. Wagner, *J. Mater. Chem. C*, 2018, **6**, 10881-10887. (e) S. Mukherjee and P. Thilagar, *Chem. Commun.*, 2016, **52**, 1070-1093. (f) B. P. Dash, R. Satapathy, J. A. Maguire, N. S. Hosmane, *New. J. Chem.*, 2011, **35**, 1955-1972. (g) J. Ochi, K. Tanaka, Y. Chujo, *Angew. Chem., Int. Ed.*, 2020, **59**, 9841-9855. (h) K. O. Kirlikovali, J. C. Axtell, A. Gonzalez, A. C. Phung, S. I. Khan, A. M. Spokoyny, *Chem. Sci.*, 2016, **7**, 5132-5138. (i) X. Wu, J. Gu, Y. Quan, W. Jia, D. Jia, Y. Chen, Z. Xie, *J. Mater. Chem. C*, 2018, **6**, 4140-4149. (j) M. S. Messina, J. C. Axtell, Y. Wang, P. Chong, A. I. Wixtrom, K. O. Kirlikovali, B. M. Upton, B. M. Hunter, O. S. Shafaat, S. I. Khan, H. B. Gray, A. N. Alexandrova, H. D. Maynard, A. M. Spokoyny, *J. Am. Chem. Soc.,* 2016, **138**, 6952-6955. (k) P. Bissinger, A. Steffen, A. Vargas, R. D. Dewhurst, A. Damme, H. Braunschweig, *Angew. Chem., Int. Ed.,* 2015, **54**, 14, 4362-4366. (l) Y. Lebedev, C. Apte, S. Cheng, C. Lavigne, A. Lough, A. Aspuru-Guzik, D. S. Seferos, A. K. Yudin, *J. Am. Chem. Soc.* 2020, **142**, 13544-13549. (m) K. K. Hollister, A. Molino, G. Breiner, J. E. Walley, K. E. Wentz, A. M. Conley, D. A. Dickie, D. J.D. Wilson, R. J. Gilliard, *J. Am. Chem. Soc.,* 2022, **144**, 590-598. (n) L. Ji, S. Griesbeck, T. B. Marder, *Chem. Sci.*, 2017, **8**, 846-863. (o) J. Wang, N. Wang, G. Wu, S. Wang, X. Li, *Angew. Chem., Int. Ed.*, 2019, **58**, 3082-3086.

2. M. G. S. Londesborough, D. Hnyk, J. Bould, L. Serrano-Andrés, V. Sauri, J. M. Oliva, P. Kubát, T. Polívka and K. Lang, *Inorg. Chem.*, 2012, **51**, 1471-1479.

A. R. Pitochelli and M. F. Hawthorne, *J. Am. Chem. Soc*., 1962, **84**, 3218-3218.

3. (a) M. G. S. Londesborough, J. Dolanský, J. Bould, J. Braborec, K. Kirakci, K. Lang, I. Císařová, P. Kubát, D. Roca-Sanjuán, A. Francés-Monerris, L. Slušná, E. Noskovičová and D. Lorenc, *Inorg. Chem.*, 2019, **58**, 10248-10259. (b) K. P. Anderson, M. A. Waddington, G. J. Balaich, J. M. Stauber, N. A. Bernier, J. R. Caram, P. I. Djurovich and A. M. Spokoyny, *Dalton Trans.*, 2020, **49**, 16245-16251. (c) M. G. S. Londesborough, J. Dolanský, T. Jelínek, J. D. Kennedy, I. Císařová, R. D. Kennedy, D. Roca-Sanjuán, A. Francés-Monerris, K. Lang and W. Clegg, *Dalton Trans.*, 2018, **47**, 1709-1725. (d) M. G. S. Londesborough, J. Dolanský, L. Cerdán, K. Lang, T. Jelínek, J. M. Oliva, D. Hnyk, D. Roca-Sanjuán, A. Francés-Monerris, J. Martinčík, M. Nikl and J. D. Kennedy, *Adv. Opt. Mater.*, 2017, **5**, 1600694. (e) V. Saurí, J. M. Oliva, D. Hnyk, J. Bould, J. Braborec, M. Merchán, P. Kubát, I. Císařová, K. Lang and M. G. S. Londesborough, *Inorg. Chem.*, 2013, **52**, 9266-9274.

4. (a) L. Cerdán, J. Braborec, I. Garcia-Moreno, A. Costela and M. G. S. Londesborough, *Nat. Commun.*, 2015, **6**, 5958. (b) J. Ševčík, P. Urbánek, B. Hanulíková, T. Čapková, M. Urbánek, J. Antoš, M. G. S. Londesborough, J. Bould, B. Ghasemi, L. Petřkovský and I. Kuřitka, *Materials*, 2021, **14**, 589. (c) J. Chen, L. Zhang, X. Huang, H. Meng, C. Tan, *Chem. Phys. Lett.*, 2020, **747**, 137328.

5. (a) M. Buffa, S. Carturan, M. G. Debije, A. Quaranta and G. Maggioni, *Sol. Energy Mater. Sol. Cells*, 2012, **103**, 114-118. (b) G. Griffini, *Front. Mater.*, 2019, **6**.

6. E. J. M. Hamilton, R.G. Kultyshev, B. Du, E.A. Meyers, S. Liu, C.M. Hadad, S.G. Shore, *Eur. J. Chem.*, 2006, **12**, 2571.

7. (a) J. R. Lakowicz, *Principles of Fluorescence Spectroscopy*, Springer, Boston, MA, 3rd edn., 2006. (b) X. Poteau, A. I. Brown, R. G. Brown. C. Holmes, D. Matthew, *Dyes Pigm.* 2000, **47**, 91-105.

8. E. P. L. Hunter and S. G. Lias, *J. Phys. Chem. Ref. Data*, 1998, **27**, 413-656.

9. (a) B. M. Graybill, J. K. Ruff and M. F. Hawthorne, *J. Am. Chem. Soc.*, 1961, **83**, 2669-2670. (b) Y. Li and L. G. Sneddon, *Inorg. Chem.*, 2006, **45**, 470-471.

10. National Institute of Standards and Technology: *Decaborane(14)*, US Department of Commerce, Washington, DC, 2021.

11. W. A. R. Franks, M. J. Kiik, and A. Nathan, *IEEE Trans. Electron Devices*, 2003, **50**, 352-358.

12. J. Salman, M. K. Gangishetty, B. E. Rubio-Perez, D. Feng, A. Yu, Z. Yang, C. Wan, M. Frising, A. Shahsafi, and D. N. Congreve, *J. Opt.*, 2021, **23**, 054001.

Chapter 4 – Synthesis and luminescence of monohalogenated B$_{18}$H$_{22}$ clusters

This chapter is a version of Anderson, K.P., Rheingold, A.L., Djurovich, P.I., Soman, O. and Spokoyny, A.M. Synthesis and luminescence of monohalogenated B$_{18}$H$_{22}$ clusters. *Submitted.*

4.1 Abstract

This work advances the foundation of *anti*-B$_{18}$H$_{22}$ chemistry by exploring cluster reactivity in the context of monohalogenation and the luminescent properties of the resulting compounds. The synthesis and photoluminescent properties of new *anti*-B$_{18}$H$_{22}$ derivatives 4-I-B$_{18}$H$_{21}$ and 7-Cl-B$_{18}$H$_{21}$ are described and benchmarked against other existing monohalogenated species reported previously. Electrophilic halogenation utilizing AlCl$_3$ and I$_2$ produces iodination at the B4 vertex to produce 4-I-B$_{18}$H$_{21}$ in 43% isolated yield. This compound exhibits oxygen-insensitive phosphorescence at 514 nm ($\Phi = 0.16$). Chlorination of the B7 vertex through treatment of the parent borane with N-chlorosuccinimide and hydrochloric acid gives 7-Cl-B$_{18}$H$_{21}$ in 76% isolated yield, which produces fluorescent emission at 418 nm and exhibits one of the highest quantum yields of B$_{18}$H$_{22}$ derivatives reported to date, $\Phi = 0.80$.

4.2 Introduction

Among the molecular luminescent materials containing boron,[1] *anti*-B$_{18}$H$_{22}$ is the only inherently fluorescent unfunctionalized polyhedral boron hydride known to date, exhibiting a quantum yield of 0.97.[2] This compound has recently gained more widespread attention due to its promise for optoelectronic applications, such as lasers, OLEDs and UV-imaging.[3] Despite this, much is still unknown regarding the synthetic diversification routes for *anti*-B$_{18}$H$_{22}$ and how substitutions at the boron vertices can alter its luminescent profile. The synthetic chemistry of *anti*-B$_{18}$H$_{22}$ is particularly more challenging given the more sophisticated cage structure compared to many other

polyhedral boranes, rendering classical spectroscopic tools such as ^{11}B NMR less informative for routine structural characterization. These challenges are particularly pronounced when analyzing asymmetrically functionalized B_{18}-based compounds, which can display up to 18 unique broad, quadrupolar chemical shifts in the ^{11}B NMR spectrum.[4] As a result, single crystal X-ray diffraction is an extremely valuable tool necessary to confirm the molecular structure of these boron clusters and has consequently proven instrumental in the synthetic investigations of this boron cluster family.

Derivatives of *anti*-$B_{18}H_{22}$ reported so far[5] give insight into the reactivity of the cluster (Figure 4.1). There have been several studies reporting the synthesis of di- and poly-functionalized B_{18}-based clusters. Interestingly, despite the report on the first monofunctionalized $B_{18}H_{22}$ clusters dating as early as 1968,[5f] chemical routes allowing to selectively position a single functional group at a predetermined vertex in this species are still lacking. For example, while several halogenation methods have led to the synthesis and isolation of 7-I and 4-Br, the 4-I and 7-Cl have been simple substituents on the fluorescent properties of *anti*-$B_{18}H_{22}$.[6] Dramatic differences in luminescent properties have already been observed between compounds with similar structures; for example, while 7-I-*anti*-$B_{18}H_{21}$ exhibits phosphorescence at 525 nm and a quantum yield of 0.41,[5d] monobrominated 4-Br-*anti*-$B_{18}H_{21}$ possesses a dual emission property in which fluorescence at 410 nm and phosphorescence at 503 nm occur simultaneously.[5c] It remains unclear if these differences are attributable to substituent identity (I vs. Br), substituent location (B7 or B4), or a
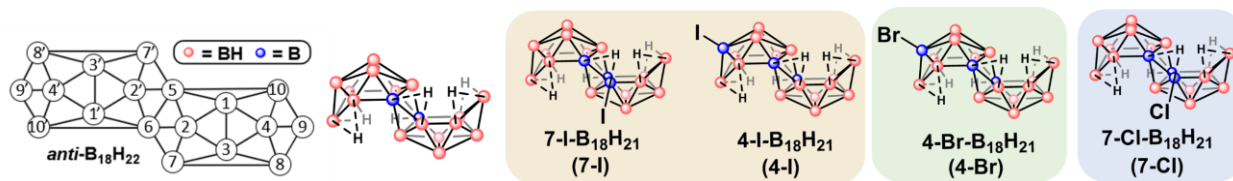
Figure 4.1. Structure and numbering scheme for *anti*-$B_{18}H_{22}$ and monohalogenated derivatives of *anti*-$B_{18}H_{22}$ in this and previously published works.[5a, 5c]

combination of both. To decouple the complex relationship between structure and luminescence, we expand the scope of monohalogenated B_{18} clusters with two new derivatives 4-I-*anti*-$B_{18}H_{21}$ (**4-I**) and 7-Cl-*anti*-$B_{18}H_{21}$ (**7-Cl**). Investigation of their luminescent properties revealed oxygen-insensitive phosphorescence in **4-I** and bright blue fluorescence in **7-Cl** that exhibits high efficiency with $\Phi = 0.80$.

4.3 Results and Discussion

Synthesis and Structural Analysis

Synthesis of 4-I-anti-B₁₈H₂₁ and 7-Cl-B₁₈H₂₁: A procedure used previously[5a] to prepare 4,4'-I_2-$B_{18}H_{20}$ was optimized to produce monohalogenated 4-I-anti-$B_{18}H_{21}$. Specifically, 1 eq. I_2 and 50 mol% $AlCl_3$ were reacted for 18 hours with *anti*-$B_{18}H_{22}$ dissolved in dichloromethane. *In situ* analysis of the resulting product mixture indicated the dominant presence of $B_{18}H_{21}I$ in the negative mode of electrospray ionization (ESI) mass spectrum (Figure S1). The pure monoiodinated compound was obtained in 43% isolated yield after purifying the crude product mixture by column chromatography on acidified silica gel. Spectroscopic characterization of purified product through ^{11}B NMR indicated an asymmetric boron cluster species with a diagnostic resonance corresponding to the newly substituted boron vertex at -49.2 ppm (Figures S2-4). Fifteen of the remaining peaks in the ^{11}B NMR spectrum show distinctive couplings to protons, overall confirming the monosubstitution pattern. Single crystal X-ray diffraction further confirmed the identity of the B4-substituted compound **4-I** (Figures 2, S15).

Success with the synthesis of **4-Br** previously and **4-I** in this study prompted us to expand this approach towards chlorination potentially targeting the B4 vertex through *in situ* generation of Cl_2 gas. This, however, proved challenging given the high reactivity of diatomic chlorine. When *anti-*$B_{18}H_{22}$ was treated with SO_2Cl_2 and $AlCl_3$ in 1,2-dichloroethane, the major species observed by electrospray ionization was $B_{18}H_{20}Cl_2$ (*m/z* = 284.24) accompanied by less intense mass peaks corresponding to $B_{18}H_{21}Cl$ and $B_{18}H_{19}Cl_3$. Purification by column chromatography on acidified silica gel produced the dichlorinated product, which appeared pure by mass spectrometry (Figure S9). However, analysis of this sample by ^{11}B NMR spectroscopy revealed two sets of boron resonances that indicated the sample contained two dichlorinated isomers (Figures S10-11). Neither modifications to this protocol nor the exploration of alternative electrophilic halogenation methods produced the desired B4-chlorinated products as a single isomer that could be successfully isolated chromatographically. Surprisingly, over the course of our studies, we discovered a set of conditions that produces a chlorinated isomer of $B_{18}H_{22}$ in which the B4 vertex remains unfunctionalized. Specifically, when the parent borane was reacted with Cl_2 gas produced *in situ* by treating N-chlorosuccinimide (NCS) with HCl/dioxane in dichloromethane[7] (Figure 4.2),
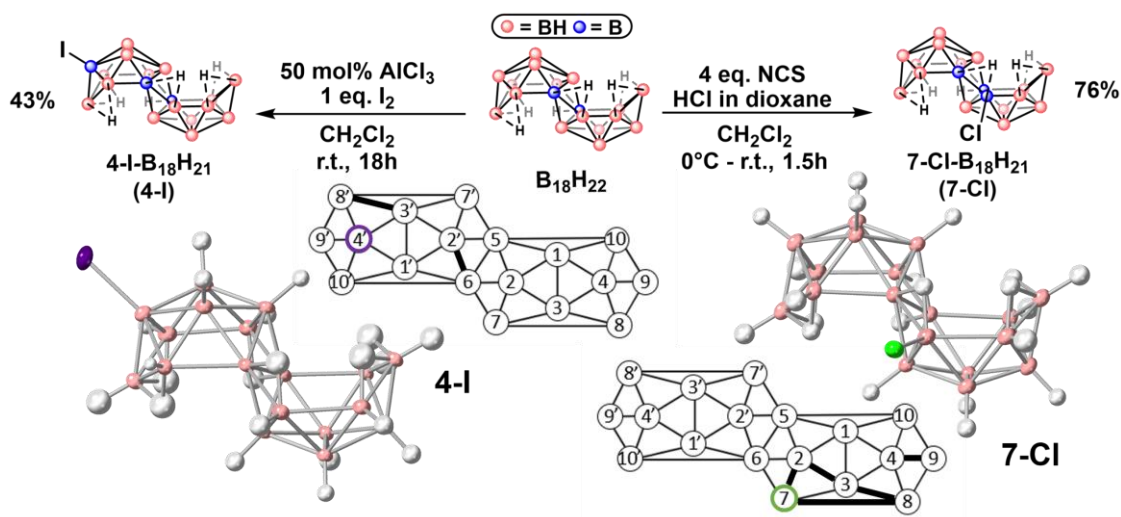
Figure 4.2. Synthetic schemes and crystal structures of **4-I** (left) and **7-Cl** (right), with significant bond lengthening denoted as bold bonds in the numbered structures. Thermal ellipsoids are drawn at 50% probability.

49

the only mass observed in the mass spectrum of the crude reaction mixture corresponded to $B_{18}H_{21}Cl$ (m/z = 250.32). After purification by filtration and an aqueous workup, the pure sample was analyzed by ^{11}B NMR (Figures S5-8). The presence of more than 9 apparent boron resonances suggested an asymmetric cluster structure, and the newly substituted boron vertex was denoted by a singlet at -0.88 ppm. The significant difference between this chemical shift and the -49.2 ppm resonance observed in **4-I** led us to suspect that the chloride substituent could reside on a vertex other than B4. Subsequent analysis by single crystal X-ray diffraction revealed that this molecule was indeed the B7-functionalized product, 7-Cl-$B_{18}H_{21}$ (Figure S16). The apparent preference for B7 chlorination under the employed conditions was surprising given that the only other B7-substituted $B_{18}H_{22}$ derivative reported to date, **7-I**, forms from the reaction of *anti*-$B_{18}H_{22}$ with I_2 in ethanol. Similarities between the **7-Cl** and **7-I** reaction conditions, such as the absence of $AlCl_3$ catalyst, suggest that vertex preference could be dictated by the reacting intermediates (i.e., X_2 vs X^+) arising from the halogenation conditions. While $AlCl_3$ assists in the formation of X^+ to yield B4 functionalization, B7 products likely form from the reaction of the parent borane with X_2, which is assisted by diatomic bond polarization from the employed solvent.[8] Notably, we attempted to synthesize the related 7-Br-*anti*-$B_{18}H_{21}$ cluster through similar means of employing N-bromosuccinimide activation. Indeed, we were able to purify a $B_{18}H_{21}Br$ compound (Figures S12-14) but have since been unable to confirm its location on the boron cage through single crystal X-ray diffraction due to our inability to grow X-ray quality crystals.

Structural Analysis of halogenated derivatives: Analysis of the monohalogenated $B_{18}H_{22}$ clusters through single crystal X-ray diffraction reveals that functionalization of the parent borane with halides leaves the overall cluster geometry intact (Table 4.1). Most bond lengths fit within three

Table 4.1. Select bond lengths (Å) of $B_{18}H_{22}$,[3] **4-I**, **7-Cl**, **7-I**,[5a] and **4-Br**[5c] with deviations from $B_{18}H_{22}$ greater than three standard uncertainties highlighted in blue. For **4-I**, connectivities are B' and B6 instead of B5 (e.g., B1'-B6).

Connectivity	$B_{18}H_{22} \cdot C_6H_6$	$4\text{-}I \cdot 2C_6H_6$	7-I	$7\text{-}Cl \cdot 2C_6H_6$	$4\text{-}Br \cdot 2C_6H_6$
B1-B2	1.786(5)	1.786(4)	1.780(5)	1.788(4)	1.750(7)
B1-B3	1.778(5)	1.786(5)	1.785(5)	1.782(4)	1.767(7)
B1-B4	1.786(5)	1.796(5)	1.806(5)	1.792(4)	1.804(6)
B1-B5 or B6	1.746(5)	1.754(4)	1.754(5)	1.757(4)	1.753(7)
B1-B10	1.74(5)	1.753(4)	1.754(5)	1.755(4)	1.766(7)
B2-B3	1.746(5)	1.766(4)	1.767(5)	1.769(4)	1.760(7)
B2-B5 or B6	1.765(5)	1.807(4)	1.800(5)	1.758(4)	1.816(7)
B2-B7	1.774(5)	1.792(5)	1.787(5)	1.799(4)	1.793(7)
B3-B4	1.774(5)	1.775(4)	1.780(5)	1.776(4)	1.772(7)
B3-B7	1.746(5)	1.756(4)	1.766(5)	1.758(4)	1.763(7)
B3-B8	1.723(5)	1.751(4)	1.761(5)	1.758(4)	1.758(7)
B4-B8	1.789(5)	1.801(4)	1.791(5)	1.802(4)	1.811(7)
B4-B9	1.702(5)	1.721(5)	1.712(5)	1.732(4)	1.735(7)
B4-B10	1.775(5)	1.781(4)	1.788(5)	1.785(4)	1.768(7)
B5 or B6-B10	1.968(5)	1.980(4)	1.971(5)	1.977(4)	1.990(7)
B5 or B6-B7	1.815(5)	1.820(5)	1.817(5)	1.823(4)	1.824(7)
B7-B8	1.946(5)	1.965(5)	1.972(5)	1.982(4)	1.973(7)
B8-B9	1.795(5)	1.797(5)	1.796(5)	1.790(4)	1.806(7)
B9-B10	1.783(5)	1.784(5)	1.778(5)	1.788(4)	1.789(7)
B-X	-	1.965(4)	2.173(5)	1.746(3)	1.906(7)

standard uncertainties compared to the parent $B_{18}H_{22}$, however the halogenated derivatives exhibit overall longer bonds. Select lengths of the newly synthesized compounds **4-I** and **7-Cl** are compared to those of $B_{18}H_{22}$ and the previously reported monohalogenated clusters **7-I** and **4-Br**. The most significant changes occur at bonds closest to the functionalized vertex. All structures exhibit a significant lengthening of B3-B8 and, except for **4-I**, B7-B8 bonds. Similarly, the B2-B5 (B2'-B6 for **4-I**) bonds show >0.035Å increases in every compound except **7-Cl**, in which it is slightly contracted. This contraction is compensated by significant lengthening in the B2-B3 and B2-B7 bonds of the chlorinated molecule. It is also worth noting that the B4-B9 connectivity is longer in all compounds, however **7-Cl** and **4-Br** show a remarkably longer B4-B9 bond than their iodinated analogues, **7-I** and **4-I**.

Photoluminescence Data

To gain insight into the effect of halogenation on the photophysical properties of B_{18}-based clusters, absorption and emission data of **4-I** and **7-Cl** were gathered in cyclohexane solution (Figure 4.3). The features in the absorption spectrum of **4-I** remain similar to the parent borane, but the absorptivity is diminished to ε = 4400 $M^{-1}cm^{-1}$, which is close to the absorptivity of **7-I** (Table 4.2, Figure S17). Like **7-I**, **4-I** exhibits phosphorescence albeit at a slightly higher emission energy of 514 nm, with no evidence of the dual luminescence observed in **4-Br**. This can be attributed to the heavy atom effect, which lends spin-orbit coupling (SOC) to the molecule that permits intersystem crossing (ISC) from the excited singlet to triplet state. In this case, the increased size and weight of iodide compared to bromide results in greater SOC/ISC and therefore complete phosphorescence. These data suggest that the absorption coefficient, emission wavelength, and nature of the luminescent process (fluorescence vs. phosphorescence) are primarily dictated by the identity of the substituent rather than its location. However, the 50%
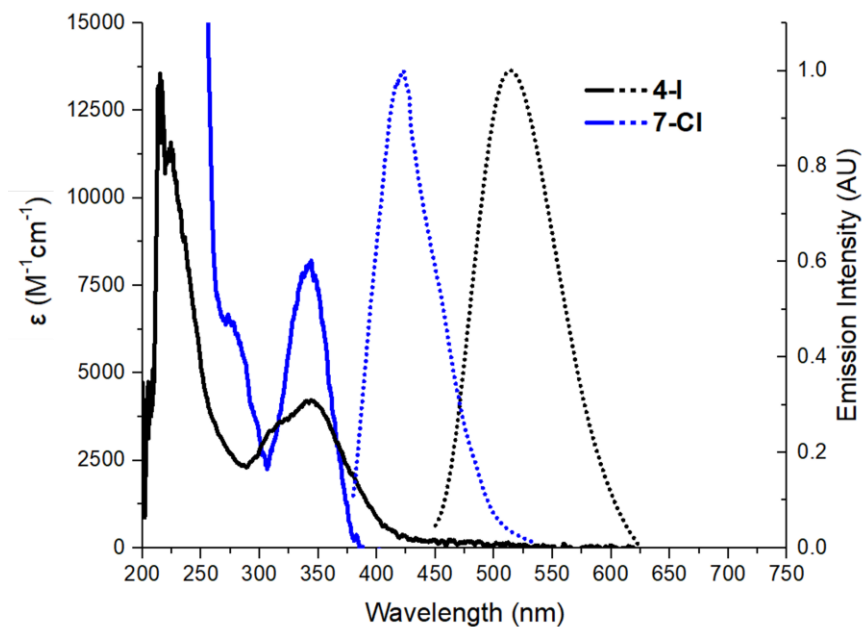
Figure 4.3. Absorption (solid) and emission (dotted) spectra of **4-I** and **7-Cl** in cyclohexane. λ_{exc} = 340 nm.

reduction in quantum yield when iodide resides at B4 (Φ = 0.16) as opposed to B7 (Φ = 0.41)

highlights the potentially inconspicuous effects of substituent location. Another interesting

distinction between the emission features of the two iodinated clusters is oxygen sensitivity;

phosphorescence, which originates from the triplet excited state, is typically subject to quenching

by molecular oxygen. Consequently, the quantum yield of phosphorescent compounds improves

under oxygen-free conditions. While this is observed with **7-I**, the quantum yield and lifetime of

4-I remain unchanged upon degassing the cyclohexane solution (Figure S18). Typically, such

insensitivity is caused by the inability of oxygen to interact with the molecule in the excited state

due to either significant steric hindrance or obstruction of the oxygen reactive site.[9] **4-I** does not

possess enough steric bulk to apply to the former, and quenching by oxygen has been observed in

other B4-halogenated derivatives, which suggests that the latter is also unlikely. Rather, the

insensitivity of phosphorescence to quenching by oxygen could be caused by the

spatial distribution of valence orbitals in **4-I**. Specifically, the Natural Transition Orbitals (NTOs)

determined from DFT calculations for the triplet excited state of **4-I** (Figure S21) show an electron

NTO that is distributed across the entire boron cluster, whereas the hole NTO resides mainly

localized on the iodide substituent. As phosphorescence quenching by oxygen takes place via

triplet energy transfer using a Dexter mechanism, sufficient overlap is required between the

valence orbitals of the interacting species (**4-I** and O_2).[10] Therefore, spatial confinement of the hole

Table 4.2. Summary of photophysical data of monohalogenated $B_{18}H_{22}$ clusters in cyclohexane solution.[3,5a,c,e] [a]Measured in oxygen-free cyclohexane. λ_{exc} = 350 nm for quantum yield measurements of **4-I** and **7-Cl**. See Figures S11-13 for data.

Compound	λ_{abs} (nm)	ε (M^{-1}cm^{-1})	λ_{em} (nm)	Φ	τ (μs)
$B_{18}H_{22}$	335	6800	408	0.97	0.0112
4-I-$B_{18}H_{21}$ (**4-I**)	342	4400	514	0.16[a]	1.2[a]
7-I-$B_{18}H_{21}$ (**7-I**)	365	4900	525	0.41[a]	27[a]
7-Cl-$B_{18}H_{21}$ (**7-Cl**)	344	8200	418	0.80	0.0083
4-Br-$B_{18}H_{21}$ (**4-Br**)	341	1900	410, 503	0.07[a]	0.0103, 11.6[a]

NTO in **4-I** could inhibit energy transfer by offering ineffective overlap with the corresponding molecular orbital on oxygen.

7-Cl also exhibited interesting absorption and emission properties (Figure S19). First, the absorptivity (ε = 8200 M^{-1}cm^{-1}) exceeds that of B$_{18}$H$_{22}$ and is on par with the absorptivity of the only other chlorinated compound reported to date.[5d] In contrast to the other halogenated compounds, **7-Cl** exhibits completely fluorescent emission at 418 nm. The absence of phosphorescence can be explained in part by the lighter and smaller nature of the chloride substituent compared to iodide or bromide. In addition, the difference in energy between the HOMO and HOMO-1 is large (ΔE = 0.9 eV). These orbitals have large contributions from orthogonal p-orbitals on the chloride atom and, following El-Sayed's rules,[11] are responsible for the change in angular momentum needed for effective SOC. The large energy separation between the filled valence orbitals results in poor SOC and raises the energy for the S$_2$ and T$_2$ states (HOMO-1 $\rightarrow$ LUMO, S$_2$ = 5.5 eV, T$_2$ = 5.1 eV), which further contributes to the inefficient ISC (Figure S22). While population of the excited triplet state does occur, phosphorescence is only visible as a shoulder at ~500 nm in the emission spectrum at 77 K (Figures S19-20). Therefore, the fluorescent nature of emission is maintained under ambient conditions and is red-shifted only slightly from the parent compound. The lifetime (8.3 ns) of this process is too fast to permit luminescence quenching by oxygen, and therefore does not change between ambient and degassed solutions. The quantum yield of **7-Cl** is also one of the highest of all B$_{18}$-based compounds reported to date, with Φ = 0.80.

4.4 Conclusion

The syntheses of two new halogenated *anti*-B$_{18}$H$_{22}$ derivatives, 4-I-*anti*-B$_{18}$H$_{21}$ (**4-I**) and 7-Cl-*anti*-B$_{18}$H$_{21}$ (**7-Cl**) have been reported and benchmarked in the context of previously reported

54

monohalogenated analogues. While electrophilic halogenation at the B4 vertex has successfully produced **4-Br** and **4-I**, attempts to synthesize the analogous chlorinated structure in this work instead resulted in **7-Cl**, which is the only reported B7-substituted $B_{18}H_{22}$ derivative apart from **7-I**. The structures of these compounds derived from single crystal X-ray diffraction show the overall cluster geometry is unperturbed, however significant bond lengthening between the B3-B8 and B7-B8 connectivities is observed for most clusters. In contrast to the other halogenated compounds, **7-Cl** exhibits B2-B5 bond contraction coupled with lengthening between the neighboring B2-B3 and B2-B7 bonds. While these minor structural differences exist, it is clear from the photophysical data that the absorption, emission, and quantum yields are greatly influenced by the identity and placement of halides. The bathochromic shifts in emission become successively larger from chlorine to iodine, with the heavier iodide and bromide substituents increasing the compound's phosphorescent character. Interestingly, ε seems to be largely affected by the halide identity, with only **7-Cl** exhibiting improved absorptivity over the unfunctionalized borane. In contrast, the quantum yield is highly susceptible to all aspects of structural modification; significant differences are not only observed between different halides, but also in vertex-differentiated clusters containing the same halide. As research into the synthetic and photoluminescent properties of *anti*-$B_{18}H_{22}$ derivatives grows, structure-function relationships will become an increasingly important aspect of chromophore design. To that end, this work expands the foundation of synthetic modification of *anti*-$B_{18}H_{22}$, provides additional structural evidence through single crystal X-ray crystallography, and expands our understanding of the resulting luminescent properties of the substituted compounds.

4.5 References

1. Recent representative examples: (a) K. K. Hollister, A. Molino, G. Breiner, J. E. Walley, K. E. Wentz, A. M. Conley, D. A. Dickie, D. J. D. Wilson and R. J. Gilliard, *J. Am. Chem. Soc.*, 2022, **144**, 590-598. (b) W. Yang, K. E. Krantz, L. A. Freeman, D. A. Dickie, A. Molino, A. Kaur, D. J. D. Wilson and R. J. Gilliard Jr, *Chem. Eur. J.*, 2019, **25**, 12512-12516. (c) X. Su, T. A. Bartholome, J. R. Tidwell, A. Pujol, S. Yruegas, J. J. Martinez and C. D. Martin, *Chem. Rev.*, 2021, **121**, 4147-4192. (d) K. O. Kirlikovali, J. C. Axtell, K. Anderson, P. I. Djurovich, A. L. Rheingold and A. M. Spokoyny, *Organometallics*, 2018, **37**, 3122-3131. (e) Z. Huang, S. Wang, R. D. Dewhurst, N. V. Ignat'ev, M. Finze and H. Braunschweig, *Angew. Chem. Int. Ed.*, 2020, **59**, 8800-8816. (f) Y. Lebedev, C. Apte, S. Cheng, C. Lavigne, A. Lough, A. Aspuru-Guzik, D. S. Seferos and A. K. Yudin, *J. Am. Chem. Soc*, 2020, **142**, 13544-13549. (g) H. S. Soor, D. B. Diaz, K. I. Burton and A. K. Yudin, *Angew. Chem. Int. Ed.*, 2021, **60**, 16366-16371. (h) X. Wu, J. Guo, Y. Quan, W. Jia, D. Jia, Y. Chen and Z. Xie, *J. Mater. Chem. C*, 2018, **6**, 4140-4149. (i) J. Wang, N. Wang, G. Wu, S. Wang and X. Li, *Angew. Chem. Int. Ed.*, 2019, **58**, 3082-3086. (j) K. Zhang, Y. Shen, X. Yang, J. Liu, T. Jiang, N. Finney, B. Spingler and S. Duttwyler, *Chem. Eur. J.*, 2019, **25**, 8754-8759. (k) Ž. Ban, Z. Karačić, S. Tomić, H. Amini, T. B. Marder and I. Piantanida, *Molecules*, 2021, **26**. (l) J. He, F. Rauch, A. Friedrich, J. Krebs, I. Krummenacher, R. Bertermann, J. Nitsch, H. Braunschweig, M. Finze and T. B. Marder, *Angew. Chem. Int. Ed.*, 2021, **60**, 4833-4840. (m) A. V. Marsh, M. J. Dyson, N. J. Cheetham, M. Bidwell, M. Little, A. J. P. White, C. N. Warriner, A. C. Swain, I. McCulloch, P. N. Stavrinou, S. C. J. Meskers and M. Heeney, *Adv. Electron. Mater.*, 2020, **6**, 2000312. (n) J. Ochi, K. Tanaka and Y. Chujo, *Angew. Chem. Int. Ed.*, 2020, **59**, 9841-9855. (o) L. Ji, S. Griesbeck and T. B. Marder, *Chem. Sci.*, 2017, **8**, 846-863. (p) J. C. Axtell, K. O. Kirlikovali, P. I. Djurovich, D. Jung, V. T. Nguyen, B. Munekiyo, A. T. Royappa, A. L.

Rheingold and A. M. Spokoyny, *J. Am. Chem. Soc.*, 2016, **138**, 15758-15765. (q) K. O. Kirlikovali, J. C. Axtell, A. Gonzalez, A. C. Phung, S. I. Khan and A. M. Spokoyny, *Chem. Sci.*, 2016, **7**, 5132-5138. (r) P. Li, D. Shimoyama, N. Zhang, Y. Jia, G. Hu, C. Li, X. Yin, N. Wang, F. Jäkle and P. Chen, *Angew. Chem. Int. Ed.*, 2022, **61**, e202200612. (s) Z. Wu, J. Nitsch, J. Schuster, A. Friedrich, K. Edkins, M. Loebnitz, F. Dinkelbach, V. Stepanenko, F. Würther, C. M. Marian, L. Ji and T. B. Marder, *Angew. Chem. Int. Ed.*, 2020, **59**, 17137-17144. (t) T. Butler, M. Zhuang and C. L. Fraser, *J. Phys. Chem. C*, 2018, **122**, 19090-19099. (u) S. Ohtani, M. Gon, K. Tanaka and Y. Chujo, *Macromolecules*, 2019, **52**, 3387-3393. (v) J. Li, J. Xu, L. Yan, C. Lu and H. Yan, *Dalton Trans.*, 2021, **50**, 8029-8035. (w) K. L. Martin, J. N. Smith, E. R. Young and K. R. Carter, *Macromolecules*, 2019, **52**, 7951-7960. (x) S. Sinha, Z. Kelemen, E. Hümpfner, I. Ratera, J.-P. Malval, J. P. Jurado, C. Viñas, F. Teixidor and R. Núñez, *Chem. Commun.*, 2022, **58**, 4016-4019. (y) X. Wu, J. Guo, Y. Cao, J. Zhao, W. Jia, Y. Chen and D. Jia, *Chem. Sci.*, 2018, **9**, 5270-5277. (z) A. V. Marsh, N. J. Cheetham, M. Little, M. Dyson, A. J. P. White, P. Beavis, C. N. Warriner, A. C. Swain, P. N. Stavrinou and M. Heeney, *Angew. Chem. Int. Ed.*, 2018, **57**, 10640-10645. (aa) S. Kim, J. H. Lee, H. So, M. Kim, M. S. Mun, H. Hwang, M. H. Park and K. M. Lee, *Inorg. Chem. Front.*, 2020, **7**, 2949-2959.

2. J. Ševčík, P. Urbánek, B. Hanulíková, T. Čapková, M. Urbánek, J. Antoš, M. G. S. Londesborough, J. Bould, B. Ghasemi, L. Petřkovský and I. Kuřitka, *Materials*, 2021, **14**.

3. L. Cerdán, J. Braborec, I. Garcia-Moreno, A. Costela and M. G. S. Londesborough, *Nat. Commun.*, 2015, **6**, 5958.

4. M. G. S. Londesborough, J. Dolanský, T. Jelínek, J. D. Kennedy, I. Císařová, R. D. Kennedy, D. Roca-Sanjuán, A. Francés-Monerris, K. Lang and W. Clegg, *Dalton Trans.*, 2018, **47**, 1709-1725.

5. (a) M. G. S. Londesborough, J. Dolanský, J. Bould, J. Braborec, K. Kirakci, K. Lang, I. Císařová, P. Kubát, D. Roca-Sanjuán, A. Francés-Monerris, L. Slušná, E. Noskovičová and D. Lorenc, *Inorg. Chem.*, 2019, **58**, 10248-10259. (b) V. Saurí, J. M. Oliva, D. Hnyk, J. Bould, J. Braborec, M. Merchán, P. Kubát, I. Císařová, K. Lang and M. G. S. Londesborough, *Inorg. Chem.*, 2013, **52**, 9266-9274. (c) K. P. Anderson, M. A. Waddington, G. J. Balaich, J. M. Stauber, N. A. Bernier, J. R. Caram, P. I. Djurovich and A. M. Spokoyny, *Dalton Trans.*, 2020, **49**, 16245-16251. (d) M. G. S. Londesborough, K. Lang, W. Clegg, P. G. Waddell and J. Bould, *Inorg. Chem.*, 2020, **59**, 2651-2654. (e) K. P. Anderson, A. S. Hua, J. B. Plumley, A. D. Ready, A. L. Rheingold, T. L. Peng, P. I. Djurovich, C. Kerestes, N. A. Snyder, A. Andrews, J. R. Caram, A. M. Spokoyny, preprint DOI: 10.26434/chemrxiv-2022-h70dk. (f) F. P. Olsen, R. C. Vasavada, M. F. Hawthorne. *J. Am. Chem. Soc.*, 1968, **90**, 3946-3951.

6. (a) M. G. S. Londesborough, D. Hnyk, J. Bould, L. Serrano-Andrés, V. Sauri, J. M. Oliva, P. Kubát, T. Polívka and K. Lang, *Inorg. Chem.*, 2012, **51**, 1471-1479. (b) M. G. S. Londesborough, J. Dolanský, L. Cerdán, K. Lang, T. Jelínek, J. M. Oliva, D. Hnyk, D. Roca-Sanjuán, A. Francés-Monerris, J. Martinčík, M. Nikl and J. D. Kennedy, *Adv. Opt. Mater.*, 2017, **5**, 1600694. (c) L. Cerdán, A. Francés-Monerris, D. Roca-Sanjuán, J. Bould, J. Dolanský, M. Fuciman and M. G. S. Londesborough, *J. Mater. Chem. C*, 2020, **8**, 12806-12818.

7. Synthesis derived from: A. Nishiguchi, K. Maeda and S. Miki, *Synthesis*, 2006, 4131.

8. (a) W. Lorpaiboon and P. Bovonsombat, *Org. Biomol. Chem.*, 2021, **19**, 7518-7534. (b) M. Zhang and C. R. F. Lund, *J. Phys. Chem. A*, 2002, **106**, 10294-10301. (c) G. L. Borosky, S. Stavber and K. K. Laali, *Top. Catal.*, 2018, **61**, 636-642.

9. (a) L. Straub, D. González-Abradelo and C. A. Strassert, *Chem. Comm.*, 2017, **53**, 11806-11809. (b) T. Zhang, C. Wang and X. Ma, *Ind. Eng. Chem. Res.*, 2019, **58**, 7778-7785. (c) I. O. Koshevoy, Y.-C. Lin, Y.-C. Chen, A. J. Karttunen, M. Haukka, P.-T. Chou, S. P. Tunik and T. A. Pakkanen, *Chem. Comm.*, 2010, **46**, 1440-1442.

10. (a) G. L. Closs, P. Piotrowiak, J. M. MacInnis, G. R. Fleming, *J. Am. Chem. Soc.*, 1988, **110**, 2643-2655. (b) G. L. Closs, M. D. Johnson, J. R. Miller, P. Piotrowiak, *J. Am. Chem. Soc.*, 1989, **111**, 3751-3753. (c) S. K. Lower and M. A. El-Sayed, *Chem. Rev.*, 1966, **66**, 199-241.

Chapter 5 – Metal-Catalyzed and Metal-Free Nucleophilic Substitution of 7-I-B$_{18}$H$_{21}$

This chapter is a version of Anderson, K.P., Djurovich, P.I., Rubio, V. P., Liang, A. and Spokoyny, A.M. Metal-Catalyzed and Metal-Free Nucleophilic Substitution of 7-I-B$_{18}$H$_{21}$. *Submitted.*

5.1 Abstract

In this work, two pathways of reactivity are investigated to generate site-specific substitutions at the B7 vertex of the luminescent boron cluster, *anti*-B$_{18}$H$_{22}$. First, a palladium-catalyzed cross-coupling reaction utilizing the precursor 7-I-B$_{18}$H$_{21}$ and a series of model nucleophiles was developed, ultimately producing several B-N and B-O substituted species. Interestingly, the B-I bond in this cluster can also be substituted in an uncatalyzed fashion, leading to the formation of various B-N, B-O, and B-S products. This work highlights intricate differences corresponding to these two reaction pathways and analyzes the role of solvents and additives on the product distributions. As a result of our synthetic studies, seven new B$_{18}$-based clusters were synthesized, isolated, and characterized by mass spectrometry and Nuclear Magnetic Resonance (NMR) spectroscopy. The photoluminescent properties of two structurally similar ether and thioether products were further investigated, with both exhibiting blue fluorescence in solution at 298 K and long-lived green or yellow phosphorescence at 77 K. Overall, this work shows for the first time the ability to perform substitution of a boron-halogen bond with nucleophiles in a B$_{18}$-based cluster, resulting in the formation of photoluminescent molecules.

5.2 Introduction

Boron-halogen (B-X) bond substitution has proven to be a general and versatile transformation that permits precise placement of various substituents on different polyhedral boron cages.[1] This reactivity has led to broad accessibility of new and interesting molecular architectures, particularly

for *closo*-boranes such as carboranes and dodecaborate-based clusters.[2] B-X bond substitution in these species is usually achieved through metal-mediated means, such as cross-coupling, that can procure B-C, B-N, B-O, B-P, and B-S bonds.[3] Other methods include light-promoted homolytic cleavage of the boron-halogen bond leading to the formation of a B-centered radical, which can then undergo further substitution reaction.[4] Another strategy for activating a boron-halogen bond centers on the oxidation of the halogen, resulting in the formation of an iodonium substituent that permits a more facile nucleophilic attack at the boron.[5] Interestingly, in contrast to the classical alkyl C-X bonds, nucleophilic substitution of B-X cluster bonds is generally intractable, with only a handful of reports to date.[6] This can be generally ascribed to the increased strength of B-X bonds and the steric bulk of the cage that prevents nucleophilic attack on the side opposite the halide.[7]

Anti-$B_{18}H_{22}$ is a boron cluster which has gained recent attention as an inherently fluorescent boron hydride (λ_{em} = 410 nm, Φ = 0.97) that has potential for various photoluminescence applications.[8] In order to tune the luminescent properties of the parent compound, selective derivatization methods for this cluster are needed. While there exist a number of routes that can place a halogen moiety onto various vertices of this boron hydride, surprisingly, there have been no reports so far exploring the post-functionalization of these boron-halogen bonds. Unlike *closo*-based clusters for which boron-halogen substitution chemistry has been established, the open-face polyhedral cage configuration of *anti*-$B_{18}H_{22}$ presents several distinct synthetic challenges, including the presence of acidic bridging hydrogens (pK_a = 2.7 and 7.5)[9] and reduced stability profile (Figure 5.1A).[8h] In this work, we report our initial assessment for the feasibility of substituting a boron-iodine bond at the B7 vertex of the *anti*-$B_{18}H_{22}$ cluster. Specifically, we report the discovery of metal-catalyzed and metal-free pathways capable of producing B-N, B-O, and B-S bonds, ultimately leading to new B_{18}-based chromophores with tunable photoluminescent properties. Overall, this work

61

represents the first example of B-X bond substitution in *anti*-$B_{18}H_{22}$ and provides a potential roadmap toward the development of a broad scope of B_{18}-based luminescent materials.

5.3 Results and Discussion

To examine the feasibility of metal-catalyzed cross-coupling for halogenated *anti*-$B_{18}H_{22}$ clusters, we decided to employ the Buchwald-Hartwig amidation conditions previously reported for B-iodo-carboranes.[10] Monoiodinated 7-I-$B_{18}H_{21}$ (**1**) was selected as the borane precursor due to its straightforward and high-yielding synthesis[8c] and 2,2,2-trifluoroacetamide (**I**) was used as a coupling partner. This nucleophile was specifically chosen for its inability to undergo β-hydride elimination and its low pK_a resulting in facile deprotonation during the transmetallation step.[11] The reaction progress and products formed were monitored *in situ* by electrospray ionization mass spectrometry in the negative mode (ESI(-)MS). While the initially selected conditions did not result in significant conversion of the starting material as observed by ESI(-)MS (Figure 5.1C, Entry 1), a mass consistent with product **2** was observed when the ligand and catalyst loading were increased from 10 mol% and 5 mol% to 50 mol% and 25 mol%, respectively (Figure 5.1C, Entry 2). However, degradation to a non-cluster species was also indicated by a significant amount of a water-soluble solid that manifested as a sharp singlet at ~13 ppm in the ^{11}B NMR spectrum. The formation of this unidentified byproduct was observed to a lesser extent when 1,4-dioxane was used as a solvent, however only $B_{18}H_{22}$ was observed by ESI(-)MS, suggesting a competing reduction pathway (Figure 5.1C, Entry 3). We previously employed palladium-based precatalysts in combination with biaryl phosphine ligands, which proved superior in cross-coupling efficiency
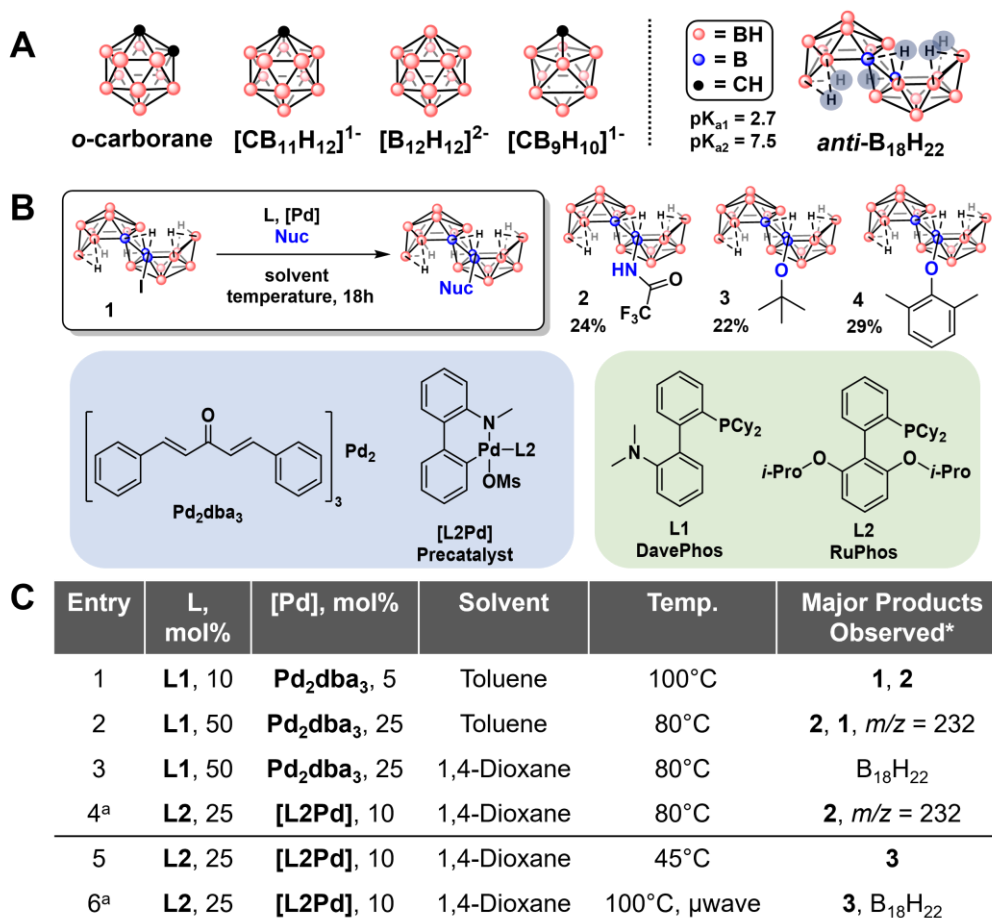
Figure 5.1. A) Select *closo*-boranes that can undergo metal-catalyzed cross-coupling vs. the *nido anti*-B$_{18}$H$_{22}$ cluster. B) General cross-coupling conditions, ligands and catalysts used, and resulting products **2**-**4** with isolated yields. C) Screening conditions employed to produce products **2** and **3**. See SI for general screening conditions procedure. [a]Done on a 30mg scale. *In order of decreasing intensity by ESI(-)MS.

for B-halo-carboranes compared to the conventional Pd$_2$dba$_3$ (Tris(dibenzylideneacetone)dipalladium(0)) precursor (Figure 5.1B).[12] Gratifyingly, improved conversion to product **2** in 1,4-dioxane was thereby achieved with a RuPhos/RuPhos Pd G4 precatalyst system (L2/[L2Pd], Figure 5.1B). Further optimization revealed that L2/[L2Pd] loading could be reduced to 25 mol%/10 mol% while maintaining nearly complete conversion (Figure 5.1C, Entry 4). With these optimized conditions we were able to purify the product mixture and isolate **2** as an analytically pure solid in 24% yield. The significant yield reduction is attributed to both the competing reduction pathway that produces B$_{18}$H$_{22}$ and the acidified silica gel column

chromatography conditions, which results in loss of the product material.[6c,13] Nevertheless, the reaction conditions also proved effective with a K*t*BuO substrate (**II**) to yield the monosubstituted boron cluster product, **3** (Figure 5.1C, Entry 5). This B-O cross-coupling can also be conducted in a microwave reactor at 100°C for 45 minutes (Figure 5.1C, Entry 6). In addition to appending the alkyl *t*BuO substituent, we found that this reaction is suitable for the bulky aromatic substrate potassium 2,6-dimethylphenolate to yield **4**. The metal-mediated nature of these reactions is supported by Figure S46.

With the isolated B-N and B-O products in hand, we turned to heteronuclear NMR spectroscopy for further characterization of compounds **2-4**; each were subject to ^{13}C, $^{1}H\{^{11}B\}$, ^{11}B NMR and $^{1}H\{^{11}B\}$-$^{11}B\{^{1}H\}$ Heteronuclear Multiple Quantum Coherence (HMQC) analysis (Figures S8-12). Taking **3** as an example, the presence of the *tert*-butyl group is supported by characteristic resonances in the ^{13}C NMR spectrum (-29.95 ppm and-78.24 ppm) and the singlet at 1.48 ppm in the $^{1}H\{^{11}B\}$ NMR spectrum. Also present in the $^{1}H\{^{11}B\}$ NMR spectrum are resonances corresponding to the 15 terminal and 6 bridging hydrogen nuclei on the boron cage, which is consistent with a monosubstituted product. The 18 boron nuclei are represented in the $^{11}B\{^{1}H\}$ NMR spectrum, and analysis of the corresponding ^{11}B NMR spectrum shows that all but three of these resonances exhibit doublet splitting, indicating they are bound to a terminal hydrogen. The three singlets at 8.33, 0.71, and -1.10 ppm should correspond to vertices B5, B6, and the newly substituted B7 (see Figure 5.2 for the numbering scheme). Integration of the boron resonances indicate that while 18 boron nuclei are present, several share similar chemical shifts, which makes definitive assignment of the boron resonances between 5 and -5 ppm more challenging. Therefore, a HMQC study of the $^{11}B\{^{1}H\}$ and $^{1}H\{^{11}B\}$ NMR spectra was conducted to assign the boron resonances and to confirm the overall structure of the molecule (Figure 5.2). The bridging

hydrogen resonances in the HMQC spectrum provide an ideal starting point for the analysis of the 2D spectrum because they correspond to two separate boron nuclei. For example, the identification of the B8-B9 bridging hydrogen H8-9 resonance at -2.90 ppm[10c] leads to the assignment of the resonances at -3.08 ppm and 2.62 ppm to the boron nuclei B8 and B9, respectively. In addition, the B9 resonance corresponds to a proton resonance at -0.26 ppm, which then correlates to two different boron resonances. This must signify the B9-B10 bridging hydrogen, which in turn leads to the assignment of the resonance at 9.63 ppm to the B10 nucleus. Continuing this process leads to the identification of the bridging hydrogens H5-7' and H6-7 *via* their resonances at -0.66 and 0.98 ppm, respectively. From this, one can assign the B5 (0.71 ppm), B6 (8.33 ppm), and B7 (-1.10 ppm) nuclei to the initially observed singlets in the ^{11}B NMR spectrum. The significant
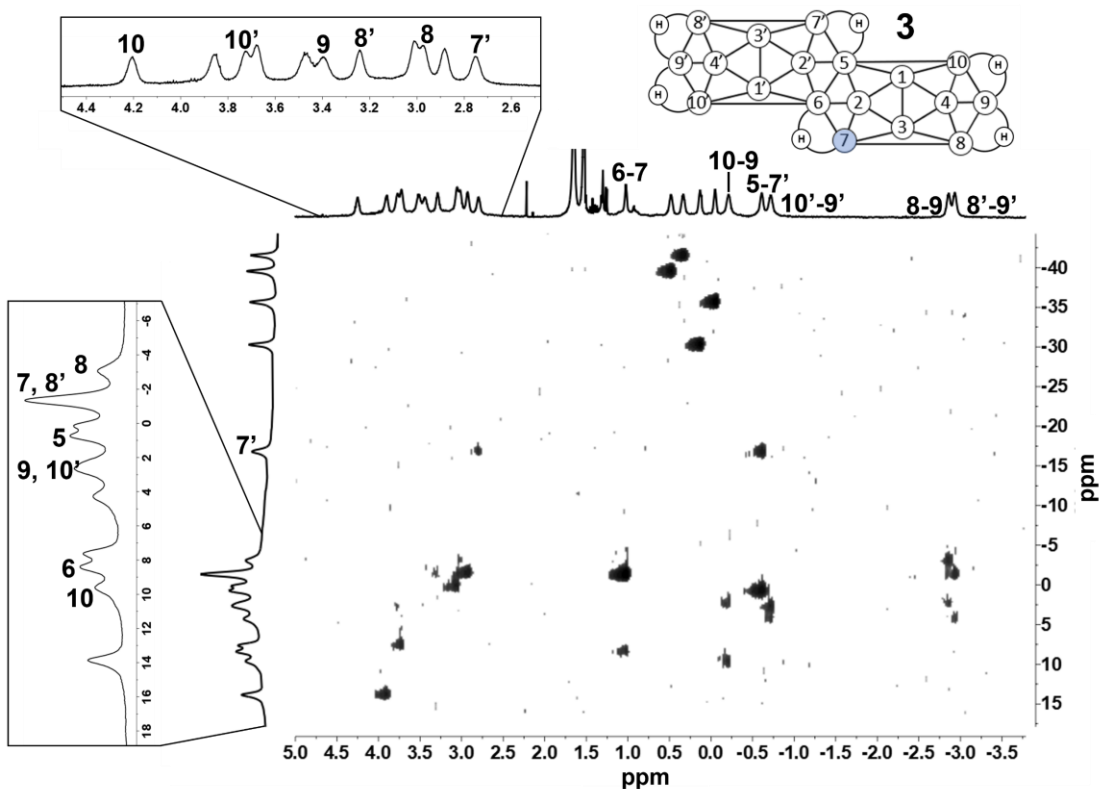
**Figure 5.2.** ^{1}H{^{11}B}-^{11}B{^{1}H} HMQC of **3** with select boron and hydrogen resonances labeled according to the numbering scheme at the top (substituted B7 vertex is highlighted in blue).

downfield shift of the B7 resonance compared to the B7' resonance and the absence of a B7 terminal hydrogen resonance is consistent with the B7-substituted nature of the cluster.

As we turned our attention to expanding the scope of cross-coupling to forge B-S bonds, we noticed product masses in the ESI(-)MS of the crude reaction mixtures that were not observed in previous reactions. For example, when the cross-coupling conditions were applied to potassium 2,6-dimethylthiophenolate (**III**), a mass corresponding to the desired B-S substituted cluster product plus a dioxane solvent molecule ($m/z = 440.38$) was the major species by ESI(-)MS. Similar results were observed when the reaction was conducted in THF ($m/z = 424.38$) (Figure S19). Upon isolation of this THF-containing compound, analysis by 1D and 2D ^{11}B NMR spectroscopy indicated a monosubstituted cluster pattern, with the functionalized B7 resonance at -3.83 ppm. The ^{1}H$\{^{11}$B$\}$ NMR spectrum contained resonances corresponding to 21 cluster hydrogens (-3 to 5 ppm) and the thioether group (7.11 and 2.57 ppm), but the distinctive THF resonances at 1.85 and 3.76 ppm were not observed. Instead, triplets at 3.97 and 2.73 ppm and multiplets at 1.82 and 1.71 ppm were present, suggesting the presence of a linear alkyl ether motif rather than an intact ethereal ring (Figure S20). This observation was further supported by ^{13}C and ^{13}C APT NMR spectroscopic experiments (Figures S23-25), which depict carbon resonances for both the thioether (143.20, 133.78, 128.25, 128.23, 22.8 ppm) and alkyl ether (70.33, 35.21, 30.49, and 36.56 ppm). In total, these data led us to conclude that the compound consisted of a B7-O bound, ring-opened THF molecule that resides between the electrophilic boron cluster and nucleophilic substrate (**5**).

To our surprise, further control experiments that excluded the palladium-based precatalyst and ligand from the reaction led to significant formation of **5** when the mixture was analyzed by ESI(-

)MS *in situ*. This observation ultimately suggested that nucleophilic substitution of 7-I-B$_{18}$H$_{21}$ can potentially proceed *via* a separate mechanism that does not involve oxidative addition of Pd(0) into a B-I bond. This is significant considering that a metal-free route toward B$_{18}$H$_{22}$ functionalization could alleviate some of the limitations observed in the metal-catalyzed reactions, specifically the competing reduction process that produces B$_{18}$H$_{22}$ and the slow reductive elimination step that necessitates sterically bulky substrates.[16] To explore this opportunity further, we examined the conditions under which products similar to **5** could form for various substrates (Figure 5.3A). When individual substrates **I-V** were combined with **1** in THF at 80-100°C, the ESI(-)MS spectrum of each reaction mixture exhibited only the mass corresponding to its respective alkyl ether product derived from THF ring-opening. The only exception was the K^{t}BuO (**II**) reaction mixture, which also contained a mass corresponding to the direct nucleophilic substitution product **3**. To determine if interconversion between these two compounds was possible, the reaction mixture was further refluxed for 18 hours but showed no change in the
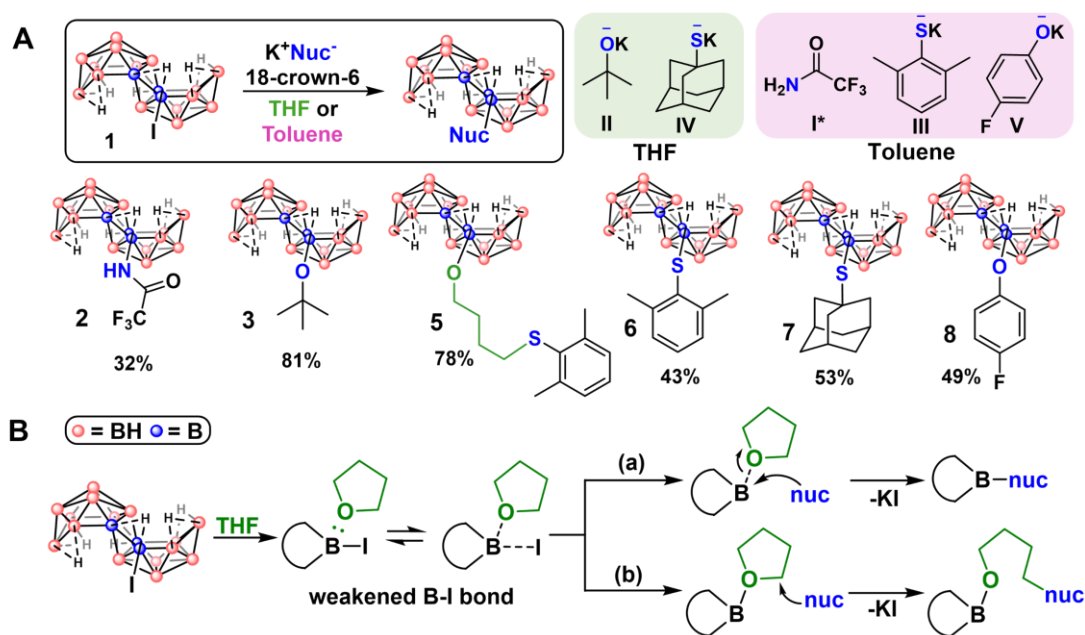
Figure 5.3. A) Reaction for nucleophilic substitution, substrates employed, and resulting products. Substrates can undergo substitution in THF (green) or toluene (pink). B) Pathways of reactivity for nucleophiles reacting with **1** in THF solution. *K$_3$PO$_4$ is included in the reaction mixture.

67

product distribution as observed by ESI(-)MS. This finding led us to consider two possible pathways of reactivity for this reaction (Figure 5.3B). The Lewis acidic B_{18}-based cluster can interact with THF[10h] to weaken the B-I bond, providing sufficiently nucleophilic substrates such as **II** the opportunity to attack the boron atom (Figure 5.3B(a)). Weaker nucleophiles, however, will react at the THF carbon to yield the ring-opened product (Figure 5.3B(b)). To probe the conditions under which each pathway could be potentially favored, we reacted **1** with **II** in THF at room temperature. This provided nearly full conversion to **3** as observed by ESI(-)MS, suggesting that the ring-opened product is favored at elevated temperatures. These results, however, were exclusive to **3**; only the THF-derived products were observed by ESI(-)MS for the other substrates, even when the reactions were conducted at -78°C. While sulfur-based reagents **III** and **IV** are more nucleophilic than their oxygen counterparts, the thermodynamic preference for B-O bond formation compared to B-S congener renders the formation of products **6** and **7** less favorable than the corresponding THF-derived products.[17] In an effort to overcome this, we found that incorporation of 18-crown-6 in the reaction mixture increases conversion to products **3** and **7** as observed by ESI(-) MS, possibly due to the increased Lewis basicity of the substrate caused by sequestration of the cation.[17] The remaining substrates **I**, **III**, and **V** however, still required a more inert solvent to avoid the ring-opening pathway altogether (Figure 5.3A, pink). As such, when **I**, **III**, and **V** are reacted with **1** in toluene there is no conversion observed by ESI(-)MS, yet including 18-crown-6 in the reaction mixture ultimately produces the desired compounds **2**, **6**, and **8**. Overall, the ability for substrates **I**, **III** and **V** to undergo nucleophilic substitution is aided not only by the crown ether but also toluene, which has a destabilizing effect on the nucleophile by solvating it to a lesser degree than THF.[18] Compounds **2**, **3**, and **5**-**8** can be easily isolated from the corresponding reaction mixtures. Structural formulations of these products were confirmed by ESI(-)MS and

$^1H\{^{11}B\}$, $^{11}B\{^1H\}$, ^{11}B, ^{13}C, ^{19}F, HMQC NMR spectroscopy. Interestingly, neither the reactions in THF nor toluene led to significant formation of **4**, potentially due to its weak nucleophilicity. Cross-coupling therefore remains the most viable route for producing **4** and other structures unsuitable for nucleophilic substitution. Still, the ability for 7-I-$B_{18}H_{21}$ to undergo metal-free nucleophilic substitution at the B-I bond is remarkable given the comparatively inert nature of boron-halogen bonds in other polyhedral borane clusters.

Given that this is the first report of ether and thioether-functionalized *anti*-$B_{18}H_{22}$, we wanted to benchmark the luminescent properties of these new derivatives. Specifically, the structurally similar compounds **4** and **6** were assessed to gauge the effects of oxygen vs. sulfur on cluster luminescence (Figure 5.4). In cyclohexane solution, the absorption of both compounds is largely in the UV region, with ($\varepsilon_{346} = 6600$ $M^{-1}cm^{-1}$ for **4** and $\varepsilon_{392} = 3300$ $M^{-1}cm^{-1}$ for **6**). Emission spectra of these solutions show blue fluorescence at 427 nm and 460 nm in **4** and **6**, respectively (Figure 5.4, S50, S52). Notably, this emission was exceptionally weak, with quantum yields (Φ) less than 0.01. However, when the measurements were repeated at 77 K the luminescence was significantly red-shifted to 530 nm and 572 nm in **4** and **6**, respectively. The measured lifetimes (τ) at these wavelengths show long-lived, phosphorescent processes, with $\tau = 360$ ms for **4** and $\tau = 7.7$ ms for **6**. (Figures S51, S53). Phosphorescence is typically seen in molecules containing heavy atoms, which lend the molecule spin-orbit coupling (SOC) that increases the efficiency of intersystem crossing (ISC) from the singlet excited state to the triplet excited state. Based on the weak fluorescence in these two compounds, it appears that SOC arising from oxygen and sulfur leads to efficient ISC. This is consistent with TD-DFT calculations of **4** and **6**, in which the orbitals participating in electronic transitions (Figures S54-55) support El-Sayed's rules for efficient ISC.[19] Despite this, the extraordinarily long phosphorescent lifetimes in **4** and **6** provide ample

opportunity for non-radiative decay to occur (e.g., through molecular motion), ultimately resulting in minimal luminescence at ambient conditions. At 77 K, however, the molecules are constrained in a frozen matrix that renders non-radiative decay processes less favorable and thus permits strong phosphorescence. This data highlights the varying effects that substituents can have on the photophysical properties of *anti*-$B_{18}H_{22}$ and shows that B-O and B-S connectivities alter the absorption, emission, and fluorescent behavior of the corresponding B_{18}-based cluster.
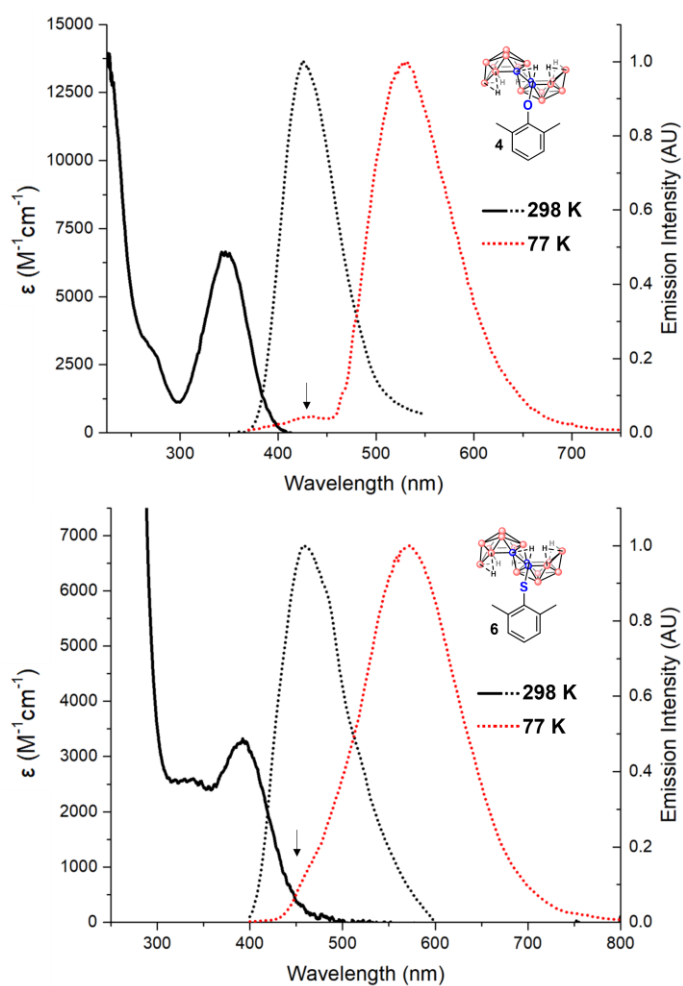
Figure 5.4. Absorption (solid line) and emission (dotted line) spectra of compounds **4** (top) and **6** (bottom). Emission spectra at 298 K and 77 K display fluorescence and phosphorescence, respectively. The arrows indicate fluorescent shoulders visible in the 77 K spectra. For **4**, λ_{exc} = 340 nm at 298 K, λ_{exc} = 350 nm at 77 K. For **6**, λ_{exc} = 380 nm.

5.4 Conclusion

In this work we detail two new and complementary strategies for generating nitrogen, oxygen, and sulfur-functionalized *anti*-$B_{18}H_{22}$ analogues from 7-I-$B_{18}H_{21}$. We first demonstrate that palladium-catalyzed cross-coupling can forge B-N and B-O bonds at the B7 vertex with sterically hindered substrates. To our surprise, we discovered that these connectivities could be produced through a metal-free nucleophilic substitution pathway, which also proved applicable for generating B-S functionalized clusters. In addition to unveiling this unique reactivity of monoiodinated $B_{18}H_{22}$, we demonstrate that the luminescence of the parent borane can be modulated through cage functionalization. Aside from a rare example of a metal-free nucleophilic substitution chemistry of a boron-halogen moiety in a boron cluster, this work

5.5 References

1.   (a) Grimes, R.N. *Carboranes, 3ʳᵈ ed.* Academic Press, 2016. (b) Lipscomb, W.N. *Boron Hydrides.* Courier Corporation, 2013.

2.   Recent reviews: (a) Fisher, S.P.; Tomich, A.W.; Lovera, S.O.; Kleinsasser, J.F.; Guo, J.; Asay, M.J.; Nelson, H.M.; LaVallo, V. Nonclassical Applications of *closo*-Carborane Anions: From Main Group Chemistry and Catalysis to Energy Storage. *Chem. Rev.* 2019, *119*, 8262-8290. (b) Dash, B.P.; Satapathy, R.; Maguire, J.A.; Hosmane, N.S. Polyhedral boron clusters in materials science. *New J. Chem.* 2011, *35*, 1955-1972. Núñez, R.; Tarrés, M.; Ferrer-Ugalde. A.; de Biani, F.F.; Teixidor, F. Electrochemistry and Photoluminescence of Icosahedral Carboranes, Boranes, Metallacarboranes, and Their Derivatives. *Chem. Rev.* **2016**, *116*, 14307-14378.

3.   Recent reviews: (a) Dziedzic, R.M. and Spokoyny, A.M. Metal-catalyzed cross-coupling chemistry with polyhedral boranes. *Chem. Commun.* 2019, *55*, 430-442. (b) Olid, D.; Núñez,R.; Viñas, C.; Teixidor, F. Method to produce B-C, B-P, B-N and B-S bonds in boron clusters. *Chem. Soc. Rev.* 2013, *42*, 3318-3336.

4. Key select examples: (a) Trofimenko, S. Photoinduced Nucleophilic Substitution in Halogenated Clovoboranes. *J. Am. Chem. Soc.* 1966, *88*, 1899-1904. (b) Li, S. and Xie, Z. Visible-Light-Promoted Nickel-Catalyzed Cross-Coupling of Iodocarboranes with (Hetero)Arenes via Boron-Centered Carboranyl Radicals. *J. Am. Chem. Soc.* **2022**, *144*, 7960-7965.

5. Key select examples: (a) Marshall, W.J.; Young, R.J.; Grushin, V.V. Mechanistic Features of Boron-Iodine Bond Activation of B-Iodocarboranes. *Organometallics* **2001**, *20*, 523-533. (b) Kaszyński, P. and Ringstrand, B. Functionalization of *closo*-Borates via Iodonium Zwitterions. *Angew. Chem. Int. Ed.* **2015**, *54*, 6576-6581. (c) Zhu, T.-C.; Xing, Y.-Y.; Sun, Y.; Duttwyler, S.;

Hong, X. Directed B-H functionalization of the *closo*-dodecaborate cluster *via* concerted iodination-deprotonation: reaction mechanism and origins of regioselectivity. *Org. Chem. Front.* **2020**, *7*, 3648-3655.

6. Key select examples: (a) Buades, A.B.; Arderiu, V.S.; Olid-Britos, D.; Viñas, C.; Sillanpää, R.; Haukka, M.; Fontrodona, X.; Paradinas, M.; Ocal, C.; Teixidor, F. Electron Accumulative Molecules. *J. Am. Chem. Soc.* **2018**, *140*, 2957-2970. (b) Stogniy, M. Y.; Anufriev, S.A.; Shmal'ko, A.V.; Antropov, S.M.; Anisimov, A.A.; Suponitsky, K.Y.; Filippov, A.O.; Sivaev, I.B. The unexpected reactivity of 9-iodo-*nido*-carborane: from nucleophilic substitution reactions to the synthesis of tricobalt tris(dicarbollide) Na[4,4',4"-(MeOCH$_2$CH$_2$O)$_3$-3,3',3"-Co$_3$(μ^3-S)(1,2-C$_2$B$_9$H$_{10}$)$_3$]. *Dalton Trans.* **2021**, *50*, 2671-2688. (c) Ewing, W. C.; Carroll, P.J.; Sneddon, L.G. Syntheses and Surprising Regioselectivity of 5- and 6-Substituted Decaboranyl Ethers via the Nucleophilic Attack of Alcohols on 6- and 5-Halodecaboranes. *Inorg. Chem.* **2011**, *50*, 4054-4064. (d) Wright, J. H.; Kefalidis, C.E.; Tham, F.S.; Maron, L.; Lavallo, V. Click-like Reactions with the Inert HCB$_{11}$Cl$_{11}$$^-$ Anion Lead to Carborane-Fused Heterocycles with Unusual Aromatic Character. *Inorg. Chem.* **2013**, *52*, 6223-6229. (b) Finze, M.; Sprenger, J.A.P.; Schaack, B.B. Salts of the 1-cyanocarba-*closo*-dodecaborate anions [1-NC-*closo*-1-CB$_{11}$X$_{11}$]$^-$ (X = H, F, Cl, Br, I). *Dalton Trans*. **2010**, *39*, 2708-2716.

7. (a) Zakharkin, L. N. and Kalinin, V. N. Action of nucleophilic reagents on B-halocarboranes. *BACCA* **1971**, *20*, 2185-2187. (b) Winberg, K.J.; Mume, E.; Tolmachev, V.; Sjöberg, S. Radiobromination of *closo*-carboranes using palladium-catalyzed halogen exchange. *J. Label. Compd. Radiopharm.* **2005**, *48*, 195-202.

8.   (a) Pitochelli, A. R. and Hawthorne, M.F. The Preparation of a New Boron Hydride $B_{18}H_{22}$. *J. Am. Chem. Soc.* **1962**, *84*, 3218. (b) Cerdán, L.; Braborec, J.; Garcia-Moreno, I.; Costela, A.; Londesborough, M.G.S. A borane laser. *Nature Commun.* **2015**, *6*, 5958. (c) Londesborough, M. G. S.; Dolanský, J.; Bould, J.; Braborec, J.; Kirakci, K.; Lang, K.; Císařová, I.; Kubát, P.; Roca-Sanjuán, D.; Francés-Monerris, A.; Slušná, L.; Noskovičová, E.; Lorenc, D. Effect of Iodination on the Photophysics of the Laser Borane *anti*-$B_{18}H_{22}$: Generation of Efficient Photosensitizers of Oxygen. *Inorg. Chem.* **2019**, *58*, 10248-10259. (d) Anderson, K.P.; Waddington, M.A.; Balaich, G.J.; Stauber, J.M.; Bernier, N.A.; Caram, J.R.; Djurovich, P.I.; Spokoyny, A.M. A molecular boron cluster-base chromophore with dual emission. *Dalton Trans.* **2020**, *49*, 16245-16251. (e) Londesborough, M. G. S.; Dolanský, J.; Jelínek, T.; Kennedy, J.D.; Císařová, I.; Kennedy, R.D.; Roca-Sanjuán, D.; Francés-Monerris, A.; Lang. K.; Clegg, W. Substitution of the laser borane *anti*-$B_{18}H_{22}$ with pyridine: a structural and photophysical study of some unusually structured macropolyhedral boron hydrides. *Dalton Trans.* **2018**, *47*, 1709-1725. (f) Chen, J.; Xiong, L.; Zhang, L.; Huang, X.; Meng, H.; Tan, C. Synthesis, aggregation-induced emission of a new *anti*-$B_{18}H_{22}$-isoquinoline hybrid. *Chem. Phys. Lett.* **2020**, *747*, 137328. (g) Saurí, V.; Oliva, J.M.;0 Hnyk, D.; Bould, J.; Braborec, J.; Merchán, M.; Kubát, P.; Císařová, I.; Lang, K.; Londesborough, M.G.S. Tuning the Photophysical Properties of *anti*-$B_{18}H_{22}$: Efficient Intersystem Crossing between Excited Singlet and Triplet States in New 4,4'-$(HS)_2$-*anti*-$B_{18}H_{20}$. *Inorg. Chem.* **2013**, *52*, 9266-9274. (h) Anderson, K.P.; Hua, A.S.; Plumley, J.B.; Ready, A.D.; Rheingold, A.L.; Peng, T.L.; Djurovich, P.I.; Kerestes, C.; Snyder, N.A.; Andrews, A.; Caram, J.R.; Spokoyny, A.M. Benchmarking the dynamic and luminescent properties and UV stability of $B_{18}H_{22}$-based materials. *Dalton Trans.* **2022**. Article ASAP. DOI: 10.1039/D2DT01225A.

9. (a) Stanko, V. I.;Chapovskii, Y.A.; Brattsev, V.A.; Zakharkin, L.I. The Chemistry of Decaborane and its Derivatives. *Russ. Chem. Rev.* **1965**, *34*, 424-439. (b) G. A. Guter and G. W. Schaeffer, The Strong Acid Behavior of Decaborane. *J. Am. Chem. Soc.* **1956**, *78*, 3546. (c) King, R.B. Defective Vertices in *closo*- and *nido*-Borane Polyhedra. *Inorg. Chem.* **2001**, *40*, 6369-6374. (d) Simpson, P.G. and Lipscomb, W.N. Molecular, Crystal, and Valence Structures of $B_{18}H_{22}$. *J. Chem. Phys.* **1963**, *39*, 26-34. (e) Olsen, F.P.; Vasavada, R.C.; Hawthorne, M.F. The chemistry of n-$B_{18}H_{22}$ and i-$B_{18}H_{22}$. *J. Am. Chem. Soc.* **1968**, *90*, 3946-3951.

10. Sevryugina, Y.; Julius, R.L.; Hawthorne, M.F. Novel Approach to Aminocarboranes by Mild Amidation of Selected Iodo-carboranes. *Inorg. Chem.* **2010**, *49*, 10627-10634.

11. (a) Bagno, A. and Comuzzi, C. Deprotonation of Amides and Polyfunctional Imides Probed by Heteronuclear NMR and Quantum Chemical Calculations. *Eur. J. Org. Chem.* **1999**, 287-295. (b) Reis, O.; Koyuncu, H.; Esiringu, I.; Sahin, Y.; Gulcan, O. A new method for the synthesis of rasagiline. European Patent EP2663545B1, January 13, 2011.

12. (a) Dziedzic, R.M.; Saleh, L.M.A.; Axtell, J.C.; Martin, J.L.; Stevens, S.L.; Royappa, A.T.; Rheingold, A.L.; Spokoyny, A.M. B-N, B-O, and B-CN Bond Formation via Palladium-Catalyzed Cross-Coupling of B-Bromo-Carboranes. *J. Am. Chem. Soc.* **2016**, *138*, 9081-9084. (b) Dziedzic, R.M.; Martin, J.L.; Axtell, J.C.; Saleh, L.M.A.; Ong, T.-C.; Yang, Y.-F.; Messina, M.S.; Rheingold, A.L.; Houk, K.N.; Spokoyny, A.M. Cage-Walking: Vertex Differentiation by Palladium-Catalyzed Isomerization of B(9)-Bromo-*meta*-Carborane. *J. Am. Chem. Soc.* **2017**, *139*, 7729-7732. (c) Mu, X.; Hopp, M.; Dziedzic, R.M.; Waddington, M.A.; Rheingold, A.L.; Sletten, E.M.; Axtell, J.C.; Spokoyny, A.M. Expanding the Scope of Palladium-Catalyzed B-N Cross-Coupling Chemistry in Carboranes. *Organometallics*, **2020**, *39*, 4380-4386. (d) Kataki-

Anastasakou, A.; Axtell, J.C.; Hernandez, S.; Dziedzic, R.M.; Balaich, G.J.; Rheingold, A.L.; Spokoyny, A.M.; Sletten, E.M. Carboranes Guests for Cucurbit[7]uril Facilitate Strong Binding and On-Demand Removal. *J. Am. Chem. Soc.* **2020**, *142*, 20513-20518. (e) Dziedzic, R.M.; Axtell, J.C.; Rheingold, A.L.; Spokoyny, A.M. Off-Cycle Processes in Pd-Catalyzed Cross-Coupling of Carboranes. *Org. Process Res. Dev.* **2019**, *23*, 1638-1645. (f) Biscoe, M.R.; Fors, B.P.; Buchwald, S.L. A New Class of Easily Activated Palladium Precatalysts for Facile C-N Cross-Coupling Reactions and the Low Temperature Oxidative Addition of Aryl Chlorides. *J. Am. Chem. Soc.* **2008**, *130*, 6686-6687. (g) Bruno, N.C.; Tudge, M.T.; Buchwald, S.L. Design and preparation of new palladium precatalysts for C-C and C-N cross-coupling reactions. *Chem. Sci.* **2013**, *4*, 916-920. (h) Bruno, N.C. and Buchwald, S.L. Synthesis and Application of Palladium Precatalysts that Accommodate Extremely Bulky Di-*tert*-butylphosphino Biaryl Ligands. *Org. Let..* **2013**, *15*, 2876-2879. (i) Bruno, N.C.; Niljianskul, N.; Buchwald, S.L. *N*-substituted 2-Aminobiphenylpalladium Methanesulfonate Precatalysts and Their Use in C-C and C-N Cross-Couplings. *J. Org. Chem.* **2014**, *79*, 4161-4166.

13. Loffredo, R. E.; Drullinger, L.F.; Slater, J.A.; Turner, C.A.; Norman, A.D. Preparation and properties of 6-ethoxy-, 6-phenyl-, and 6-trimethylsiloxydecaborane(14). *Inorg. Chem.* **1976**, *15*, 478-480.

14. Tian, J.; Wang, G.; Qi, Z.-H.; Ma, J. Ligand Effects of BrettPhos and RuPhos on Rate-Limiting Steps in Buchwald-Hartwig Amination Reaction Due to the Modulation of Steric Hindrance and Electronic Structure. *ACS Omega*, **2020**, *5*, 21385-21391.

15. Finch, A.; Gardner, P.J.; Watts, G.B. Thermochemistry of the trialkylthioboranes and triphenylthioborane. *J. Chem. Soc. Faraday Trans.* **1967**, *63*, 1603-1607.

16.   Hamlin, T.A.; Swart, M.; Bickelhaupt, F.M. Nucleophilic Substitution (S_N2): Dependence on Nucleophile, Leaving Group, Central Atom, Substituents, and Solvent. *ChemPhysChem* **2018**, *19*, 1315-1330.

17.   (a) Lower, S. K. and El-Sayed, M.A. The Triplet State and Molecular Electronic Processes in Organic Molecules. *Chem. Rev.* **1966**, *66*, 199-241. (b) Marian, C.M. Spin-orbit coupling and intersystem crossing in molecules. *WIREs Comput. Mol. Sci.* **2012**, *2*, 187-203.

18. Key select examples: (a) Mukherjee, S. and Thilagar P., Boron clusters in luminescent materials. *Chem. Commun.* **2016**, *52*, 1070-1093. (b) Wu, X.; Guo, J.; Quan, Y.; Jia, W.; Jia, D.; Chen, Y.; Xie, Z. Cage carbon-substitute does matter for aggregation-induced emission features of *o*-carborane-functionalized anthracene triads. *J. Mater. Chem. C*, **2018**, *6*, 4140-4149. (c) Kim, S.; Lee, J.H.; So, H.; Kim, M.; Mun, M.S.; Hwang, H.; Hwan, M.P.; Lee, K.M. Insights into the effects of substitution position on the photophysics of mono-*o*-carborane-substituted pyrenes. *Inorg. Chem. Front.*, **2020**, *7*, 2949-2959. (d) Marsh, A.V.; Cheetham, N.J.; Little, M.; Dyson, M.; White, A.J.P.; Beavis, P.; Warriner, C.N.; Swain, A.C.; Stavrinou, P.N.; Heeney, M. Carborane-Induced Excimer Emission of Severely Twisted Bis-*o*-Carboranyl Chyrsene. *Angew. Chem. Int. Ed.*, **2018**, *57*, 10640-10645. (e) Sinha, S.; Kelemen, Z.; Hümpfner, E.; Ratera, I.; Malval, J.-P.; Jurado, J.P.; Viñas, C.; Teixidor, F.; Núñez, R.; *o*-Carborane-based fluorophores as efficient luminescent systems both as solids and as water-dispersible nanoaprticles. *Chem. Commun.*, **2022**, *58*, 4016-4019. (f) Martin, K.L.; Smith, J.N.; Young, E.R.; Carter, K.R. Synthetic Emission Tuning of Carborane-Containing Poly(dihexylfluorene)s. *Macromolecules*, **2019**, *52*, 7951-7960. (g) Li, J.; Xu, J.; Yan, L.; Lu, C.; Yan, H. A "flexible" carborane-cored luminogen: variable emission behaviours in aggregates. *Dalton Trans.*, **2021**, *50*, 8029-8035. (h) Ochi, J.; Tanaka, K.; Chujo, Y. Recent Progress in the Development of Solid-State Luminescent *o*-Carboranes with Stimuli

Responsivity. *Angew. Chem. Int. Ed.*, **2020**, *59*, 9841-9855. (i) Zhang, K.; Shen, Y.; Yang, X.; Liu, J.; Jiang, T.; Finney, N.; Spingler, B.; Duttwyler, S. Atomically Defined Monocarborane Copper(I) Acetylides with Structural and Luminescence Properties Tuned by Ligand Sterics. *Chem. Eur. J.*, **2019**, *25*, 8754-8759.

Perspective

Research on boron cluster-based luminescent molecules has gained traction over the past decade owing to their unique and interesting photophysical properties. While investigations on carborane-containing luminescent compounds comprise a great portion of this interest, research on the inherently luminescent borane $anti$-$B_{18}H_{22}$ is comparatively nascent. This dissertation provides a starting point to explore several aspects of $anti$-$B_{18}H_{22}$ chemistry. While iodination, bromination, and chlorination has been covered in this work, fluorination of the cluster has not yet been demonstrated. One could potentially utilize the methods described herein to access more complex molecular architectures, such as perhalogenated clusters or mixed halogen clusters that could potentially be used as precursors in subsequent nucleophilic substitution reactions. While this focuses on the functionalization of $anti$-$B_{18}H_{22}$ at the B4 and B7 vertices, much remains unknown regarding selective substitution at other boron atoms in the 18-vertex cage. Preliminary results from our lab show that the bridging hydrogens of $anti$-$B_{18}H_{22}$ undergo deuterium exchange when stirred in deuterated methanol at room temperature. The facile abstraction of these hydrogen atoms could be utilized to develop a new route for cluster functionalization. Alternatively, existing $B_{18}H_{22}$ derivatives could be used to produce substitutions at vertices other than B4 and B7; a recent publication[1] reported the functionalization of the B5 vertex of decaborane(14) from a B6-halogenated precursor, suggesting that a similar reaction could be feasible in halogenated B_{18}-based clusters. This fundamental synthetic knowledge will become increasingly important for the design of B_{18}-based chromophores and the production of more complex molecular architectures that require site-specific substitutions on the boron cluster cage.

With the development of new synthetic methods for $anti$-$B_{18}H_{22}$, investigation of the photoluminescent properties of the resulting analogues will be essential to establishing guiding

principles on B_{18}-based chromophore design. As demonstrated in this work, establishing how structural modification and the solvent/film environment alters the properties of this cluster is a significant challenge. Consequently, there are non-synthetic aspects of *anti*-$B_{18}H_{22}$ that also require attention. For example, the solvatochromism study conducted in Chapter 3 showed that *anti*-$B_{18}H_{22}$ is highly susceptible to its solvent environment, and that derivatives of this cluster will not necessarily exhibit the same solvent-dependent luminescence as the parent borane. While we suspect that these changes arise from a combination of steric and electronic effects, the exact cause of the observed changes in absorption and emission remains unknown. It is also likely that different "classes" of solvents (aromatic, protic, ethereal, etc.) interact with the cluster differently and therefore effect distinctly different changes in luminescence. Therefore, comprehensive investigations of cluster-solvent interactions are necessary to fully understand, and better predict, the luminescent properties of B_{18}-based molecules in solution and in films. Other relevant research areas include assessing B_{18}-based cluster stability as solids, films, and in various solvents. Mechanistic investigations of the cluster cage deconstruction observed in Chapter 3 could also elucidate potential causes of instability and methods to combat it.

References

1. W. C. Ewing, P. J. Carroll and L. G. Sneddon. *Inorg. Chem.* **2011**, *50*, 4054-4064.